NOTICE

The quality of this microform is heavily dependent upon the quality of the original thesis submitted for microfilming. Every effort has been made to ensure the highest quality of reproduction possible.

If pages are missing, contact the university which granted the degree.

Some pages may have indistinct print especially if the original pages were typed with a poor typewriter ribbon or if the university sent us an inferior photocopy.

Previously copyrighted materials (journal articles, published tests, etc.) are not filmed.

Reproduction in full or in part of this microform is governed by the Canadian Copyright Act, R.S.C. 1970, c. C-30.

AVIS

La qualité de cette microforme dépend grandement de la qualité de la thèse soumise au microfilmage. Nous avons tout fait pour assurer une qualité supérieure de reproduction.

S'il manque des pages, veuillez communiquer avec l'université qui a conféré le grade.

La qualité d'impression de certaines pages peut laisser à désirer, surtout si les pages originales ont été dactylographiées à l'aide d'un ruban usé ou si l'université nous a fait parvenir une photocopie de qualité inférieure.

Les documents qui font déjà l'objet d'un droit d'auteur (articles de revue, tests publiés, etc.) ne sont pas microfilmés.

La reproduction, même partielle, de cette microforme est soumise à la Loi canadienne sur le droit d'auteur, SRC 1970, c. C-30.

Canada

THE UNIVERSITY OF ALBERTA

Thermal Measurements on Clearwater Shale utilizing a Transient Heat Probe and Direct Electrical Heating

by

© David Goulbourne

A Thesis

submitted to the Faculty of Graduate Studies and Research

in partial fulfilment of the requirements for the Degree

of Master of Science

Department of Electrical Engineering

Edmonton, Alberta

Spring, 1988

ISBN 0-315-42726-4

THE UNIVERSITY OF ALBERTA

RELEASE FORM

NAME OF AUTHOR: DAVID GOULBOURNE

TITLE OF THESIS: Thermal Measurements on Clearwater Shale Utilizing a Transient Heat Probe and Direct Electrical Heating

DEGREE: MASTER OF SCIENCE

YEAR THIS DEGREE GRANTED: Spring 1988

Permission is hereby granted to THE UNIVERSITY OF ALBERTA LIBRARY to reproduce single copies of this thesis and to lend or sell such copies for private, scholarly or scientific research purposes only.

The author reserves other publication rights, and neither the thesis nor extensive extracts from it may be printed or otherwise reproduced without the author's written permission.

David Goulbourne

(Student's signature)

Present Address:
108 Woodlands Road,
St.Albert, Alta.,
T8N-3H2

Date: January 19/88

THE UNIVERSITY OF ALBERTA

FACULTY OF GRADUATE STUDIES AND RESEARCH

The undersigned certify that they have read, and recommend to the Faculty of Graduate Studies and Research, for acceptance, a thesis entitled THERMAL MEASUREMENTS ON CLEARWATER SHALE UTILIZING A TRANSIENT HEAT PROBE AND DIRECT ELECTRICAL HEATING submitted by DAVID GOULBOURNE in partial fulfilment of the requirements for the degree of MASTER OF SCIENCE in ELECTRICAL ENGINEERING.

F.E. Vermeulen

Supervisor

A.E. Cote

Supervisor

J.D. Dahl

J.R. Winkler

Robert Fedosejevs

Date January 19/88

Abstract

The objective of this Thesis was to determine the thermal conductivity and heat capacity of Clearwater shale. Core samples were obtained from two wells in the Syncrude Canada Limited mine site at Mildred Lake, Alberta, at depths ranging from 11.3m to 53.9m. The Clearwater shale overlies the oilsand payzone and the thermal properties of Clearwater shale are required for the continuing research in the recovery of bitumen from the Alberta oilsands using in-situ electromagnetic techniques.

Two methods were used to measure these properties. They were the transient heat probe method and the transient heat capacity method.

For the transient heat probe method, which measures thermal conductivity, a probe was built using criteria which account for the finite dimensions of the sample and probe. These criteria, however, are based upon analytical models which only approximate the actual physical phenomena that occur with the transient heat probe. Hence the criteria are generally very conservatively chosen. A simulation program, MEGAERA, was utilized to assess these criteria and to establish more accurate design information.

The transient heat capacity method involved heating the shale samples electrically and monitoring the temperature rise of the sample. By placing the thermocouples well within the sample, heat losses from the sample were negligible, at the thermocouple locations, for the first few minutes of an experiment. The heat capacity of the sample could then be easily determined, from the

temperature rise of the sample and the electrical energy delivered to the sample.

Acknowledgments

I would like to express my appreciation to the following people:

To my supervisors Dr. Chute and Dr. Vermeulen, for having enough confidence in my abilities to consider me as a graduate student and for their guidance and advice.

To Jim Fearn and his technical skills which he used to build the apparatus used in this research - Thanks Jim.

To Dr. Ed Sumbar, for his many useful comments and suggestions regarding my work and graduate studies in general.

To Dr. Fedosejevs and his extraordinary mathematical skills which he was willing to share with me when I encountered difficulties.

To the Alberta Oil Sands Technology and Research Authority and the Natural Sciences and Engineering Research Council for financial support.

Finally, I wish to thank my parents who delayed many of their plans while I completed my work.

TABLE OF CONTENTS

LIST OF TABLES

LIST OF FIGURES

List of Symbols and Abbreviations

AWG	American wire gauge
c	specific heat $\left(\frac{J}{g\,^{\circ}C}\right)$
D	thermal diffusivity (m^2/s)
E	energy (J)
ΔE	change in energy (J)
$g(r,t)$	heating rate (W/m^3) at position r(m) and time t(s)
γ	Euler's constant (0.57722...)
H	thermal conductance $\left(\frac{W}{m^2\,^{\circ}C}\right)$
I.D.	inner diameter
K	thermal conductivity $\left(\frac{W}{m\,^{\circ}C}\right)$
O.D.	outer diameter
ϕ	porosity
Q	heating rate per unit volume (W/m^3)
q	heating rate per unit length (W/m)
$q(r,t)$	heat flux vector (W/m^2) at position r(m) and time t(s)
ρ	density (g/cm^3 or kg/m^3)
ρc	volumetric heat capacity $\left(\frac{J}{m^3\,^{\circ}C}\right)$
S_w	water saturation
σ	electrical conductivity (S/m)
t	time (s)
T	temperature ($^{\circ}C$)
ΔT	change in temperature ($^{\circ}C$)

1.0 Introduction

The in-place crude bitumen reserves of Alberta are estimated at 268 billion cubic metres. The bitumen generally occurs in layers that are 3 metres to 41 metres thick, which are overlain by extensive overburden. In regions where the overburden is less than 75 metres thick, surface mining methods are applicable. However, only approximately 11.9 billion cubic metres can be recovered using this method. For the rest of the reserves, the overburden thickness is greater than 75 metres and some type of in-situ method has to be applied to recover the bitumen.[1]

In-situ techniques usually involve heating the formation to lower the viscosity of the bitumen, which in its natural state is virtually immobile. Methods which have been suggested to heat the formation are steam and hot water injection, in-situ combustion, and even underground nuclear explosions. More recently electromagnetic methods have become of interest.

Presently the Applied Electromagnetic Laboratory at the University of Alberta is involved in developing electromagnetic heating techniques for the oilsands. The studies that are being undertaken involve both numerical and physical modelling and require extensive information on the physical properties of the oilsands and surrounding overburden and underburden. The purpose of

---

[1]Alberta Energy Resources Conservation Board (ERCB), December 31, 1986

this research was to determine the thermal properties of Clearwater shale. This material is a major constituent of the overburden of the oilsand payzone.

There are many methods for determining the thermal properties of materials. For instance, there are steady state methods, transient methods, and even methods which involve using a weighted average of the thermal properties of the various constituents in composite materials to determine the effective thermal properties of the original composite material. These methods will be discussed further in the chapter *2.0 Theory and Literature Review* of this thesis.

For shale samples it is believed that transient methods, lasting a few seconds to several minutes, are better than steady state methods which generally require more time. With transient methods the sample will have less time to change *physically* during the experiment. Consequently, two transient methods were chosen. These methods will be presented in detail in the following chapters.

The Chapter *2.0 Theory and Literature Review* will discuss the theory upon which the transient methods used in this research are based and will also discuss some of the methods used by other researchers.

In the chapters *3.0 Design and Testing of the Transient Heat Probe Apparatus and Method* and *4.0 Design and Testing of the Transient Heat Capacity Apparatus and Method*, a detailed description of the apparatus and methods used in this research, to determine the thermal properties of shale, are presented. In

addition, these chapters show how the transient heat probe and heat capacity methods were tested using a numerical simulation program and by performing experiments on materials with published thermal properties. Chapters 3.0 and 4.0 also present the experimental results found for Clearwater shale samples, using the transient heat probe and heat capacity methods.

Finally, in the chapter *5.0 Conclusions and Suggested Modifications* a summary of the experimental results determined during this research and some suggested modifications to the transient methods used in this research are presented.

2.0 Theory and Literature Review

There are many methods for determining the thermal properties of materials. However, before proceeding to present in detail the theory required to understand the apparatus used in this research, it may be useful to briefly discuss some of the other methods used to determine thermal properties of materials.

From two equations of heat transfer, the heat flux equation or Fourier's Law[2]

$$q(r,t) = -K\nabla T(r,t) \qquad (2.1)$$

where K = the thermal conductivity $\left\{ \frac{W}{m\,^{\circ}C} \right\}$

$\nabla T(r,t)$ = the gradient of the temperature($^{\circ}C/m$) at a position r(m) and time t(s)

$q(r,t)$ = the heat flux vector (W/m^2) at r(m) and t(s)

(Note: Since heat flows from high to low temperatures, the negative sign in Fourier's Law is required.)

---

[2] Özişik, pp1-4, (1980)

and the differential equation of heat conduction[3] for a vanishingly small volume V

$$K\nabla^2 T(r,t) + g(r,t) = \rho c \frac{\partial T}{\partial t} \qquad (2.2)$$

where K = the thermal conductivity $\left[\frac{W}{m^{\circ}C}\right]$

ρ = density (g/m^3)

c = specific heat $\left[\frac{J}{g^{\circ}C}\right]$

ρc = volumetric heat capacity $\left[\frac{J}{m^{3\circ}C}\right]$

$g(r,t)$ = rate of heat generation(W/m^3) at a position r(m) and time t(s) of the vanishingly small volume V

$K\nabla^2 T(r,t)$ = net rate of heat entering the vanishingly small volume V through its surface S (W/m^3)

$\rho c \frac{\partial T}{\partial t}$ = rate of change of heat stored at the vanishingly small volume $V(W/m^3)$

two categories for determining thermal properties of materials may be found. There are steady state methods $\left[\frac{\partial T}{\partial t} = 0\right]$ and transient methods $\left[\frac{\partial T}{\partial t} \neq 0\right]$.

In steady state methods a temperature distribution that is

---

[3] Özisik, pp4-7, (1980).

constant in time $\left[\frac{\partial T}{\partial t} = 0\right]$ is established within a sample of the material being measured. The temperature distribution may be produced by heat generated within the sample, or by heat flux passing through the sample, as in the *Hot Plate Method*[4,5,6,7,8]. Since the temperature distribution does not vary with time, the rate of change of heat stored in the sample is zero (i.e. $\rho c\frac{\partial T}{\partial t} = 0$) and therefore the volumetric heat capacity, ρc, cannot be determined using steady state methods. However, by choosing an appropriate geometry for the sample, an analytic solution for the temperature distribution may be derived and the thermal conductivity of the sample can be found.

Using transient methods one can determine all the thermal properties of a sample. Transient methods usually involve changing the heat of the sample and measuring these changes in heat along with changes in the temperature distribution of the sample as a function of time. A simple example of a transient method used to determine the volumetic heat capacity, ρc, of a homogeneous sample involves changing the heat of the sample and measuring the change

---

[4]Nancorrow, (1933)

[5]Cervenan, Vermeulen, and Chute, (1981)

[6]Lillico, (1986)

[7]ASTM, C 177-85, (1985)

[8]ASTM, C 1044-85, (1985)

in the temperature of the sample. By integrating the differential equation of heat conduction, equation (2.2), over the volume of the sample and with respect to time, one obtains the following result, after solving for ρc.

$$\rho c = \frac{\int_t \int_v (K\nabla^2 T(r,t) + g(r,t)) \partial v \partial t}{\int_t \int_v \frac{\partial T}{\partial t} \partial v \partial t} \qquad (2.3a)$$

$$= \frac{\Delta E(t)}{\int_v \Delta T(r,t) \partial v} \qquad (2.3b)$$

where $\Delta E(t)$ = the total change in the heat of the sample as a function of time t(s)

$\Delta T(r,t)$ = the change in the temperature ($^\circ$C) of the sample as a function of position r(m) and time t(s)

If the change in the temperature distribution is uniform throughout the sample then

$$\rho c = \frac{\Delta E(t)}{(VOL)\Delta T(t)}$$

where (VOL) = the total volume of the sample (m^3)

This method is very similar to the transient heat capacity method used in this research and will be discussed in more detail later in this thesis. Two difficulties with this method are the accurate measurement of the change in the energy of the sample, $\Delta E(t)$, and the production of a uniform temperature change in the sample. More elaborate transient methods exist which can measure all of the thermal properties of the sample.

Hanafi and Karim[9] measured the thermal conductivity of oilsands by monitoring the temperature response, at the center of spherical samples, due to a step temperature change at the surface of the spherical samples. By using an approximate analytic solution, the thermal conductivity of the oilsand samples was determined.

Glatzmaier and Ramirez[10] used the transient hot wire method, which is very similar to the transient heat probe method (refer to *2.1 Transient Heat Probe Method*), to determine the thermal conductivity and diffusivity (ratio of the thermal conductivity to the volumetric heat capacity) of glycerin, unconsolidated oil shale, and glass beads. In the transient hot wire method a very

[9]Hanafi and Karim, (1986)

[10]Glatzmaier and Ramirez, (1985)

small diameter wire with a finite electrical conductivity is inserted into a cylindrical sample. The wire is electrically heated by passing a current through the wire. By monitoring the temperature rise of the wire and/or sample, the thermal properties of the sample can be determined. Other researchers, Sandberg, Andersson, and Bäckström[11] also used the transient hot wire method to determine the thermal properties of glycerol.

Iida, Ohtani, and Stephan[12] developed a very ingenious transient method which is capable of measuring the thermal diffusivity and conductivity of cylindrical sand/salt water samples. They electrically heated a cylindrical sample by passing a current through the sample and monitored the temperature rise of the sample using several thermocouples located within the sample. By taking the Laplace transform of the temperature responses of the thermocouples and using an appropriate analytic solution, the thermal diffusivity and conductivity of the sample could be determined.

A final example of a transient method is the transient heat probe method which is used in this research to determine the thermal conductivity of shale. Under appropriate conditions the transient heat probe method is capable of measuring *all of the*

---

[11] Sandberg, Andersson, and Bäckström, (1977)

[12] Iida, Ohtani, and Stephan, (1984)

thermal properties of a sample[13,14,15]; however, these conditions are difficult to achieve in actual experiments. In *2.1 Transient Heat Probe Method* this method will be discussed in detail.

A third category for determining thermal properties of materials involves finding the composition of the material being tested. The effective heat capacity of the original composite sample can then be determined by finding the weighted average of the heat capacities of each component in the original composite sample, according to the composition of the original composite sample[16,17]. For example, for a mineral sample containing water,

$$c_{eff} = (\%water)c_{water} + (\%mineral)c_{mineral} \quad (2.5)$$

where c_{eff} = the effective specific heat of the composite sample $\left[\frac{J}{g\,^{\circ}C}\right]$

%water and %mineral are the composition by mass of the composite sample

---

[13] Bruijn, Haneghem, and Schenk, (1983)

[14] Jaeger, (1958)

[15] Blackwell, (1954)

[16] Kepler, et al, (1985)

[17] Woodside and Messmer, (1961)

c_{water} and $c_{mineral}$ are the specific heat of the water and mineral components of the sample $\left(\frac{J}{g\,^{\circ}C} \right)$

Since the purpose of this research was to determine the thermal properties of shale, it was believed that transient methods, lasting approximately 10 seconds to 10 minutes, were better than steady state methods which can require several hours to make a measurement. Shale samples were usually 100% water saturated; however, the moisture in these samples very easily evaporates when are exposed to the atmosphere. With transient methods the sample will have less time to change *physically* during the experiment - i.e there is minimal water migration or evaporation in the sample during the experiment. The following two sections will present the theory underlying the two transient methods which were used in this research.

2.1 Transient Heat Probe Method

The transient heat probe method is believed to have originally been developed for use in geophysics for the in-situ measurement of thermal properties of rocks and soils.[18] Since then the basic principles of the heat probe method have found other applications.

---

[18] DeVris and Peck, (1958)

For example, these principles have been used to determine the thermal properties of liquids[19], single crystals of silicon or aluminum[20], and building materials such as bricks, concrete, and fibrous insulation[21].

2.1.1 Physical Description of Transient Heat Probe Method

In the transient heat probe method, a probe, similar to the one shown in Figure 2.1, is inserted into a sample whose thermal properties are to be determined. The probe is energized by supplying a constant input power to a heating element inside the probe and the temperature of the probe is recorded, as a function of time, by a thermocouple usually located at the mid-length of the probe. By recording the temperature response of the probe and the power supplied to the probe, the thermal properties of the sample can be determined. The design and construction of the probe illustrated in Figure 2.1 will be discussed in Section 3.2.

When the probe is initially turned on, the temperature is uniform along the entire probe length. As time passes end effects begin to create non-uniformities in the temperature distribution of the probe. These are important, as the analytic solutions, which

---

[19]Van Der Held and Van Drunen, (1949)

[20]Erdman and Schilmoeller, (1973)

[21]Batty, O'Callaghan, and Probert, (1984)

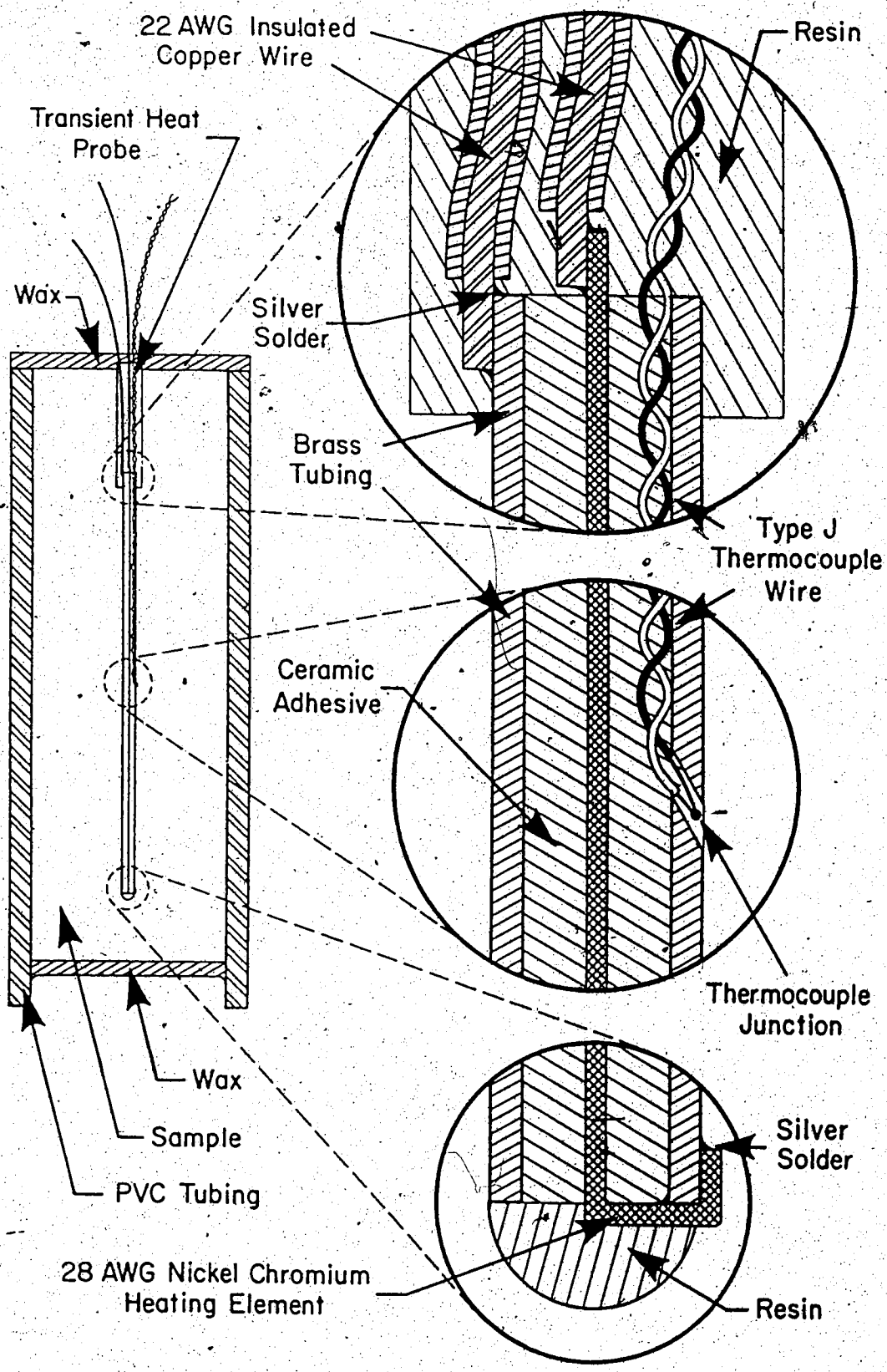

Figure 2.1 : Transient Heat Probe Apparatus

are used to estimate the thermal properties of the sample from the experimental probe temperatures, are based upon an infinitely long heat probe. Such an infinite heat probe has no end effects and hence, has a uniform temperature distribution axially for all time. Therefore, the analytic solutions are only valid at the center of the real probe during such times when the end effects are experimentally negligible. Criteria have been developed to try to determine at which times during the measurement procedure and for what probe configurations the end effects are important[22,23,24,25]. Since the analytical criteria only approximately describe the actual physical situation, the criteria have generally been very conservatively chosen.

---

[22]Blackwell, (1954)

[23]Blackwell, (1953)

[24]Blackwell, (1956)

[25]Jaeger, (1955)

2.1.2 Mathematical Description of Transient Heat Probe Method

The heat probe method is based upon the analytic solution of a continuous line heat source in an infinite homogeneous medium. In cylindrical coordinates a continuous line heat source of vanishingly small diameter, placed along the z-axis, is turned on at time t=0 and produces a heating rate q(W/m), along its entire length. From symmetry, heat flow into the sample is in the radial direction only. For this situation the infinite homogeneous medium will have the following temperature distribution[26]

$$T(r,t) = \begin{cases} \frac{-q}{4\pi K} \, Ei\left[\frac{-r^2}{4Dt}\right] & 0 \le t; 0 \le r \\ 0 & \text{otherwise} \end{cases} \qquad (2.6)$$

where T(r,t) = temperature in the infinite medium (°C)

r = radial distance from the line source (m)

t = time (s)

q = heating rate supplied to continuous line source per unit length of line source (W/m)

---

[26] Carslaw and Jaeger, pp. 261-262, (1956)

K = thermal conductivity of infinite homogeneous medium $\left[\frac{W}{m\,^{o}C}\right]$

D = thermal diffusivity of infinite homogeneous medium (ratio of the thermal conductivity to volumetric heat capacity) (m^2/s)

$-Ei(-x) = \int_x^\infty \frac{e^{-u}}{u}\,du$, which is the exponential integral.

Using the first two terms of a series expansion of Ei(-x),

$$Ei(-x) = \gamma + \ln x - x + \frac{1}{2}x^2 + \text{oooo} \qquad (2.7)$$

where $\gamma = 0.57722$, which is Euler's constant

equation (2.6) becomes

$$T(r,t) = \frac{q}{4\pi K}\left(\ln\left(\frac{4Dt}{r^2}\right) - \gamma\right) \qquad t \text{ large} \qquad (2.8)$$

Notice that at a fixed radius the temperature rises linearly with ln(t) and the slope of this line is $\frac{q}{4\pi K}$. If the heating rate q(W/m) is known, the thermal conductivity, K, of the infinite homogeneous medium can be calculated from this slope. Once the thermal conductivity, K, is found the diffusivity, D, of the infinite homogeneous medium can be found using equation (2.8).

The analytic solution presented above is for an idealized experiment. A real probe has a finite length, a non-zero thermal heat capacity, and a finite thermal conductivity. This causes probe end effects, as well as probe thermal inertia, and also results in a thermal contact resistance between the probe and the sample. In addition, in laboratory experiments the sample will have finite dimensions. Consequently when the heat front that emanates from the probe reaches the outer edge of the sample, equation (2.8), which is valid for large time in an infinite sample, will no longer hold.

Blackwell developed a more realistic analytical solution[27] which takes into account the thermal heat capacity of the probe and contact resistance at the boundary between the probe and external medium. The continuous line source is replaced by an infinitely long cylindrical probe of radius a, specific heat c_1, mass per unit length M_1, and infinite thermal conductivity (i.e. uniform temperature distribution in the probe). Initially both the probe and external medium are at zero temperature and at time t=0 the probe is turned on producing a constant heating rate per unit length q(W/m) radially along its entire length. For large times ($1 < \frac{D_2 t}{a^2}$ where D_2 is the thermal diffusivity of the external medium) the temperature of the probe is

---

[27] Blackwell, (1954)

$$T_1(t) \simeq \frac{q}{4\pi K_2}\left[\ln(4X) - \gamma + \frac{2K_2}{aH} + \frac{1}{2X}\left[\ln(4X) - \gamma + 1 - \frac{\rho_1 c_1}{\rho_2 c_2}\left[\ln(4X) - \gamma + \frac{2K_2}{aH} \right]\right] + O(X^{-2}) \right] \qquad (2.9)$$

(valid for $1<X$)

where $X = \frac{D_2 t}{a^2}$

K_2 = thermal conductivity of the medium $\left[\frac{W}{m\,^oC} \right]$

γ = Euler's constant

$\rho_1 c_1$ = volumetric heat capacity of the probe $\left[\frac{J}{m^3\,^oC} \right]$

$\rho_2 c_2$ = volumetric heat capacity of the external medium $\left[\frac{J}{m^3\,^oC} \right]$

H = thermal conductance at boundary between probe and external medium $\left[\frac{W}{m^2\,^oC} \right]$

q = heating rate produced by probe per unit length of probe (W/m)

a = radius of infinitely long cylindrical probe (m)

For small times $\left[\frac{D_2 t}{a^2} < 1\right]$

$$T(t) \simeq \frac{q}{M_1 c_1}\left[t - \frac{H\pi a}{M_1 c_1} t^2 + \frac{16H^2 a\sqrt{\pi D_2}}{15 M_1 c_1 K_2} t^{5/2} + O(t^3) \right] \qquad (2.10)$$

(valid for X<1)

where $M_1 c_1$ = the volumetric heat capacity of the probe per unit length of probe $\left[\frac{J^\circ}{m^\circ C}\right]$

It should be noted that for very large time $\left[1 << \frac{D_2 t}{a^2}\right]$ equation (2.9) yields results that are identical to the continuous line source result of equation (2.8) - i.e. for $1 << \frac{D_2 t}{a^2}$ equation (2.9) becomes

$$T(t) \simeq \frac{q}{4\pi K_2}\left[\ln\left(\frac{4D_2 t}{a^2}\right) - \gamma\right] \quad t \text{ large} \qquad (2.11)$$

Vos[28] suggests the following criterion for equation (2.11) to be valid

$$50 \frac{a^2}{4D_2} < t \qquad (2.12)$$

Blackwell further improved this model by considering the effects of a probe with finite thermal conductivity. To do this he replaced the infinitely long, perfectly conducting probe with a hollow probe having a non-zero thermal heat capacity and a finite thermal conductivity. Otherwise this model is identical to the previous model. For this improved model Blackwell found that the large time solution is identical to the large time solution of the previous model, up to the $\frac{1}{X}$ term in the series. The small time solution however changed considerably and this indicates that for small times the temperature of the probe is very dependent upon the design of the probe used in the experiment. Fortunately, the small time solution is only valid for the first few seconds of a typical shale experiment, and as a result this experimental data can be ignored. To illustrate this consider the following. Typical thermal properties for shale are

---

[28]Vos, (1955)

$$K_2 = 1.7 \text{ to } 2.3 \quad \frac{W}{m\,^{o}C}$$

$$\rho_2 c_2 = 2.5\times10^{6} \text{ to } 3.4\times10^{6} \quad \frac{J}{m^{3}\,^{o}C}$$

$$D_2 = 5.0\times10^{-7} \text{ to } 9.2\times10^{-7} \quad \frac{m^2}{s}$$

Since the small time solution is valid for $X<1$ or $t < \frac{a^2}{D_2}$, with $a = \frac{1}{16}$ inches $\simeq$ 0.0016 metres one obtains $t < \sim 5$ seconds. If the small time solution can be derived for a given probe design, the solution would be valid for only the first ~5 seconds of a typical shale experiment.

Other analytic models have also been developed. DeVris and Peck[29] used two infinitely long concentric cylinders with different thermal properties, and a continuous line heat source along the axis of the cylinders in their analytic model. For very large time (i.e. $1 << \frac{D_2 t}{a^2}$, the asymptotic log-linear region of Blackwell's and the continuous line source models) the DeVris-Peck model produced results which are identical to equations (2.8) and (2.11). Indeed Blackwell's analytic models, the DeVris-Peck analytic model, and the continuous line source model all produce identical results for the temperature of the probe at very large times (equations

---

[29] DeVris and Peck, (1958)

(2.8) and (2.11)). It would appear that the temperature of the probe, at very large times, is independant of the design of the probe, and that accurate estimates of the thermal properties of the medium can be based on equations (2.8) and (2.11).

The previous models, however, have not considered the finite length of real probes and the axial heat losses which are associated with them. As axial heat losses become significant at large times during an experiment, equations (2.8) and (2.11) no longer hold and, therefore, the experiment must be terminated.

Many analytical models have been used[30,31,32,33] to account for end effects and there have also been physical experiments with probes[34,35,36]. The basic idea is to reduce the end effects to the point where they are experimentally undetectable at the center of the length of the probe, for a time interval that is sufficient for conducting the experiment. This will allow equations (2.8) and

---

[30]Blackwell, (1954)

[31]Blackwell, (1953)

[32]Blackwell, (1956)

[33]Jaeger, (1955)

[34]Jaeger, (1959)

[35]Batty, O'Callaghan, and Probert, (1984)

[36]Wechsler, (1966)

(2.11) to be valid at the center of the probe while the end effects are negligible.

One of the most elaborate analytic models was developed by Blackwell[37]. His model accounts for axial heat flow in the probe and sample, whereas other models have ignored the axial heat flow in the probe. Blackwell placed an infinitely long cylinder of radius a, thermal conductivity K_1, and thermal diffusivity D_1 in an infinite medium with thermal properties K_2 and D_2, and allowed only a finite length of the infinite cylinder, between +L and -L, to be heated. For this model Blackwell derived the following result, which is valid for very large times only (i.e. $1 \ll \frac{D_2 t}{a^2}$, where the temperature of the probe rises linearly with ln(t) in previous models) on the surface, r=a, and at the center of the infinitely long cylinder, z=0:

$$\left.\frac{\partial T}{\partial(\ln t)}\right|_{\substack{r=a \\ z=0}} = \frac{q}{4\pi K_2} R \qquad (2.13)$$

$$\left(\text{valid for } 1 \ll \frac{D_2 t}{a^2}\right)$$

where R = a factor causing the temperature at the center of the length of the probe to deviate from the ideal solution due to

---

[37] Blackwell, (1956)

axial losses, the presence of the probe, contact resistance, and other factors. Notice that for R=1, which is the desired result, equation (2.13) produces a result which is similar to equations (2.8) and (2.11) as expected. R is a function of the length to diameter ratio of the probe and the ratio of the thermal conductivities and heat capacities of the probe and external medium. By manipulating these parameters the ideal result of R=1 can be approached.

Blackwell showed that

$$\Delta R = 1-R = -\frac{1}{\pi}\left(-\frac{\lambda^2}{4X}\right)\left[\frac{2\sqrt{X}}{\lambda} + \frac{2(\epsilon-\eta)}{8X^{3/2}}\left(\ln(4X) - \gamma + \frac{2K_2}{aH}\right)\right] \quad (2.14)$$

where $X = \frac{D_2 t}{a^2}$ as previously defined - see equation (2.9)

$\lambda = \frac{L}{a}$ the ratio of length to diameter of the probe

$\epsilon = \frac{K_1}{K_2}$ the ratio of the thermal conductivities of probe and infinite medium

$\eta = \frac{\rho_1 c_1}{\rho_2 c_2}$ the ratio of the heat capacities of the probe and sample

$$\upsilon = \begin{cases} \frac{2d}{a}\left(1 - \frac{d}{2a}\right) \approx \frac{2d}{a} & \text{for hollow probes} \\ 1 & \text{for needle probes} \end{cases}$$

d = thickness of probe wall (m)

Using equation (2.14) one can estimate the deviation in the actual temperature of the probe from the ideal solution of equations (2.8) and (2.11).

Finally, the effect of the heat front reaching the outer surface of the finite sample must be considered. When the heat front reaches the outer surface of the sample, equations (2.8) and (2.11) are no longer valid and the experiment must be stopped. Hence, the objective is to keep the heat front from reaching the outer dimensions of the sample for a sufficient time period, for equations (2.8) and (2.11) to be used to determine the thermal properties of the sample. In general, this is accomplished by increasing the size of the sample. There are many possible criteria available to predict when the heat front reaches the outer surface of the sample.

From Carslaw and Jaeger[38] the temperature distribution due to an instantaneous point source of heat, E joules, released at a position r_1 in an infinite medium is

$$T(r,t) = \frac{E}{8\rho c(\pi Dt)^{3/2}} \exp\left[-\frac{|r-r_1|^2}{4Dt}\right] \qquad (2.15)$$

where $T(r,t)$ = temperature ($^{\circ}C$) at time t(s) and position r(m) in the infinite medium

E = the heat (J) released at time t=0 and position r_1(m)

D = the thermal diffusivity of the infinite medium (m^2/s)

ρc = the volumetric heat capacity of the infinite medium $\left[\frac{J}{m^3 {}^{\circ}C}\right]$

At a fixed time, t, the radial temperature distribution is as depicted in Figure 2.2, and at a fixed radius, r, the temperature response is as depicted by Figure 2.3.

[38] Carslaw and Jaeger, pp256-257, (1956)

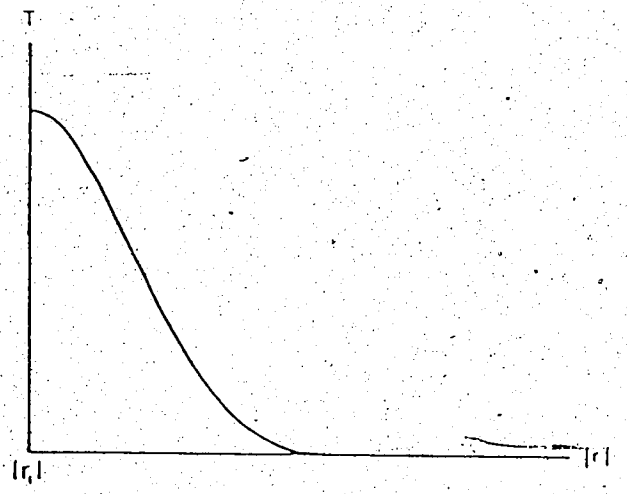

Figure 2.2 : Temperature Response of an Instantaneous Point Source of Heat Energy

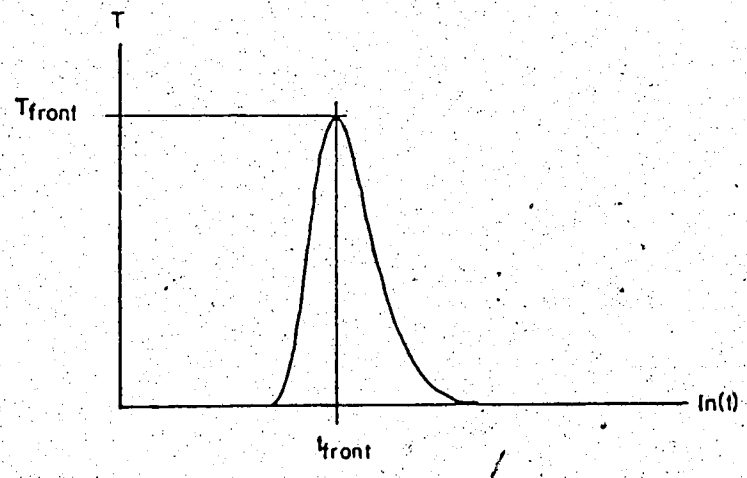

Figure 2.3 : Heat Front from an Instantaneous Point Source of Heat Energy

$$\text{where } t_{front} = \frac{|r-r_1|^2}{6D} \qquad (2.16)$$

$$\text{and } T_{front} = \frac{\bar{E}}{8\rho c|r-r_1|^3}\left(\frac{6}{\pi}\right)^{3/2}\exp\left(-\frac{3}{2}\right) \qquad (2.17)$$

If one defines the heat front from the instantaneous point source as T_{front} (see Figure 2.3), then using equation (2.16) one knows when the heat front reaches any position r in the infinite medium. To estimate when the heat front reaches the surface of the sample one could find the shortest distance, Δmin, between the probe and the outer surface of the finite sample. Then equation (2.16) may be used as follows to estimate when the heat front reaches the outer surface of the sample.

$$t_{front} = \frac{(\Delta min)^2}{6D} \qquad (2.18)$$

where Δmin = minimum distance (m) between probe and outer surface of the finite sample

D = diffusivity of the sample (m^2/s)

A modification to this result is to consider an instantaneous line source instead of an instantaneous point source. If this is done

equation (2.18) becomes

$$t_{front} = \frac{(\Delta min)^2}{4D} \qquad (2.19)$$

A further modification to this method is to replace the instantaneous line source by an instantaneous cylindrical surface source of radius a. Equation (2.19) then becomes[39]

$$0 = -I_0\left(\frac{ra}{2Dt_{front}}\right) + \frac{(r^2+a^2)}{4Dt_{front}} I_0\left(\frac{ra}{2Dt_{front}}\right) - \frac{ra}{2Dt_{front}} I_1\left(\frac{ra}{2Dt_{front}}\right) \qquad (2.20)$$

where $I_0()$ and $I_1()$ are the modified Bessel functions of zero and first order

a = radius of cylindrical surface (m)

More complicated modifications may be developed, but solving for t_{front} becomes very difficult.

Vos[40] used the following criterion to estimate when the heat front reached the outer dimensions of a finite sample

---

[39] Carslaw and Jaeger, pp259, (1956)

[40] Vos, (1955)

$$t_{front} = 0.6 \frac{(\Delta min)^2}{4D} \qquad (2.21)$$

which is similar to equations (2.18) and (2.19).

DeVris and Peck[41] estimated when the heat losses from the surface of the sample become significant and used the following result

$$\exp\left[- \frac{b^2}{4Dt_{max}} \right] = 0.02 \qquad (2.22)$$

where t_{max} = the maximum time (s) during an experiment before heat losses from the surface of the sample become significant

b = radius of sample (m)

Using a numerical simulation program in the Section *3.1 MEGAERA Testing of the Transient Heat Probe Method*, all the criteria presented here (equations (2.12), (2.14), and (2.18) to (2.22)) were tested to determine which criteria are most reliable.

---

[41] DeVris and Peck, (1958)

2.1.3 Summary of Transient Heat Probe Method

To summarize how the previous results can be used to determine the thermal properties of a sample, a transient heat probe and sample (see Figure 2.1) are considered, which satisfy the conditions given by equations (2.12), (2.14), and (2.18) to (2.22). The conditions given by equations (2.12), (2.14), and (2.18) to (2.22) are very conservative in some cases and, therefore, not all of the conditions given by these equations may be met by a given heat probe - see *3.1 MEGAERA Testing of the Transient Heat Probe Method*. Moreover, the ultimate test of a given heat probe is to test the accuracy of the probe using a sample with known thermal properties. With the probe inserted in a hole in the sample, as shown in Figure 2.1, the probe is turned on at time t=0 by supplying a constant input power per unit length, q(W/m), to the probe. The temperature of the probe is recorded as a function of time as shown in Figure 2.4. Using equation (2.8) or (2.11) one can determine the thermal conductivity of the sample from the slope of the log-linear region, $t = t_{min}$ to t_{max}, in Figure 2.4.

$$K = \frac{q}{4\pi\Delta T} \ln\left(\frac{t_2}{t_1}\right) \qquad (2.23)$$

where ΔT = the change in temperature ($^{\circ}C$) of the probe between times t_1(s) and t_2(s) (see Figure 2.4).

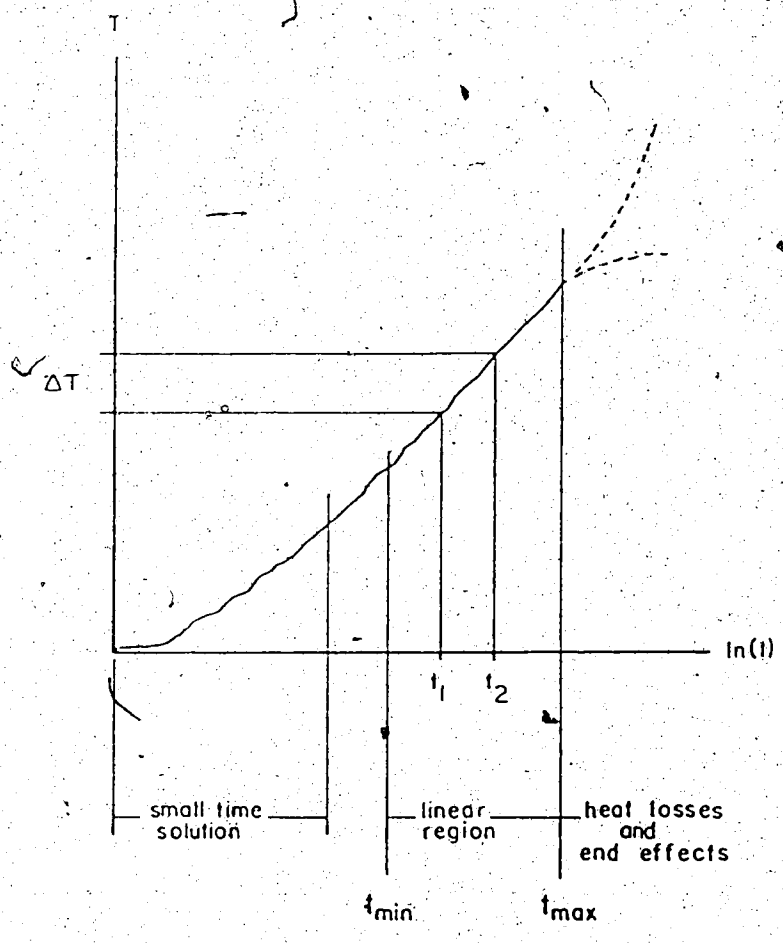

Figure 2.4 : Temperature Response of the Transient Heat Probe

If conditions in the actual experiments satisfy Blackwell's analytic model for equation (2.9), equations (2.8), (2.9) and/or (2.11) may be used to determine the diffusivity of the sample. Since Blackwell's analytic model assumes the radial thermal conductivity of the probe is infinite, actual probes must have a very high thermal conductivity radially. This condition is usually satisfied by using a metal tube for the wall of the probe, as shown in Figure 2.1. To use equations (2.8) or (2.9), the thermal conductance at the boundary between the probe and sample must also

be very large or infinite. In some cases, such as liquid or certain 100% saturated samples, the thermal conductance may be assumed to be infinite. For other cases, the thermal conductance must be known and equation (2.9) (or a truncated version of it) must be used to determine the diffusivity of the sample. Since the thermal conductance between the probe and sample varies from experiment to experiment, the thermal conductance can only be estimated. In addition, to use equation (2.9) the effective heat capacity of the probe is required. The probe, however, is a composite device and, therefore, determining the effective heat capacity of the probe is not easy.

Since the conditions presented above can not generally be met, equations (2.8), (2.9), and (2.11) usually can not be used to determine the diffusivity of the sample. Only the thermal conductivity of the sample can be determined from the slope of the log-linear region of the temperature response curve for the probe.

2.2 Transient Heat Capacity Method

The transient heat capacity method used in this research is similar to the transient method presented in *2.0 Theory and Literature Review* (refer to equation (2.4)). Some of the attractive features of this transient heat capacity method are its simplicity and very rapid determination of the heat capacity of samples (from ~10 to 100 seconds for typical shale experiments). Furthermore, when correctly designed, energy losses from the apparatus can be neglected. The following sections will give a physical and

mathematical description of the transient heat capacity method.

2.2.1 Physical Description of the Transient Heat Capacity Method

A homogeneous cylindrical sample is uniformly heated by passing an electrical current through the sample as shown in Figure 2.5.

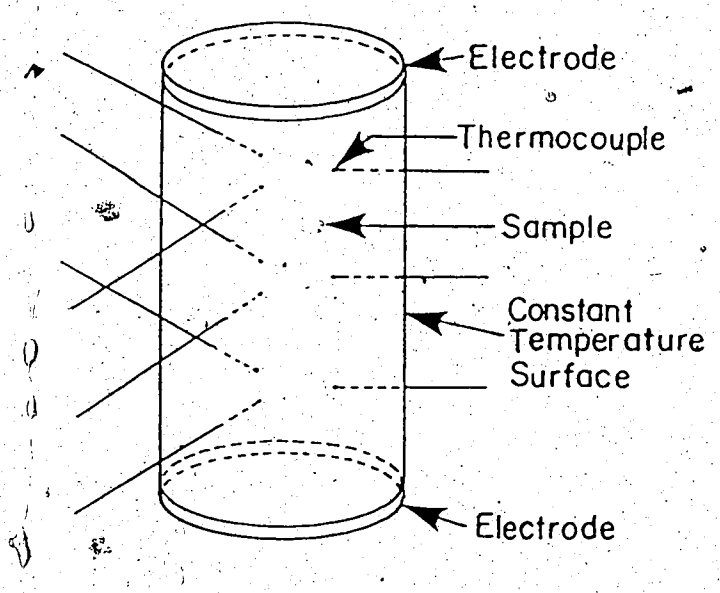

Figure 2.5 Simplified Diagram of Transient Heat Capacity Method

From the electrical energy supplied to the sample and the temperature rise measured by several thermocouples located inside the sample, the volumetric heat capacity, ρc, of the sample can be found.

$$\rho c = \frac{\Delta E}{\Delta T_{ave}} \qquad (2.24)$$

where ΔE = the electrical energy supplied per unit volume (J/m^3)

ΔT_{ave} = the average change in the temperature($^{\circ}C$) of the thermocouples

ρc = volumetric heat capacity of the sample $\left[\frac{J}{m^3 {}^{\circ}C} \right]$

When electrical energy is first supplied to the sample, the temperature rise of the sample is initially uniform. As time passes, heat losses from the surface of the sample cause non-uniformities in the temperature distribution of the sample. This is similar to the end effects in the transient heat probe method, which occur because of axial heat loss from a finitely long heat probe. If the sample is large enough and the thermocouples are positioned well within the sample, the heat losses from the sample will not be experimentally noticeable at the thermocouple locations, for a time interval which is sufficient for equation (2.24) to be used to determine ρc. Ideally, the temperature at the center of the sample should be used in equation (2.24); however, in actual experiments the sample may be non-homogeneous and, therefore, it is unwise to rely on only one thermocouple measurement. Since this method assumes the sample is homogeneous, the effects of a non-homogeneous sample and a temperature dependent electrical conductivity have to be considered. This will be done in *4.3 Testing of the Transient Heat Capacity Apparatus and Method.*

2.2.2 Mathematical Description of Transient Heat Capacity Method

Using the integral transform method described by Özisik[42], the author derived an analytic solution (see Appendix F) to a problem with greater heat losses than in actual experiments. Consider the following problem.

At time t=0, a constant heating rate $Q(W/m^3)$ is produced inside a finite cylindrical sample of radius b(m), length ℓ(m), thermal conductivity $K\left[\frac{W}{m\,^{\circ}C}\right]$, heat capacity $\rho c\left[\frac{J}{m^3\,^{\circ}C}\right]$, and diffusivity $D(m^2/s)$. Initially, the sample is at $0^{\circ}C$ and all surfaces of the sample are held at $0^{\circ}C$ (see Figure 2.6); however, any reference temperature could be used by simply added a constant to equation (2.25) which is presented below. By imposing a constant temperature boundary condition on all surfaces of the sample, heat losses from the sample in this analytic model are greater than in actual experiments. In actual experiments the sample is held in a sample holder and this sample holder acts as a partial insulator. For this analytic problem the sample has the temperature distribution given by equation (2.25).

---

[42] Özisik, pp522-593, (1980)

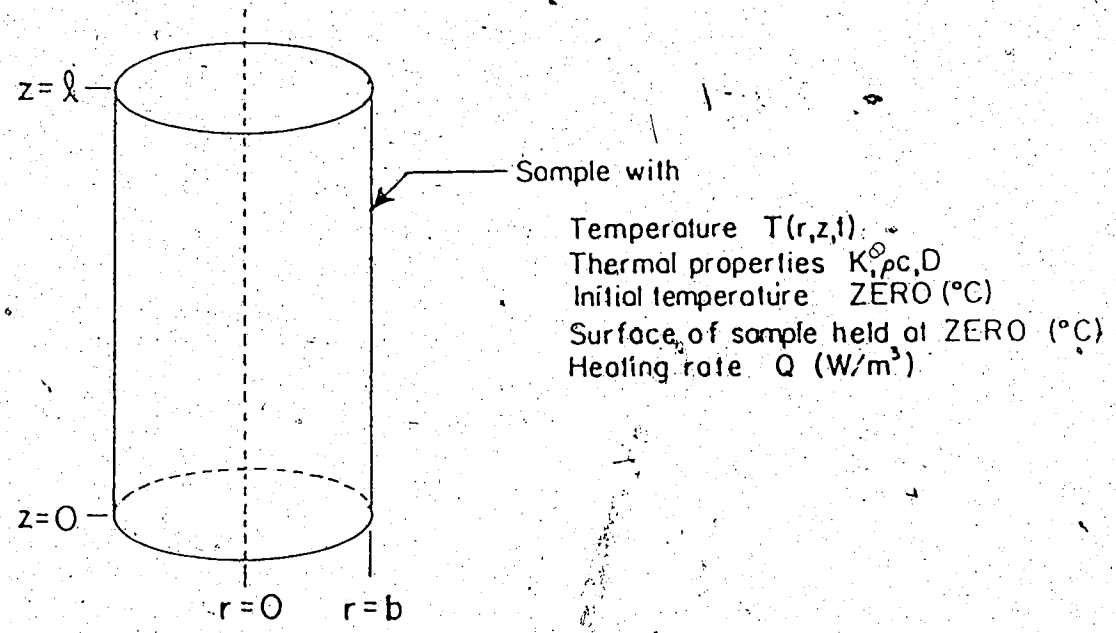

Figure2.6 : Analytic Model for Transient Heat Capacity Method

$$T(r,z,t) = \sum_{\substack{m=1 \\ (m\ odd)}}^{\infty} \sum_{n=1}^{\infty} \frac{8}{\ell b J_1(\beta_n b)} \exp(-D(\lambda_m^2 + \beta_n^2)t)$$

$$* \frac{Q}{K\lambda_m \beta_n} \sin(\lambda_m z) J_0(\beta_n r)$$

$$* \left[\frac{\exp(D(\lambda_m^2 + \beta_n^2)t) - 1}{\lambda_m^2 + \beta_n^2} \right] \quad (2.25)$$

where $T(r,z,t)$ = temperature (^{o}C) inside sample at r(m) and z(m) and time t(s)

$\lambda_m = \frac{m\pi}{\ell}$ are the z eigenvalues

β_n = are the roots of $J_0(\beta_n b)=0$ and are the r eigenvalues

b = radius of sample (m)

ℓ = length of sample (m)

$\dot{D}$ = thermal diffusivity of sample (m^2/s)

K = thermal conductivity of sample $\left[\frac{W}{m\,^{o}C}\right]$

Q = heating rate in sample (W/m^3)

The typical shape of $T(r,z,t)$ as a function of time at any position r,z inside the sample is as follows.

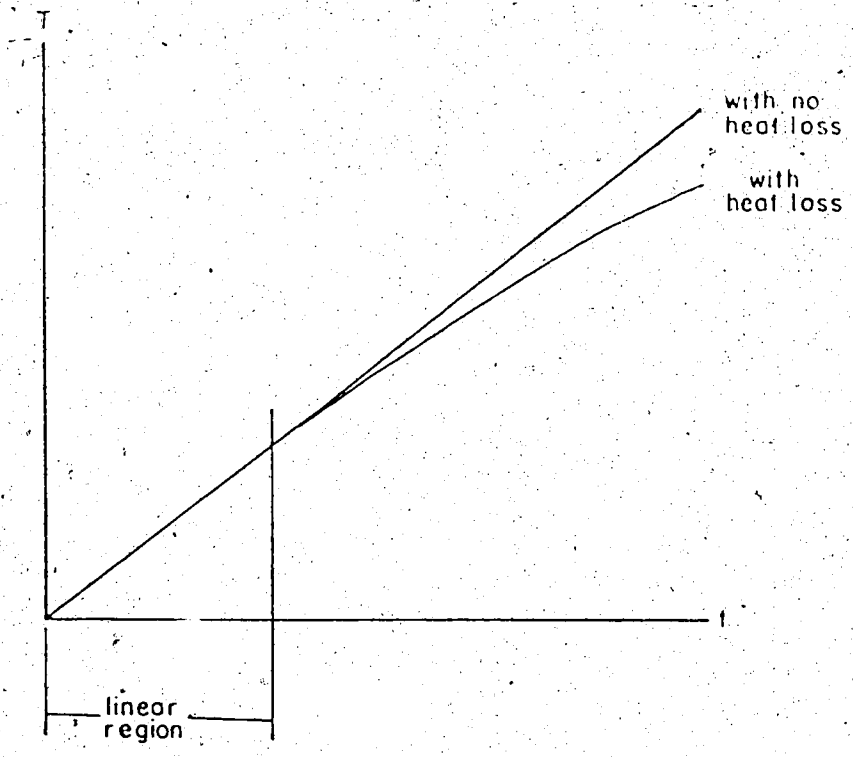

Figure 2.7 : Typical Response of Thermocouples in Analytic Model Used for Transient Heat Capacity Method

In the linear region of Figure (2.7), equation (2.24) is valid and can be used to calcalute the volumetric heat capacity, ρc, of the sample. To estimate when the heat losses become significant at the thermocouple locations one can use the instantaneous point source method as described in *2.1.2 Mathematical Description of the Transient Heat Probe Method*, equation (2.18),

$$t_{front} = \frac{(\Delta min)^2}{6D} \qquad (2.26)$$

where Δmin = the shortest distance from the thermocouple location to the outer surface of the cylinder (m)

D = diffusivity of the sample (m^2/s)

In actual experiments an additional problem arises. The thermocouples used to measure the temperature rise of the sample have noise and a lag in their response. As a result, during actual experiments, one requires a temperature change in the sample, which is large enough to make the noise and lag in the thermocouples' responses negligible. By way of illustration, consider a typical experimental run. If one uses data obtained from actual experiments and proceeds to calculate the volumetric heat capacity of the sample, ρc, using equation (2.24), one obtains the result depicted in Figure 2.8.

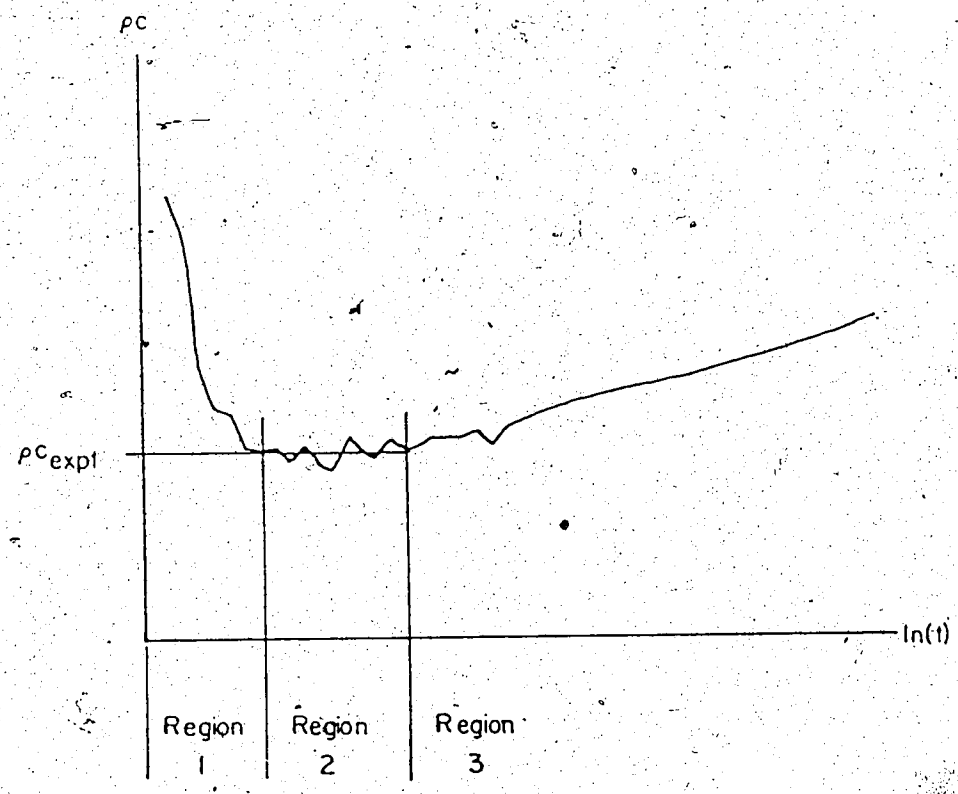

Figure 2.8 : Typical Heat Capacity Results from an Actual Transient Heat Capacity Experiment

In Region 1 of Figure 2.8 noise and a lag in the response of the thermocouples causes the apparent heat capacity of the sample to fluctuate greatly. In Region 2 the lag in the response of the thermocouples is negligible in comparison to ΔT_{ave} - the average change in the temperature response of the thermocouples. Hence in this region, the volumetric heat capacity of the sample, ρc_{expt}, can be determined using equation (2.24). The ripple on the curve in Region 2 is due to noise in the thermocouple readings. Finally in Region 3, heat losses from the sample are now significant and the experiment must be terminated.

To ensure that Regions 1 and 3 do not overlap, one has to

experimentally determine the noise, ΔT_{error}, and lag, t_{lag}, in the response of the thermocouples. Once this determination has been made, one can then estimate the end of Region 1, t_1, as

$$t_1 = \frac{\rho c(\Delta T_{error})}{Q} \quad \text{or} \quad t_1 = t_{lag} \qquad (2.27)$$

(whichever is larger)

where ρc = the volumetric heat capacity of the sample $\left[\frac{J}{m^3 {}^\circ C}\right]$

Q = the volumetric heating rate in the sample (W/m^3)

The end of Region 2 can be estimated using equation (2.26). As long as the end of Region 1 is less than the end of Region 2, Region 2 should exist.

2.2.3 Summary of the Transient Heat Capacity Method

This method for determining the heat capacity of a sample is a very reliable, fast, and simple method. A cylindrical sample is electrically heated by passing a current through the sample. The average temperature rise of the sample, due to the electrical energy, is recorded by several thermocouples inside the sample. From the average temperature rise of the sample, the heat capacity of the sample can be determined using equation (2.24). The greatest advantage of this method, over other methods for determining heat

capacity, is that energy losses from the sample can be neglected because the outer layers of the sample effectively *insulate* the middle of the sample from energy losses during the experiment.

3.0 Design and Testing of the Transient Heat Probe Apparatus and Method

The objective of this research was to determine the thermal properties of 100% water saturated Clearwater shale samples. When measuring the thermal properties of materials which contain moisture, one has to be concerned with sample changes during the course of experiments. Moisture at the surface of a typical Clearwater shale sample begins to evaporate immediately when the sample is exposed to the atmosphere at room temperature. Within a few minutes the surface of the sample is completely dry. Consequently, one avoids exposing unprotected Clearwater shale to the atmosphere whenever possible, and transient measurement techniques are preferable to long term steady state techniques.

For the transient heat probe method to work as described in *2.1 Transient Heat Probe Method*, many conditions have to be satisfied. In order to verify that the transient heat probe satisfies these conditions and produces acceptable results, a simulation program, MEGAERA, was utilized and many probes were built. The simulation program MEGAERA was written by A. Hiebert[43,44], and simulates the electrical heating, by electrical conduction

---

[43]Hiebert, (1983)

[44]Hiebert, (1981)

currents, of composite materials with temperature dependent electrical conductivities. The actual probes which were built, were tested on materials with previously published thermal properties and used in numerous preliminary experiments on Clearwater shale samples until satisfactory results were obtained.

The presentation of the design and testing of the transient heat probe apparatus and method is in four parts. First, the results of MEGAERA simulations of the transient heat probe method are given in Section 3.1. Following this, a description of the actual probe and method used in experiments are presented in Sections 3.2 and 3.3. Fourth, experimental results on oilsand and dry sand samples are presented in Section 3.4 and compared with previously published results for these types of material. After it has been demonstrated that the transient heat probe method produced satisfactory results in these preliminary tests, the results from Clearwater shale experiments are presented in Section 3.5.

3.1 MEGAERA Testing of the Transient Heat Probe Method

Initially it was desired to use MEGAERA to establish new empirical design criteria for the transient heat probe method. However, the large ratio of the various dimensions of the probe and sample (from tenths of a millimeter for the probe diameter, to several centimeters for the probe and sample lengths) made it difficult to use MEGAERA to simulate actual transient heat probe problems in enough detail for empirical design criteria to be found. If empirical design criteria are to be found, it is believed

that a new numerical simulation program, which is dedicated to the transient heat probe method and capable of accounting for the detailed structure of the probe, including the large length to diameter ratio, would have to be developed.

Fortunately, by using MEGAERA to simulate a simplified transient heat probe problem which is described below, the criteria presented in *2.1.2 Mathematical Description of Transient Heat Probe* (equations (2.12), (2.14), and (2.18) to (2.22)) were tested and the most reliable criteria determined. In addition, by simulating an appropriate problem, the end effects of the simulated probe can be made more severe than the end effects of actual probes. Hence, if it can be shown that the transient heat probe method can provide reliable results for such a simulation problem, one can expect actual probes to provide reliable results also. Consider the following problem, used to evaluate the criteria of Section 2.1.2.

The transient heat probe was simulated by a solid cylinder of radius a(m), length $2\ell_1$(m), thermal conductivity $K_1\left(\frac{W}{m^{\circ}C}\right)$, volumetric heat capacity $\rho_1 c_1\left(\frac{J}{m^3{}^{\circ}C}\right)$, and was heated at a constant uniform rate $Q(W/m^3)$. This solid cylinder was then surrounded by a cylindrical sample with radius b(m), length $2\ell_2$(m), thermal conductivity $K_2\left(\frac{W}{m^{\circ}C}\right)$, volumetric heat capacity $\rho_2 c_2\left(\frac{J}{m^3{}^{\circ}C}\right)$, and the outer surface of the sample held at $20^{\circ}C$. From symmetry, axial heat flow across the middle of the simulated probe and sample would be zero and, therefore, only half of the problem needed to be simulated, as shown in Figure 3.1. This allowed the limited memory

resources of MEGAERA to be used more effectively in these simulations. Furthermore, the performance of real probes should be better than predicted by these simulations, because the real probes were made from hollow brass tubes which were filled with a low thermal conductivity adhesive - Aremco high temperature ceramic adhesive, Ceramabond 552 - , while the simulated probe was a solid cylinder. As a result, axial heat losses from real probes should be less than those of the simulation.

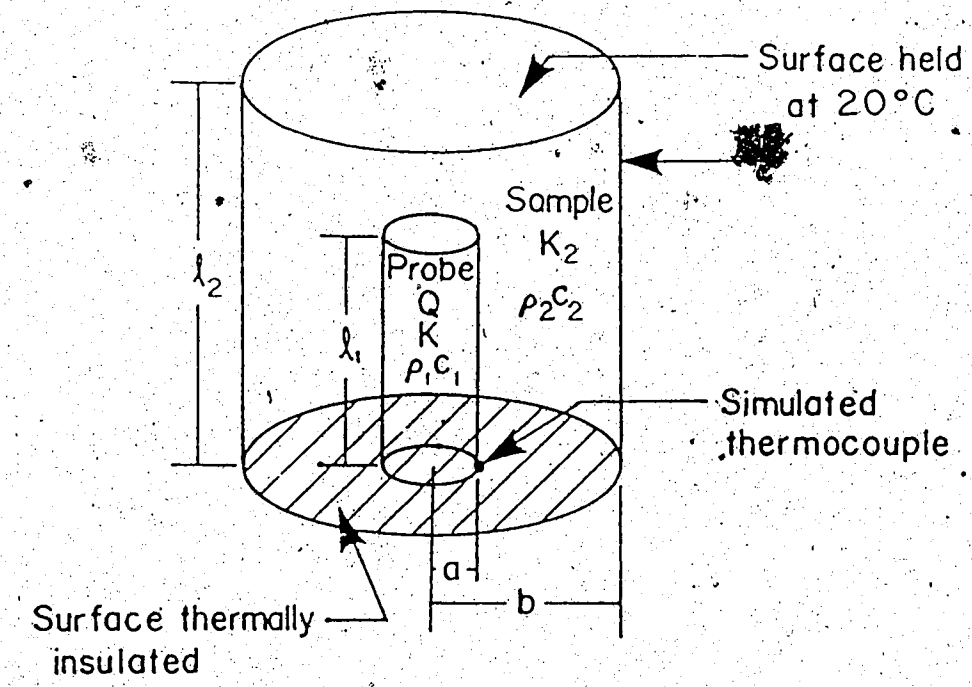

Figure 3.1 : Transient Heat Probe Problem Simulated by MEGAERA

In the evaluation of the criteria (equations (2.12), (2.14), and (2.18) to (2.22)), the objective was to determine the valid log-linear region, $t = t_{min}$ to t_{max} as shown in Figure 2.4 (where equation (2.23) is valid), of each simulation and examine the

effects of varying the parameters K_1, ρc_1, K_2, ρc_2, ℓ_1, ℓ_2, a and b, which were input into the CAERA simulations. The log-linear region of each simulation was found using a least square curve fitting routine (see Appendix A) to fit equation (3.1a), shown below, to various parts of the temperature versus ln(time) curve of the simulated probe.

$$\text{Temperature(time)} = A \ln(\text{time}) + B \qquad (3.1a)$$

where A and B are constants found by the curve fitting routine.

The part of the temperature versus ln(time) curve which best fitted equation (3.1a) was chosen as the log-linear region. Since there was round-off or quantization error in the simulated temperature response of the probe, a range of thermal conductivities was estimated in this log-linear region by fitting equation (3.1a) to various parts of this log-linear region. From the slope, A, of equation (3.1a) the thermal conductivity of the simulated sample could be estimated using

$$K_{est} = \frac{q}{4\pi A} \qquad (3.1b)$$

where K_{est} = estimated thermal conductivity of the sample $\left[\frac{W}{m\,^{\circ}C}\right]$

q = the heating rate of the probe $(\widehat{W/m})$

A = the slope of equation (3.1a) $(^{\circ}C)$

Ideally, K_{est} should be equal to K_2; however, numerical round-off error in the output from MEGAERA simulation program cause K_{est} and K_2 to differ. Once the log-linear region t_{min} to t_{max} was found, the criteria given by equations (2.12), (2.14), and (2.18) to (2.22) were then calculated and the results compared with either t_{min} or t_{max}.

Before proceeding to present the simulation results, it may be useful to recall the factors which effect the log-linear region, t_{min} to t_{max}, of Figure 2.4. Ideally one would like to use a continuous line source as a transient heat probe in an infinite sample medium. For this case t_{min} would occur when $\left|\frac{r^2}{4Dt}\right| \ll \left|\ln\left(\frac{4Dt}{r^2}\right)\right|$ as indicated by equations (2.6), (2.7), and (2.8), while t_{max} would be infinite. However, this ideal case can only be approximated by a finite probe and sample in actual experiments.

Using a finite probe and sample, the beginning of the log-linear region, t_{min}, is effected mainly by the design of the probe. For instance, a large diameter probe with a large thermal mass will take a longer time to heat up and respond appropriately to the thermal properties of the sample than will a smaller diameter probe

with a smaller thermal mass. The end of the log-linear region, t_{max}, occurs because the heat front from the probe reaches the outer dimensions of the sample. This event, in turn, is noticed at the thermocouple location on the probe.

Heat flow in the transient heat probe method can be divided into two components, which are radial and axial heat flow.

For radial heat flow, in an infinite sample medium there is no outer radius of the sample for the heat front from the probe to reach, and therefore, t_{max} is infinite. In actual experiments, however, the radial heat front will eventually reach the outer radius of the sample and the effects of this occuring will be noticeable at the thermocouple located on the probe. When this happens, the end of the log-linear region, t_{max}, is reached and the experiment terminated. Depending on the boundary condition at the radial surface of the sample, the slope of the temperature response curve for the probe may increase rapidly or decrease to zero. If the boundary condition is an insulating material, the slope of the temperature response curve will increase because heat energy will accumulate in the sample. For a constant temperature or convective boundary condition, the sample will approach some steady state temperature distribution and hence, the slope of the temperature respone curve will be zero. The speed or diffusion rate of the heat front is dependent on the thermal properties of the sample.

Recall that the analytic models developed for the transient heat probe method are infinite axially and therefore, there is no axial heat flow. In actual experiments, axial heat flow is initially

negligible and equation (2.23) can be used to estimate the thermal conductivity of the sample. As time passes, axial heat flow becomes significant and the end of log-linear region, t_{max}, is reached, ending the experiment. Again, depending on the boundary condition at the surface of the sample, the temperature response curve for the probe may increase or decrease in slope, as previously discussed.

Twenty-four of the simulations conducted are summarized in Tables 3.1a), b), c), and d). The first four runs shown in Tables 3.1 were used to verify that the problem simulated by MEGAERA was an acceptable representation of the transient heat probe method. Surprisingly, the 1st run in which $\ell_1 = \ell_2$ and hence axial heat losses from the probe were maximized, was capable of producing a satisfactory estimate for the thermal conductivity of the sample, which was only 8.3% in error. The 2nd run was another extreme case in which ℓ_1 and ℓ_2 were both infinite and consequently no axial heat flow or losses were present. An error of only -0.6% in the estimate of the thermal conductivity was found for this simulation. For the 3rd run a very thin layer of sample covers the ends of the probe. By adding this thin layer of sample to the ends of the probe, the error in the thermal conductivity estimated by the transient heat probe method decreased from 8.3% in the 1st run to 3.6% for the 3rd run. Not surprisingly, by increasing the sample material covering the end of the probe to 0.5 cm in the 4th run, the error in the estimated thermal conductivity decreases further to below 2.0%.

RUN	Thermal Properties of Probe			Thermal Properties of Sample			Dimensions of the Probe and Sample				Probe Heating Rate
	K_1 $\left(\frac{W}{m\,^\circ C}\right)$	$\rho_1 c_1$ $\left(\frac{J}{cm^3\,^\circ C}\right)$	D_1 (m^2/s)	K_2 $\left(\frac{W}{m\,^\circ C}\right)$	$\rho_2 c_2$ $\left(\frac{J}{cm^3\,^\circ C}\right)$	D_2 (m^2/s)	ℓ_1 (cm)	ℓ_2 (cm)	a (cm)	b (cm)	q - (W/cm)
1	110	3.311	3.3223E-5	1.69	2.15	7.8605E-7	5.0	5.0	0.16	2.5	281.4867
2	110	3.311	3.3223E-5	1.69	2.15	7.8605E-7	"	"	0.16	2.5	281.4867
3	110	3.311	3.3223E-5	1.69	2.15	7.8605E-7	5.0	5.0625	0.16	2.5	281.4867
4	110	3.311	3.3223E-5	1.69	2.15	7.8605E-7	5.0	6.0	0.16	2.5	281.4867
5	110	3.311	3.3223E-5	10.0	2.15	4.6512E-6	"	"	0.16	2.5	281.4867
6	110	3.311	3.3223E-5	10.0	2.15	4.6512E-6	5.0	6.0	0.16	2.5	281.4867
7	110	3.311	3.3223E-5	15.0	2.15	6.9767E-6	5.0	6.0	0.16	2.5	281.4867
8	110	3.311	3.3223E-5	20.0	2.15	9.3023E-6	"	"	0.16	2.5	281.4867
9	110	3.311	3.3223E-5	100.0	2.15	4.6512E-5	5.0	6.0	0.16	2.5	4423.3625
10	110	3.311	3.3223E-5	10.0	5.00	2.0000E-6	"	"	0.16	2.5	281.4867
11	110	3.311	3.3223E-5	10.0	1.75	5.7143E-6	"	"	0.16	2.5	281.4867
12	500	3.311	1.5101E-4	10.0	2.15	4.6512E-6	5.0	6.0	0.16	2.5	281.4867
13	50	3.311	1.5101E-5	10.0	2.15	4.6512E-6	5.0	6.0	0.16	2.5	281.4867
14	110	2.000	5.5000E-5	10.0	2.15	4.6512E-6	"	"	0.16	2.5	281.4867
15	110	5.000	2.2000E-5	10.0	2.15	4.6512E-6	5.0	6.0	0.16	2.5	281.4867
16	110	3.311	3.3223E-5	10.0	2.15	4.6512E-6	5.0	6.0	0.09	2.5	89.0642
17	110	3.311	3.3223E-5	10.0	2.15	4.6512E-6	5.0	6.0	0.13	2.4526	292.0110
18	110	3.311	3.3323E-5	10.0	5.00	2.0000E-6	"	"	0.32	2.5	1125.9468
19	110	3.311	3.3223E-5	10.0	2.15	4.6512E-6	5.0	6.0	0.16	2.0	281.4867
20	110	3.311	3.3223E-5	10.0	2.15	4.6512E-6	5.0	6.0	0.16	3.0	281.4867
21	110	3.311	3.3323E-5	20.0	2.15	9.3023E-6	"	"	0.16	3.5	281.4867
22	110	3.311	3.3223E-5	10.0	2.15	4.6512E-6	5.0	5.4375	0.16	2.5	281.4867
23	110	3.311	3.3223E-5	10.0	2.15	4.6512E-6	5.0	6.5	0.16	2.5	281.4867
24	110	3.311	3.3223E-5	10.0	2.15	4.6512E-6	2.5	3.5	0.16	2.5	281.4867

Table 3.1a) : Input Parameters to MEGAFRA Simulation Problem

RUN	Log-Linear Region				
	t_{min} (s)	t_{max} (s)	Estimated Thermal Conductivity $\left(\frac{W}{m\,^{\circ}C}\right)$	$K_2\left(\frac{W}{m\,^{\circ}C}\right)$	error(%)
1	7-8	80-90	1.83	1.69	8.3
2	9-10	170+	1.68 to 1.69	1.69	-0.6 to 0.0
3	9-10	110-120	1.74 to 1.75	1.69	3.0 to 3.6
4	9-10	170+	1.71 to 1.72	1.69	1.2 to 1.8
5	1.5	30	10.11 to 10.18	10.0	1.1 to 1.8
6	1.5-2	20-30	10.04 to 10.07	10.0	0.4 to 0.7
7	1-1.5	17-20	14.98 to 15.04	15.0	-0.1 to 0.3
8	0.6-0.7	17-20	20.13 to 20.17	20.0	-0.7 to 0.9
9	0.2-0.3	3.5-4	98.6 to 99.4	100.0	-1.4 to -0.6
10	8-10	60-70	10.60 to 10.70	10.0	6.0 to 7.0
11	1.0-1.5	17-20	9.58 to 9.73	10.0	-4.2 to -2.7
12	2	20-30	10.08 to 10.09	10.0	0.8 to 0.9
13	1.5-2	30	9.89 to 9.96	10.0	-1.1 to -0.4
14	1.5-2	30	10.43 to 10.66	10.0	4.3 to 6.6
15	2-2.5	20-30	9.40	10.0	-6.0
16	0.6-0.7	20-30	9.54 to 9.57	10.0	-4.6 to -4.3
17	1.5-2	20-30	9.84 to 9.90	10.0	-1.6 to -1.0
18	No Region		11.56 to 11.67	10.0	15.6 to 16.7
19	1.5-2	17-20	10.03 to 10.07	10.0	0.3 to 0.7
20	1.5-2	40-50	9.91 to 9.98	10.0	-0.9 to -0.2
21	1.5	30	19.63 to 19.82	20.0	-1.9 to -0.9
22	1.5-2	30	10.04	10.0	0.4
23	1.5-2	30	10.04 to 10.07	10.0	0.4 to 0.7
24	1.5	20	10.31 to 10.34	10.0	3.1 to 3.4

Table 3.1b) : Log-Linear Region of the Temperature Response of the Simulated Probe and the Estimated Thermal Conductivity Found Using Equation (3.1b)

RUN	Estimates of Time for Heat Front to Reach r=b (seconds)					Estimates for when Axial Heat Flow Significant (s)		Estimate of t_{max} from Simulation[h] (s)
	Point Source[a]	Line Source[b]	Vos[c]	Wechsler[d]	Instantaneous Cylindrical Surface[e]	Point Source[f]	Blackwell's equation for $\Delta R = 2\%$[g]	
1	116.1	174.2	104.5	50.8	198.0	12.5	146.7	80-90
2	116.1	174.2	104.5	50.8	198.0	....	.....	170+
3	116.1	174.2	104.5	50.8	198.0	12.5	146.7	110-120
4	116.1	174.2	104.5	50.8	198.0	12.5	146.7	170+
5	19.6	29.4	17.6	8.6	33.5	....	.....	30
6	19.6	29.4	17.6	8.6	33.5	12.5	38.4	20-30
7	9.5	19.6	8.5	5.7	22.3	12.5	27.6	17-20
8	9.8	14.7	8.8	4.3	16.7	....	.....	17-20
9	1.9	2.9	1.7	0.9	3.3	12.5	4.8	3.5-4
10	45.6	68.4	41.0	20.0	77.8	....	.....	60-70
11	16.0	24.0	14.4	7.0	27.2	....	.....	17-20
12	19.6	29.4	17.6	8.6	33.5	2.7	26.4	20-30
13	19.6	29.4	17.6	8.6	33.5	27.6	43.7	30
14	19.6	29.4	17.6	8.6	33.5	....	.....	30
15	19.6	29.4	17.6	8.6	33.5	18.9	39.0	20-30
16	20.8	31.2	18.7	8.6	33.6	12.5	43.5	20-30
17	19.3	29.0	17.4	8.3	32.2	12.5	40.5	20-30
18	39.6	59.4	35.6	20.0	76.8	....	.....	.....
19	12.1	18.2	10.9	5.5	21.4	12.5	38.4	17-20
20	28.9	43.4	26.0	12.4	48.2	12.5	38.4	40-50
21	20.0	30.0	18.0	8.4	32.9	....	.....	30
22	19.6	29.4	17.6	8.6	33.5	12.5	38.4	30
23	19.6	29.4	17.6	8.6	33.5	12.5	38.4	30
24	19.6	29.4	17.6	8.6	33.5	3.1	7.6	20

Table 3.1c) : Estimates of t_{max} due to Radial and Axial Heat Flow.

Notes [a]equation (2.18) used: $\text{time} = \frac{(b-a)^2}{6D_2}$

[b]equation (2.19) used: $\text{time} = \frac{(b-a)^2}{4D_2}$

[c]equation (2.21) used: $\text{time} = 0.6\frac{(b-a)^2}{4D_2}$

[d]DeVris-Peck equation (2.22) is solved for time.

[e]equation (2.20) is numerically solved for time, for the various simulations.

[f]equation (2.18) used: $\text{time} = \frac{\ell_1^2}{6D_1}$

[g]Blackwell's equation (2.14) is numerically solved for time with $\Delta R = 0.02$.

[h]Estimates for t_{max} from Table 3.1b)

RUN	Vos's t_{min} Criterion (s)	Table 3.1b) t_{min} (s)
1	40.7	7-8
2	40.7	9-10
3	40.7	9-10
4	40.7	9-10
5	6.9	1.5
6	6.9	1.5-2
7	4.6	1-1.5
8	3.4	0.6-0.7
9	0.7	0.2-0.3
10	16.0	8-10
11	5.6	1.0-1.5
12	6.9	2
13	6.9	1.5-2
14	6.9	1.5-2
15	6.9	2-2.5
16	2.2	0.6-0.7
17	4.5	1.5-2
18	64.0	No Region
19	6.9	1.5-2
20	6.9	1.5-2
21	3.4	1.5
22	6.9	1.5-2
23	6.9	1.5-2
24	6.9	1.5

Table 3.1d) : Vos's criterion for t_{min} (equation (2.12))

Once it was verified that MEGAERA could simulate the transient heat probe method, the effect of varying the input parameters K_1, ρc_1, K_2, ρc_2, ℓ_1, ℓ_2, a, and b on the log-linear region (see Figure 2.4) could be studied and the analytic criteria given by equations (2.12), (2.14), and (2.18) to (2.22) could be tested. In assessing the data presented in Tables 3.1, Runs 5 and 6 generally can be used as base cases for comparison with the other runs in Tables 3.1.

By increasing the thermal conductivity of the sample from 1.69 $\frac{W}{m\,^{o}C}$ in Runs 2 and 4 to 10 $\frac{W}{m\,^{o}C}$, 15 $\frac{W}{m\,^{o}C}$, 20 $\frac{W}{m\,^{o}C}$, and 100 $\frac{W}{m\,^{o}C}$ in Runs 5 and 6, 7, 8, and 9 respectively, the thermal diffusivity of the sample is also increased and, as a result, the temperature distribution of the sample changes more rapidly. This causes t_{min} and t_{max} to decrease as shown in Table 3.1b).

Similarly, by decreasing the heat capacity of the sample from 5 $\frac{J}{cm^{3}\,^{o}C}$ in Run 10 to 2.15 $\frac{J}{cm^{3}\,^{o}C}$ in Runs 5 and 6, and 1.75 $\frac{J}{cm^{3}\,^{o}C}$ in Run 11, the thermal diffusivity of the sample again increases and t_{min} and t_{max} decrease as indicated in Table 3.1b). It should be noted that if the heat capacity of the sample is made much less than that of the probe, the temperature response curve for the probe will initially cross the asymptote to the log-linear region before approaching a log-linear response, as shown in Figure 3.2 and by Vos (1955).

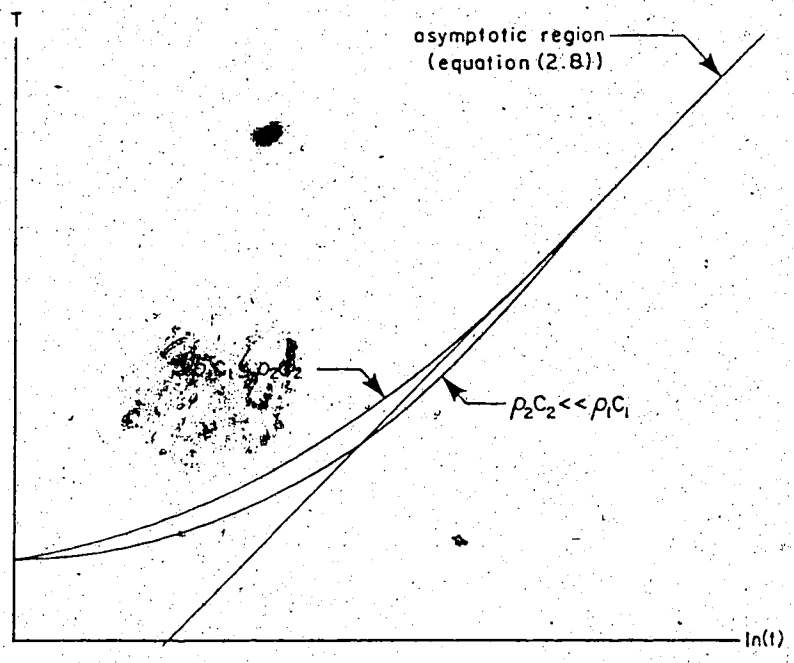

Figure 3.2 : Effect of $\rho_2 c_2 \ll \rho_1 c_1$ on Temperature Response of the Transient Heat Probe

From Runs 12 and 13 it may be seen that changes to the thermal conductivity of the probe had no measurable effect on t_{min}; however, when the temperature versus ln(time) curves of the 12th and 13th runs were directly compared with each other, a slight increase in t_{max} was noticable as the thermal conductivity of the probe decreased. This can be attributed to lower axial heat losses from the probe as its thermal conductivity decreased.

When the heat capacity of the probe is increased, Runs 14 and 15, the thermal mass of the probe also increased. It then follows that the probe should heat-up more slowly and consequently respond more slowly - i.e. t_{min} increases as shown in Table 3.1b).

As the radius of the probe decreases, Runs 16 and 17, the probe

responds faster and, therefore, t_{min} decreases while t_{max} increases. Unfortunately, when the radius of a real probe decreases, the temperature gradient at the wall of the probe increases very rapidly and very large temperature gradients tend to force moisture away from the probe. For the 18th run, the radius of the probe was too large and no log-linear region was found.

By increasing the radius of the sample, Runs 19, 20, and 21, the end of the log-linear region also increases, because the heat front from the probe takes longer to reach the outer surface of the sample.

Similarly, by varying the length of the probe and sample, Runs 1 and 3, and Runs 22, 23, and 24, the end of the log-linear region, t_{max}, again can be varied. For instance, by increasing the length of the sample and probe t_{max} is also increased.

Using the results presented in Tables 3.1 the criteria given by equations (2.12), (2.14), and (2.18) to (2.22) were tested and the reliability of these criteria investigated.

For the runs in Table 3.1, in which ℓ_1 and ℓ_2 were infinite, only radial heat flow was present and hence the radial criteria, equations (2.18) to (2.22) were examined. By comparing the t_{max} results in Table 3.1 with the results from the radial criteria, one finds that the line source criterion, equation (2.19), and the instantaneous cylindrical surface criterion, equation (2.20), were the most reliable. Therefore, the effects of the heat front reaching the radial surface of the sample were best predicted by the line source and instantaneous cylindrical surface criteria,

equations (2.19) and (2.20) respectively, while the other radial criteria were generally far too conservative. In other words, the effective log-linear region extends much further than these criteria would predict.

Vos's criterion, equation (2.12), for the start of the log-linear region, t_{min}, was the only criterion used to estimate t_{min}. When the probe is initially turned on the probe and sample appear to be infinite at the thermocouple location on the probe, until the heat front from the probe reaches the outer dimensions of the sample, and/or axial heat flow becomes significant. As a result, the initial temperature response of the probe is independent of the external dimensions of the probe and sample and, hence, all the MEGAERA simulation runs shown Table 3.1 could be used to evaluate Vos's criterion. When this was done, Vos's criterion for t_{min} was found to be too conservative. The log-linear region extends to significantly shorter times than predicted on the basis of Vos's criterion. However, it should be noted that in actual experiments t_{min} is likely very dependent on the probe design and the contact resistance between the probe and sample. These factors were not taken into account by Vos's criterion or the MEGAERA simulations.

In order to test the axial criteria given by equations (2.14) and (2.18), runs in Tables 3.1 where axial heat losses occur before radial heat losses were utilized. These runs were 1 and 3, where $\ell_1 - \ell_2$ and ℓ_1 and ℓ_2 differ by only 0.0625 cm respectively, and Run 24, in which the probe and sample were only 2.5 cm and 3.5 cm

in length. To test Blackwell's criterion for axial heat losses, given by equation (2.14), a 2% deviation in the temperature of the probe from the ideal solution of equations (2.8) and (2.11) was arbitrarily chosen; however, any small deviation (less than ~10%) should have been sufficient for axial heat losses to be significant. Therefore, equation (2.14) was set equal to 2% (i.e. $\Delta R = 0.02$) and numerically solved for time. The results are listed in Table 3.1c). From the results for Runs 1, 3, and 24, one sees that Blackwell's criterion for axial heat losses was unable to consistently predict when axial heat losses became significant. For Runs 1 and 3, the estimate for when axial losses became significant (t_{max}) was too large, while for Run 24, Blackwell's criterion was too conservative. One possible explanation for this discrepancy is that Blackwell's analytic model for equation (2.14) does not accurately represent a finite length probe. Recall that Blackwell's analytic model used an infinitely long probe which was heated over only a finite portion, as previously described in Section 2.1.2, while the MEGAERA simulation actually modelled a probe of finite length. Similarly, the point source criterion, equation (2.18), was also unable to predict when axial heat losses became significant and was found to be too conservative for Runs 1, 3, and 24.

From these MEGAERA simulation tests of the various design criteria available in the literature, only the radial line source and the instantaneous cylindrical surface criteria, equations (2.19) and (2.20), respectively, were found to be reliable for predicting when radial heat losses were significant. The other

criteria for both radial and axial heat losses were found to be too conservative; however, all the criteria given by equations (2.12), (2.14), and (2.18) to (2.22) can still be used in the design of the transient heat probes, with the understanding that they are very conservative. In addition, these MEGAERA simulations of the transient heat probe method were performed over a wide range of thermal properties and physical dimensions with generally good estimates for the thermal conductivity, K_2, of the simulated sample. For Runs 1, 3, and 24, in which axial heat flow would be in excess of the axial heat flow in actual transient heat probe experiments, MEGAERA demostrated that the transient heat probe method was still capable of producing acceptable estimates for the thermal conductivity of the sample. MEGAERA also indicated that axial heat loss could be significantly reduced by simply covering the ends of the probe with sample material, as demostrated in Runs 1, 3, and 4 of Tables 3.1. With axial heat loss significantly reduced, the effects of the heat front reaching the outer surface of the sample would be the dominant factor effecting t_{max}, and the line source and instantaneous cylindrical surface criteria were found to be reliable radial criteria for predicting when this occurred. Furthermore, to ensure that the actual transient heat probes would also produce good results, these probes were designed so as to perform better than those used in the MEGAERA simulations. This was accomplished by using hollow probes which were longer than those in the MEGAERA simulations and hence had lower axial heat flow. The dimensions of the samples used in actual experiments were

also larger then those in the simulation and, therefore, the heat front takes more time to reach the outer dimensions of the sample. A more detailed description of the probe and sample are given in the next section.

3.2 Physical Description of the Probes

Several probes were built and tested before an acceptable probe was developed. Initially the probes were 0.2381 cm in diameter by 10.16 cm in length, and 0.2381 cm in diameter by 12.7 cm in length with a thermocouple soldered to the outer surface of the brass tube. Although these probes produced acceptable results, the thermocouple junction was found to be too fragile and broke many times during experiments. As a result it was decided that the thermocouple would have to be placed inside the brass sheath.

The probes as finally designed (see Figure 3.3 which is a repeat of Figure 2.1) were built by first cutting a 12.7 cm length of 0.3175 cm O.D. by 0.2388 cm I.D. brass tubing which was used as a brass sheath. A small hole was drilled through the brass sheath at the mid-length of the probe. This hole was later used to mount the thermocouple junction. Twenty-two AWG copper wire was silver soldered to one end of the brass tube and also to an appropriate

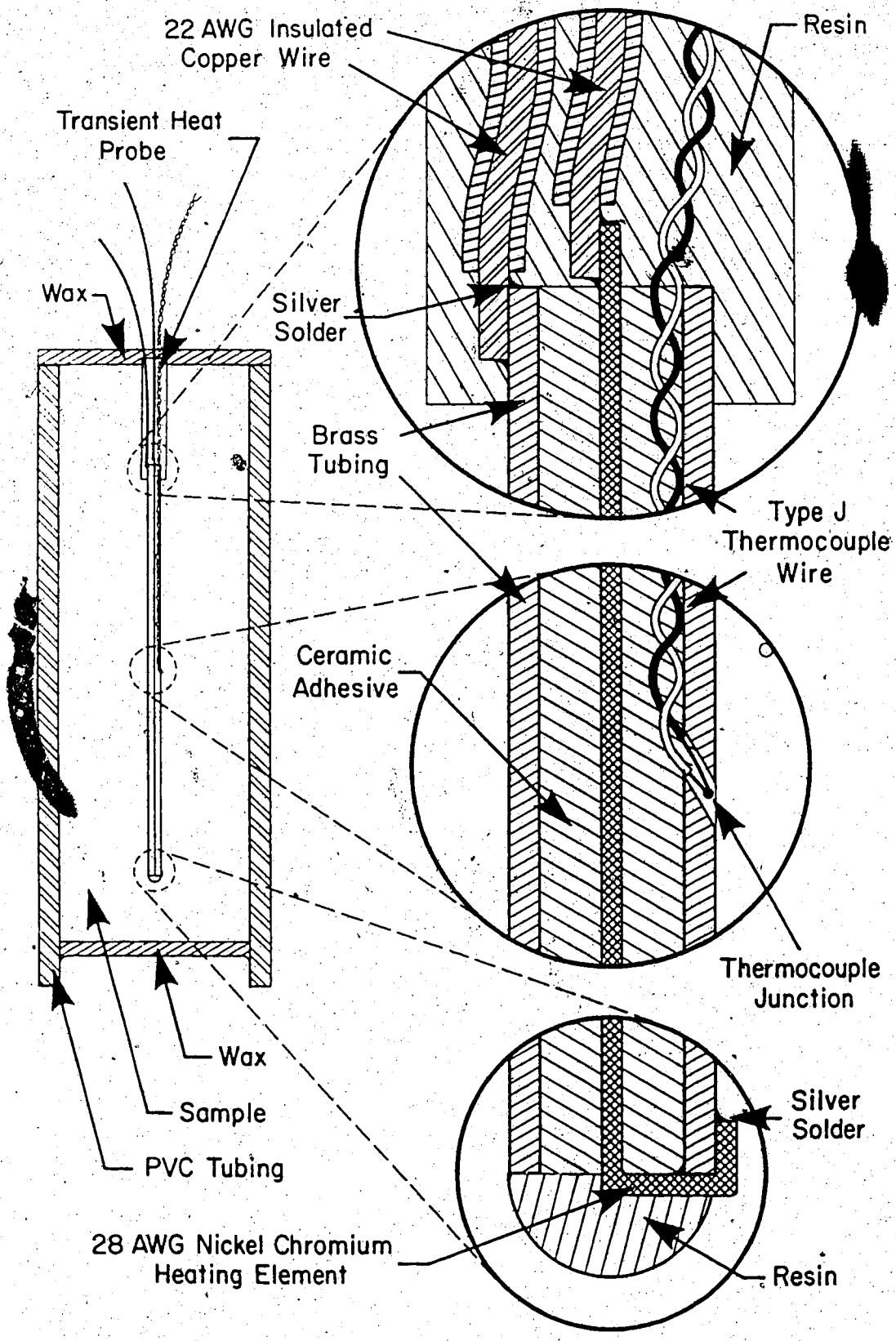

Figure 3.3 : Transient Heat Probe Apparatus

length of nickel-chromium wire, which was used as a heating element. A thermocouple junction was soft soldered into the small hole previously drilled through the brass sheath. The nickel-chromium heating element was then positioned along the axis of the brass sheath and held in place using clamps and shims. Aremco high temperature ceramic adhesive, Ceramabond 552, was inserted into the brass sheath using a syringe and the probe was placed in an oven for 2 hours at 200 °F to cure the Ceramabond 552. Once the Ceramabond 552 had cured the nickel-chromium heating element was silver soldered to the brass sheath. Electrical insulators were placed over the copper wires and resins (Torr Seal and Orthodontic resin) were placed at the ends of the probe, as shown in Figure 3.1, to protect the probe during the experiments.

During experiments the probe was connected to an HP 6274B DC power supply and the voltage and current delivered to the probe were monitored by two Fluke 8000A digital multimeters (see circuit diagram in Figure 3.4). Fortunuately the electrical properties of the nickel-chromium heating element remained constant as it was heated. Therefore, it was not necessary to adjust the HP 6274B DC power supply during the experiments. The temperature rise of the probe was monitered by an HP 3952A Automatic Data Acquisition System.

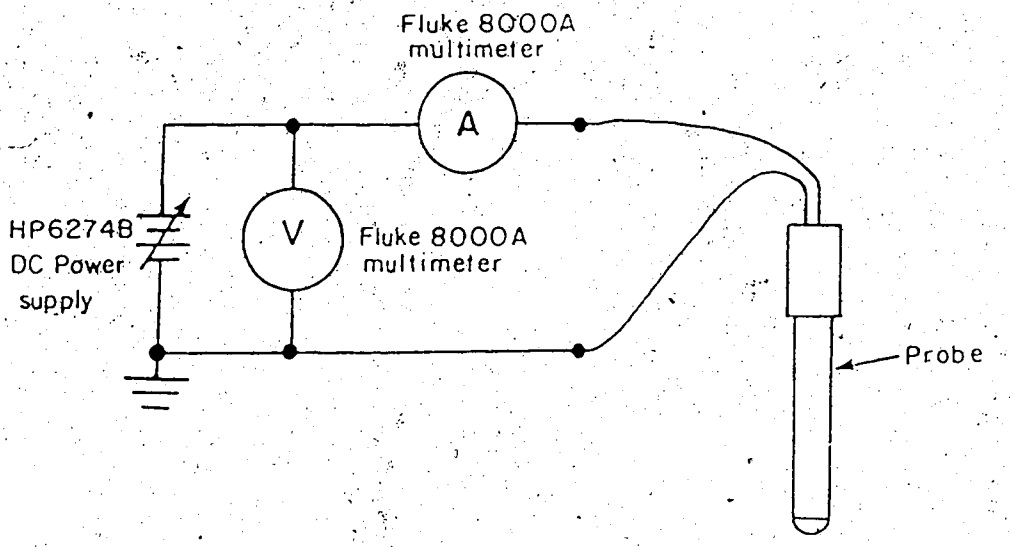

Figure 3.4 : Circuit Diagram for Transient Heat Probe Method

The probe was inserted in shale samples, which ranged in length from 13.4 cm to 18.8 cm with a radius of 3.1 cm. These shale samples were placed in a PVC tube which was sealed using wax as illustrated in Figure 3.3.

When the probe design criteria given by equations (2.12), (2.19), and (2.20) were calculated and a MEGAERA simulation done with the following estimated thermal and physical properties for the probe and sample

$$K_1 = 110 \frac{W}{m^{\circ}C} \qquad K_2 = 1.94 \frac{W}{m^{\circ}C}$$

$$\rho c_1 = 3.311 \times 10^6 \frac{J}{m^3{}^{\circ}C} \qquad \rho c_2 = 2.99 \times 10^6 \frac{J}{m^3{}^{\circ}C}$$

$$a = 0.0016 \text{ m} \qquad b = 0.031 \text{ m}$$

the following results were obtained.

The MEGAERA simulated temperature response of the probe is given

in Figure 3.5. From this temperature response curve, a log-linear region of 15 s to 350 s was determined using equations (3.1a) and (3.1b) as previously outlined, and the estimated thermal conductivity of the sample in this region was found to be 1.97 - 1.99 $\frac{W}{m\,^{\circ}C}$ (1.5 - 2% error).

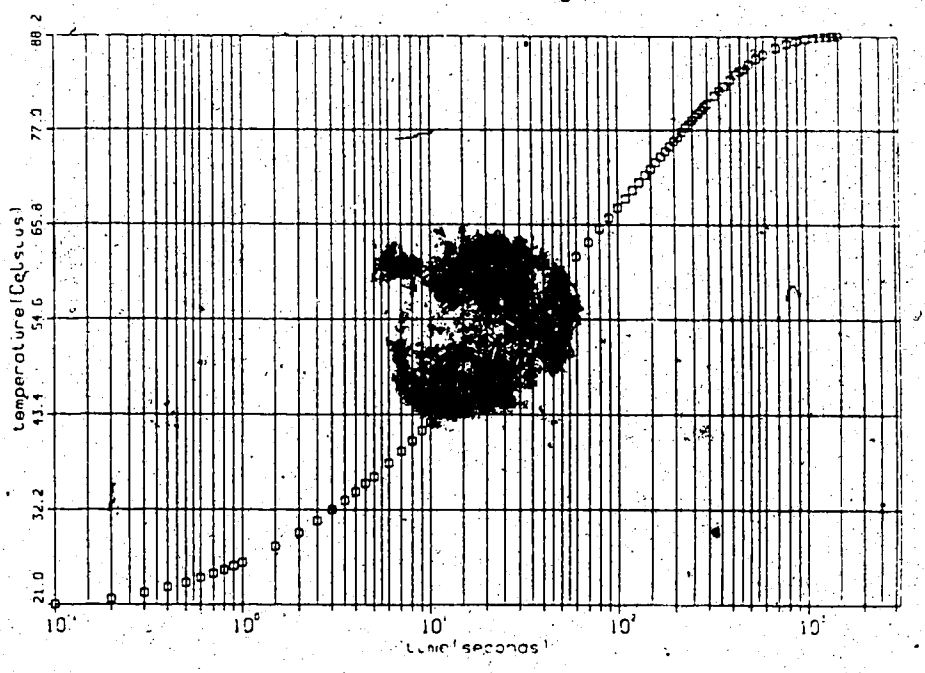

Figure 3.5 : Temperature Response of Probe in MEGAERA Simulation

For the line source and instantaneous cylindrical surface criteria, equations (2.19) and (2.20) respectively, the following estimates for t_{max} were calculated. It should be recalled that these two criteria were found to be the most reliable criteria during MEGAERA simulations of the transient heat probe method.

Equation	t_{max} (s)
(2.19)	330
(2.20)	370

Using Vos's very conservative criterion for t_{min}, equation (2.12), one obtains

$$t_{min} \cong 41 \text{ s}$$

The results of the criteria given by equations (2.12), (2.19), and (2.20) indicate that a log-linear region of approximately 41 s to 350 s should be expected during actual experiments on Clearwater shale. From actual experimental results on Clearwater shale samples, given in APPENDA E, typical log-linear regions averaged 8.7 s to 515 s, which compares favourably with the log-linear regions predicted by MEGAERA and the criteria given by equations (2.12), (2.19), and (2.20).

The following section will outline the actual method used during experiments.

3.3 Description of the Experimental Procedure for the Transient Heat Probe Method

The procedure used in the transient heat probe method underwent many modifications before a satisfactory approach was established.

Initially the probes were successfully tested on wax, dry sand, and oilsands samples. However, when the probes were then used on

shale samples additional problems arose. Moisture migration in the shale samples appeared to be a major problem. For example, when shale samples were initially tested, the power supplied to the probes was found to be too high. This seemed to cause moisture in the samples to be driven away from the probes. As a result, the thermal conductivity of the sample adjacent to the probes would decrease, creating an artifically low thermal conductivity region. In addition, this lower thermal conductivity region would cause the probe to heat up very rapidly, resulting in higher than usual axial heat losses and non-uniformities in the axial temperature distribution along the probe. Therefore, the power supplied to the probe had to be reduced to the point where noise and drift in the thermocouple readings became significant. The drift in the thermocouple readings was found to be due to the HP 3952A Automatic Data Acquisition System slowly heating up when initially turned on. When the HP 3952A system was left turned on overnight this drift disappeared. However, leaving the HP 3952A system on for extended periods of time was deemed to be an impractical solution. Hence, to account for the drift in the thermocouple readings a reference thermocouple in ice water was used.

The following outline is for the final procedure adopted for the transient heat probe method.

Procedure:

1) A shale sample is selected.

The Clearwater shale samples used in this research

were obtained in January 1985, from two Syncrude Canada Ltd. wells designated as 34-51-0-0 and 36-51-0-0. These wells were located northeast of the Syncrude mine site at Section 8, Township 93, Range 11, west of the 4th Meridian. The depths of the wells were 15.2m to 53.9m for 34-51-0-0, and 11.3m to 50.9m for 36-51-0-0. The shale cores from well 34-51-0-0 were sealed in twenty-nine, 1.5m long × 6.35 cm diameter PVC tubes, while the shale cores from well 36-51-0-0 were sealed in twenty-eight, 1.5m long × 6.35 cm diameter PVC tubes. These tubes were stored in a constant temperature/humidity room at ~8°C to prevent moisture loss from the shale cores. Before a selected shale sample could be tested, the appropriate PVC tube containing the shale sample was removed from the constant temperature/humidity room and the core divided into smaller lengths of 25mm to 250mm. These smaller core samples were then separately sealed in wax to prevent moisture loss and labeled. The samples not immediately used were placed back in the constant temperature/humidity room. A typical sample identification label is shown below

Mar 3/87 ⇐ *date tube was opened.*

34-51-0-0 ⇐ *well identification number.*

P24,"A" ⇐ *tube number* (P29) *and sample* ("A") *from tube.*

52.4-53.3m ⇐ *depth at which samples in this tube were obtained.*

2) Composition of shale sample is determined before experiment.

a) [redacted]ble is weighed ($M_{thimble}$) using a Mettler P[redacted] mass balance, with a resolution of 1 mg and a maximum capacity of 16 g.

b) Small pieces of the shale sample are cut off and placed in the paper thimble and weighed (M_{total}).

c) The paper thimble containing the small pieces of shale is placed in a Thelco Model 14 oven to evaporate all the moisture from the shale.

d) Once the moisture has completely evaporated from the sample, the paper thimble containing the small pieces of shale is weighed (M_{dried}), to determine the mass of mineral in the shale.

e) The composition by mass of the shale can be determined as follows.

$$\%\text{mineral} = \frac{M_{dried} - M_{thimble}}{M_{total} - M_{thimble}} \qquad (3.2)$$

$$\%\text{water} = \frac{M_{total} - M_{dried}}{M_{total} - M_{thimble}} \qquad (3.3)$$

3) The shale sample is placed in the PVC sample holder, as shown in Figure 3.3, and sealed in wax.

a) The mass of the PVC sample holder (M_{pvc}) is determined using a triple beam mass balance, with a resolution of 0.1 g and a maximum capacity of 2610 g .

b) The shale sample is placed in the 3.1 cm radius PVC sample holder. Since the original core samples were only slightly larger in radius (3.175 cm) than the PVC sample holder and the radial surfaces of the cores were covered with soft drilling mud, the shale samples could be inserted into the PVC sample holder by simply applying pressure to one end of the shale sample.

c) After placing the sample into the PVC sample holder, the mass of the PVC sample holder with the sample inside is determined (M_{total}), using the triple beam balance of step 3a). Knowing the mass of the PVC sample holder (M_{pvc}), the mass of the sample can be found.

$$M_{sample} = M_{total} - M_{pvc} \qquad (3.4)$$

d) The sample is sealed in wax to prevent the moisture from leaving the sample and to allow the experiment to be repeated several times on the same sample.

e) From the diameter of the PVC sample holder and the length of the sample, the volume of the sample (V_{sample}) can be calculated and therefore the average density of the sample known.

$$\rho_{sample} = \frac{M_{sample}}{V_{sample}} \qquad (3.5)$$

4) The probe is inserted into the sample.

a) A hole is hand drilled along the axis of the cylindrical sample. The reason for hand drilling this hole, rather than using an electric drill, is that electric drilling was found to damage the sample.

b) Water is poured into this hole and then drained from it. This is done to make the shale sample *stick* to the probe when it is inserted and consequently reduce contact resistance between the probe and sample. Since the samples were usually 100% water saturated, it is believed

that this procedure should not significantly affect the sample. Using water is much simpler than introducing some foreign substance, such as a thermal compound, into the sample, to reduce contact resistance. Moreover, the use of water to reduce contact resistance was found to be so successful that the shale samples sometimes had to be destroyed in order to remove the probe from the sample.

c) The probe is inserted into the hole.

d) The wax around the probe is re-melted to ensure that the sample is completely sealed.

5) The probe is connected to the DC power supply and HP 3052A Automatic Data Acquisition System.

a) An HP 6274B DC power supply is set to a voltage which will produce a heating rate of about 2 to 4 W/m in the probe.

b) The probe is connected to the power supply as shown in Figure 3.4 and the thermocouple located on the probe is connected to the HP 3052A Automatic Data Acquisition System.

c) The ice water which is used as a constant reference temperature is prepared and a second thermocouple, also connected to the HP 3052A system is inserted into it.

6) The actual thermal conductivity measurement begins. The HP 3052A Automatic Data Acquisition System, under program control, is used to monitor and record the response of the probe thermocouple and the ice water thermocouple.

a) A program controlling the HP 3052A system is started (see Appendix B for the program) and begins to record the response of the probe and ice water thermocouples every second for the first 100 seconds of the experiment and then every 10 seconds for the next 1400 seconds.

b) The HP 6274B DC power supply, which heats the probe, is turned on.

c) In order to determine the power delivered to the probe, two Fluke 8000A digital multimeters monitor the voltage and current supplied to the probe - refer to Figure 3.4. Since the length of the probe is known, the heating per unit length of probe is easily determined.

d) After 25 minutes the HP 6274B DC power supply is turned off.

e) The program then proceeds, from the data collected, to calculate and print out the temperature of the probe and ice water, with and without drift correction in the temperature

readings.

7) As previously mentioned at the beginning of Section 3.3, the power supplied to the probe had to be reduced to the point where noise and drift in the temperature readings became significant. Since the temperature measurements are very noisy, steps 5) and 6) are repeated 2 to 6 times, once per day, in order to obtain an average thermal conductivity value for the sample. The reason for performing only one experiment per day, on the same sample, is to allow the moisture in the sample, which may have migrated away for the probe due to large temperature gradients near the probe, to redistribute itself uniformly throughout the sample.

8) Composition and water saturation of the sample are determined after the experiment is completed.

   a) The sample is removed from the apparatus and the composition of part of the sample is found using the procedure of step 2). The rest of the sample is saved, if possible, by sealing it in wax for future analysis.

   b) The water saturation, S_w, of the sample is estimated as follows.

$$S_w = \frac{\begin{bmatrix}\text{Volume of water}\\ \text{in the sample}\end{bmatrix}}{\begin{bmatrix}\text{Total void volume}\\ \text{within the sample}\end{bmatrix}}$$

or

$$S_w = \frac{\rho_{sample}(\%water)}{1 - \frac{\rho_{sample}(\%mineral)}{\rho_{solid}}} \qquad (3.6)$$

where ρ_{sample} = the density of the sample (g/m^3) - see step 3d)

%water and %mineral are the composition of the sample by mass - see step 2)

$\rho_{solid} \cong 2.8\ g/cm^3$ - estimated density of the shale particles[45]

Since ρ_{solid} is only estimated, this equation can only estimate the water saturation and, therefore, one can obtain values for S_w greater than 100%.

[45] Holtz and Kovacs, pp14-15, (1981)

9) The calculation of the thermal conductivity of the sample is performed.

Various parts of the temperature response curve for the probe are numerically fitted to the following equation, which is similar to equation 3.1a), using least squares curve fitting techniques - see Appendix A for program.

$$T(t) = A \ln(t) + B \qquad (3.7)$$

where $T(t)$ = the temperature ($^{\circ}C$) probe at time $t(s)$

A and B are constants found by the curve fitting method.

The part of the temperature response curve which best fits equation (3.7) is chosen as the log-linear region. Since there is noise associated with the thermocouple response, equation (3.7) is fitted to various parts of the log-linear region to obtain a range of estimates for the thermal conductivity of the sample. From the slope of equation (3.7), constant A, the thermal conductivity of the sample can be found. Thus

$$K_{expt} = \frac{q}{4\pi A} \qquad (3.8)$$

where K_{expt} = the estimated thermal conductivity of the sample $\left[\frac{W}{m\,^{o}C}\right]$

q = the heating rate of the probe (W/m)

3.4 Experimental Results on Materials with Published Thermal Properties

In order to further test the transient heat probe method, experiments on materials with published thermal properties were performed. The results of two of these experiments are shown below.

Dry sands experiment # 68

Dry sand (>325 mesh) was loosely packed in a 2000ml beaker with dimensions of 12.7 cm in diameter by 16.5 cm high. The probe was then inserted into the dry sand.

The density of the loosely packed sand was estimated twice by measuring the mass and volume of sand poured into a graduated cylinder.

Density of sand: ρ = 1.47 to 1.56 g/cm^3

The porosity of the sand was estimated using the following

equation.

$$\phi \cong 1 - \frac{\rho}{\rho_s} \qquad (3.9)$$

where $\rho_s = 2.65$ g/cm^3 - the density of the solid particles of sand[46]

Using equation (3.9) one obtains,

Porosity of sand: $\phi = 41.1$ to 44.5 %

A previously published value for the thermal conductivity of the dry sand was found using the empirical relation given by equation (3.10). Somerton et al performed many thermal conductivity measurements on dry sand and sand-fluid systems using the *hot plate method*, in order to develop this empirical relation:[47]

$$K_{Somerton} = 1.27 - 2.25\phi + 0.39K_s\sqrt{S_w} \qquad (3.10)$$

---

[46] Holtz and Kovacs, p14-15, (1981)

[47] Somerton, Keese, and Chu, (1974)

where $K_s = 7.4 \frac{W}{m\,^oC}$ - thermal conductivity of the solid phase of the sand[48]

and $S_w = 0.0$ %

It follows that

$$K_{Somerton} \approx 0.27 \text{ to } 0.35 \frac{W}{m\,^oC}$$

Two experiments were conducted, at different probe power levels. The results are shown in Figure 3.6a) and b), and experimental results for K_{expt} were calculated using the curve fitting routine presented in Appendix A.

Run	q $\left(\frac{W}{m}\right)$	K_{expt} $\left(\frac{W}{m\,^oC}\right)$	log-linear range (s)
1	12.76	0.31 - 0.32	30.0 - end of run
2	3.60	0.31	30.0 - 235

[48] Cervenan, Vermeulen, and Chute, (1981)

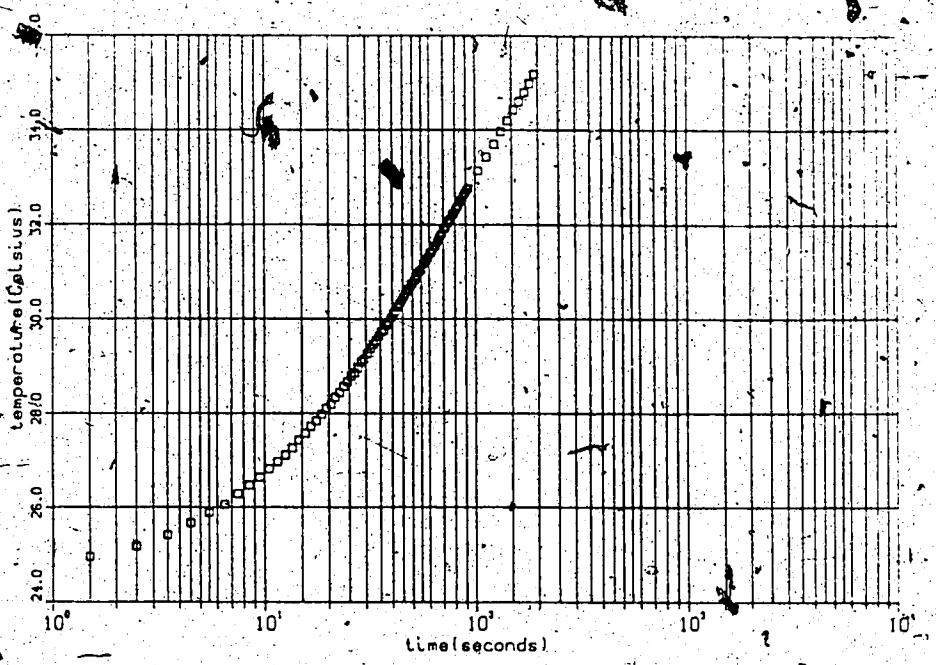

Figure 3.6a) : Temperature Response of Probe for Experiment # 68, 1st Run

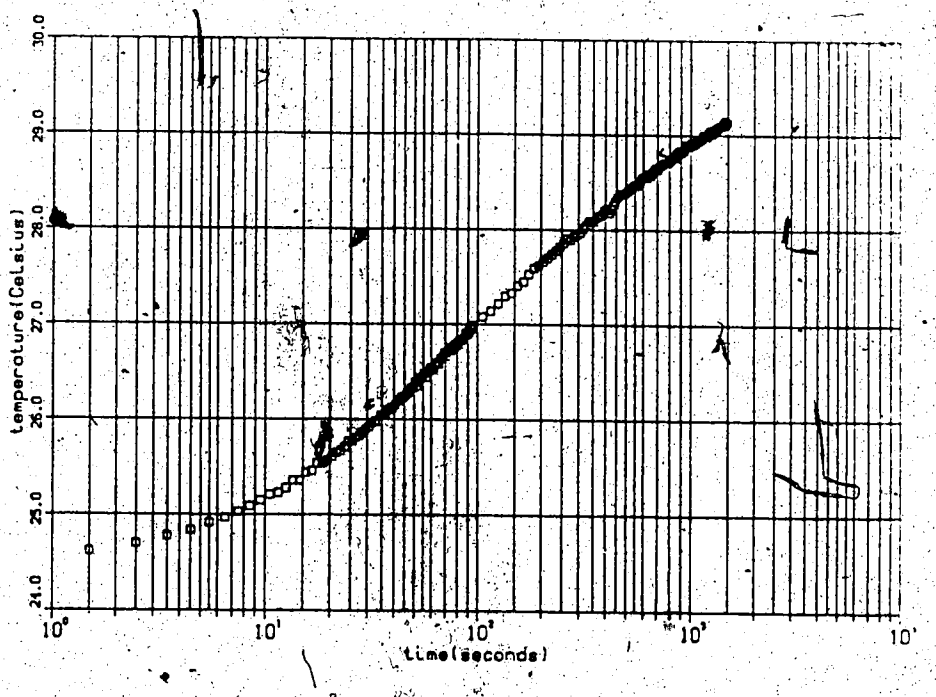

Figure 3.6b) : Temperature Response of Probe for Experiment # 68, 2nd Run

Notice that the increase in the temperature of the probe is ~10 °C for the 1st run (Figure 3.6a)) and ~4 °C for the 2nd run (Figure 3.6b)). As a result, noise and drift in the thermocouple readings, which are approximately ±0.1 °C and up to -1 °C respectively, are negligible.

The experimental and Somerton values for the thermal conductivity of the dry sand agree very well.

Oilsand experiment #70

Oilsand was packed into the PVC sample holder shown in Figure 3.3 (the dimensions of the sample holder and probe were given in Section 3.2) and the thermal conductivity probe inserted as described in *3.3 Description of the Experimental Procedure for the Transient Heat Probe Method*.

The composition of the sample was found using a Dean Stark compositional analysis apparatus. In this apparatus toluene vapor is flushed through a known mass of oilsand, causing the water and bitumen in the oilsand sample to be removed. The water which is removed from the sample is collected and later used to determine the mass fraction of water in the oilsand sample. After all the water and bitumen has been flushed from the sample only the mineral component of the oilsand sample remains and the mass fraction of mineral in the oilsands can be determined. Once the mass of the water and mineral components of the sample are known, the mass of

the bitumen in the sample can also be determined and thus the mass composition of the sample is known. For the sample under test

$$\text{bitumen} \cong 9.1\%$$

$$\text{water} \cong 5.8\%$$

$$\text{mineral} \cong 85.1\%$$

the density of sample was

$$\rho \cong 1.96 \text{ g/cm}^3$$

the porosity of the sample (using equation (3.9)) was

$$\phi \cong 37 \%$$

and the water saturation of sample (using equation (3.6) with $\rho_{solid} \cong 2.65$ g/cm^3 for the solid mineral particles[49]) was

$$S_w \cong 39.7 \%$$

Two previously published values for the thermal conductivity of oilsands samples are given below.

---

[49]Holtz and Kovacs, pp14-15, (1981)

1) Using Somerton's empirical equation (3.9) to determine the thermal conductivity of the oilsand sample under test, yields

$$K_{Somerton} \cong 2.27 \ \frac{W}{m\,^{o}C}$$

(Note that equation (3.9) does not account for the bitumen in the sample. The work of Cervenan et al[50] suggests that for the water saturation exhibited by the sample, Somerton's expression leads to a value of thermal conductivity that may be slightly too large.)

2) The second published thermal conductivity value for oilsand was determined by Seto[51]. Seto used the transient heat probe method to determine this value of thermal conductivity for a Water-Bitumen saturated oilsand sample which was held in a triaxial compression test cell. This test cell was capable of producing confining and fluid pressures up to 10 MPa, and had a temperature range of 20 °C to 200 °C. For a

---

[50] Cervenan, Vermeulen, and Chute, (1981)

[51] Seto, (1985)

sample whose composition was

bitumen - 12.3%

water - 4.5%

mineral - 83.2%

and whose water saturation was

S_w - 27%

Seto found a thermal conductivity of

$$K_{Seto} - 2.009 \frac{W}{m\,^{o}C} \quad @\ 20\ ^{o}C$$

(Note that the composition of Seto's sample was slightly different from that of the sample under test. As the water saturation increases the thermal conductivity of the oilsand increases and Seto's results will then agree more closely with the results of this experiment, which are given below.)

Two experiments were conducted, at different probe power levels. The results are shown in Figure 3.7a) and b), and experimental results for K_{expt} were found using the curve fitting routine presented in Appendix A.

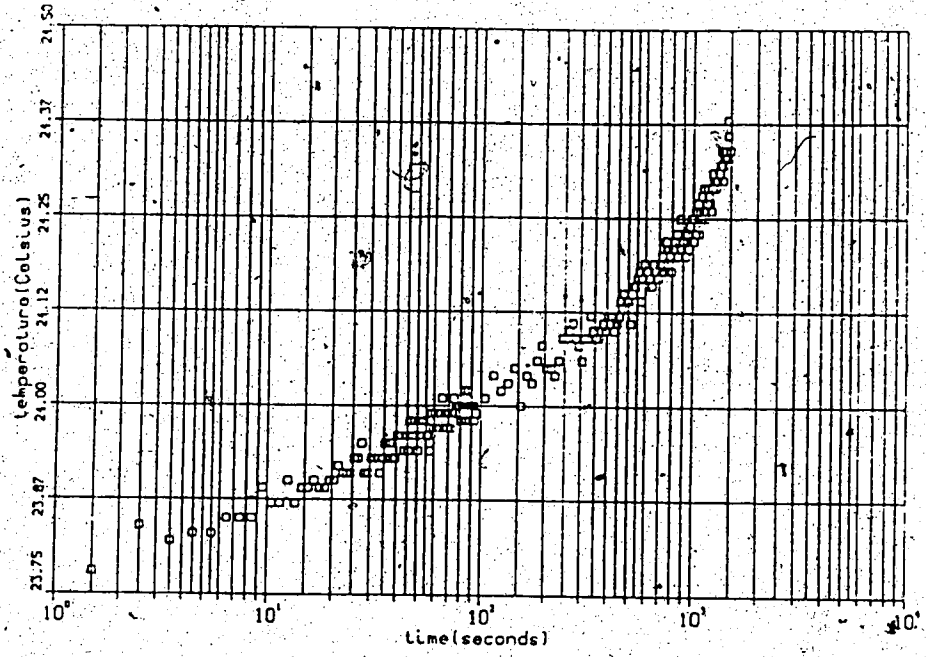

Figure 3.7a) : Temperature Response of Probe for Experiment # 70, 1st Run

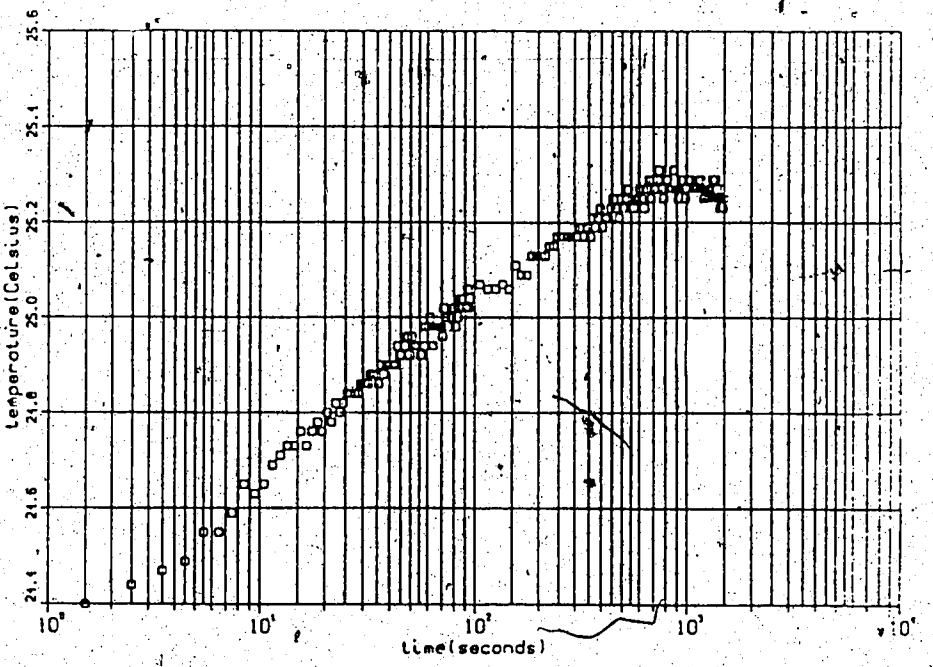

Figure 3.7b) : Temperature Response of Probe for Experiment # 70, 2nd Run

Run	q $\left[\frac{W}{m}\right]$	K_{expt} $\left[\frac{W}{m\,^{\circ}C}\right]$	log-linear range (s)
1	1.82	2.10 - 2.23	4.5 - 480
2	1.33	2.09 - 2.11	9.5 - 105.5

The thermocouple drift in the 1st run was corrected using an ice water reference thermocouple as previously described in Section 3.3 and Appendix B, while for the 2nd run, thermocouple drift was not corrected. Note that due to this drift, the end of the temperature versus ln(time) curve in Figure 3.7b) is bent down.

Also, notice that the increase in the probe temperature is less than 1 °C, and, therefore, noise and drift in the thermocouple readings are very significant. As mentioned before, a small temperature is necessary to avoid fluid migration near the probe.

It is seen that the Somerton and Seto values for thermal conductivity of the oilsand agree well with the experimentally determined value. In interpreting this result it must be borne in mind that Seto's sample is of somewhat different composition from that of the sample considered by the author, and that noise and drift in the thermocouple readings may have affected the values of thermal conductivities measured by the author.

Successful experiments were also conducted on wax samples. These were preliminary experiments using the transient heat probe method,

in which the probes were 0.2381 cm in diameter by 10.16 cm in length. The results of these transient heat probe experiments, when compared with steady state thermal conductivity results obtained for wax using the hot plate method[52] agreed well. Since the physical properties of wax are very different from shale, these experiments were of limited use. Consequently, the results of these experiments are simply presented here without any details, and can be used as another indication of the validity of the transient heat probe method.

The steady state hot plate method produced the following thermal conductivity for wax (experiment #17, with relative error estimated from the uncertainty in the thermocouple position and reading).

$$K_{wax} = 0.29 \frac{W}{m\,^{o}C} \pm 20\%$$

From the transient heat probe method the following results were found.

$$K_{wax} = 0.30 \frac{W}{m\,^{o}C} \text{ (experiment \#13)}$$

$$0.29 \frac{W}{m\,^{o}C} \text{ (experiment \#15)}$$

---

[52] Cervenan, Vermeulen, and Chute, (1981)

The experimental results obtained for dry sand, oilsand, and wax samples gave confidence in the reliability of the heat probe method, which was then applied to obtain thermal conducutivity of shale samples.

3.5 Experimental Thermal Conductivity Results On Shale

The following tables summarize the experimental thermal conductivity results obtained on Clearwater shale samples. A more thorough description of the experiments presented in Tables 3.2a) and b) is given in Appendix E.

For well 36-51-0-0

Experiment Number	Sample	K $\left(\frac{W}{m\,^{o}C}\right)$	Composition by Mass	
			%Mineral	%Water
71	P25,M	1.74± 8%	84.5	15.5
72	P9 ,D	1.76± 8%	81.2 to 79.1	18.8 to 20.9
73	P16,D	2.09± 7%	86.4 to 85.5	13.6 to 14.5
75	P24,A	1.99±12%	76.2 to 73.1	23.8 to 26.9

Table 3.2a) : Thermal Conductivity results for well 36-51-0-0

For well 34-51-0-0

[illegible]nt	Sample	K $\left[\frac{W}{m^{\circ}C}\right]$	Composition by Mass	
			%Mineral	%Water
78	P28,I	1.76±12%	90.3 to 88.1	9.7 to 11.9
	P21,C	1.70±10%	77.2 to 75.8	22.8 to 24.2
79	P29,G	2.26± 3%	88.6 to 87.5	11.4 to 12.5
	P 8,D	2.23±5.4%	86.4 to 83.0	13.4 to 17.0

Table 3.2b) : Thermal Conductivity results for well 34-51-0-0

These results for Clearwater shale may be compared to previously published results for shale. Somerton (1958) found the following thermal conductivity value for shale using a steady state thermal measurement method.

$$K = 1.69 \frac{W}{m^{\circ}C}$$

The shale used by Somerton, however, is believed to be different from the Clearwater shale used in this research. Somerton indicated that his shale samples were hard and laminated, with a porosity of 7.1%. The Clearwater shale samples used in this research were generally soft with a consistency similar to cheese and a porosity of about 20 to 30%.

4.0 Design and Testing of the Transient Heat Capacity Apparatus and Method

Several versions of the transient heat capacity apparatus were built and tested before a final satisfactory configuration was found. The following three sections will give a physical description of the final version of the heat capacity apparatus, an outline of the method used during actual experiments, results from a numerical simulation program, and experimental results for materials with published thermal properties.

4.1 Physical Description of the Transient Heat Capacity Apparatus

From Section 2.2.1 the heat capacity of a sample is determined by electrically heating a cylindrical sample and monitoring the temperature rise of the sample using several thermocouples located within the sample.

To accomplish this in actual experiments, shale samples, of radius 2.54 cm and length 8.9 cm to 11.5 cm, were held in a cylindrical plexiglas sleeve with electrodes placed at the ends of the sample as depicted in Figure 4.1. The sample was then electrically heated by passing a current between the two electrodes. Ideally, to reduce heat losses from the sample and hence lengthen the linear region of Figure 2.7, an insulating material should be used instead of the plexiglas sleeve. However,

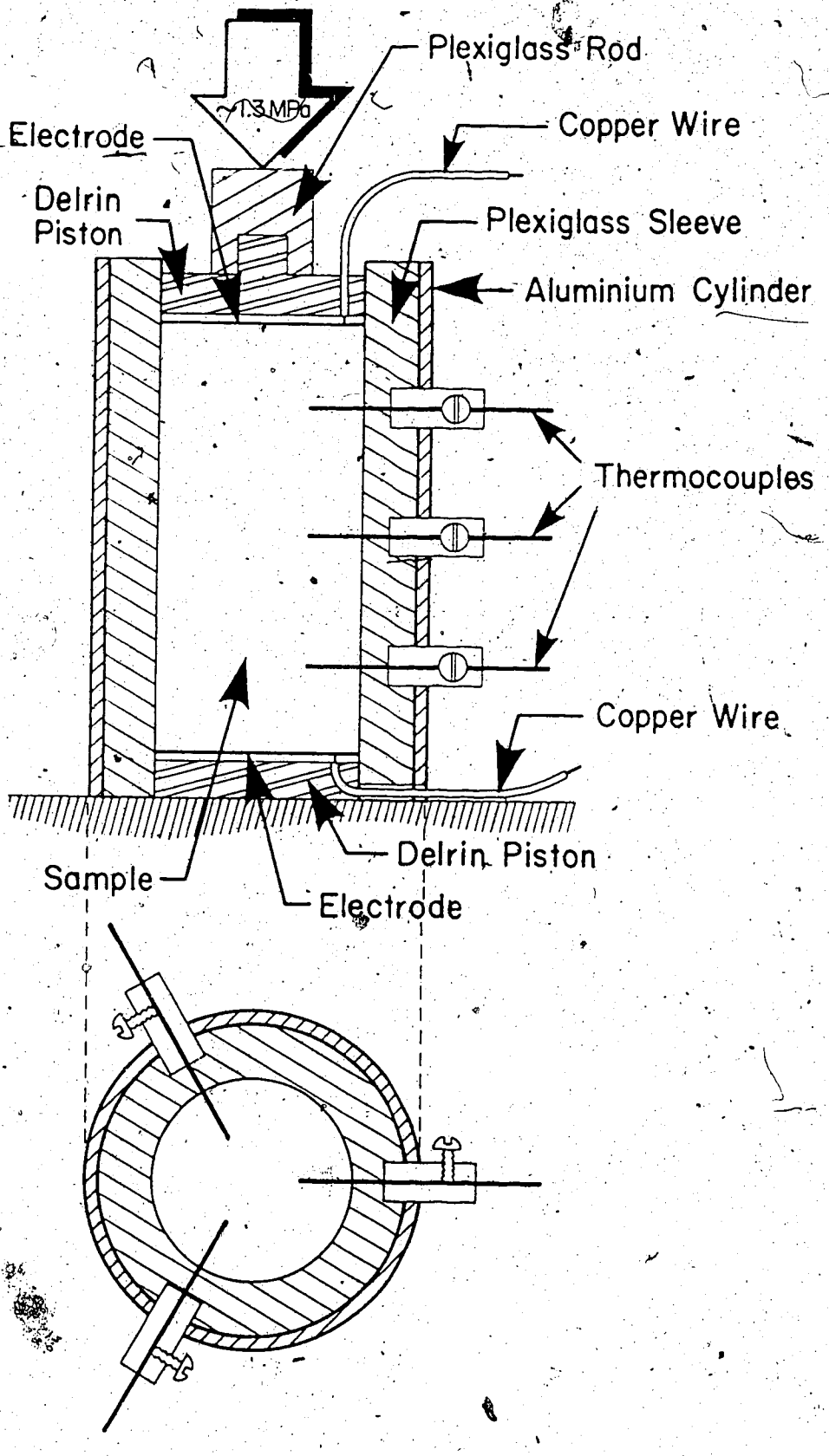

Figure 4.1 : Transient Heat Capacity Apparatus

to ensure good electrical contact between the sample and electrodes, pressure (~1.3 MPa) was applied to the electrodes and insulating materials generally are not strong enough to withstand this pressure. Even though plexiglas was used, an aluminum cylinder surrounds the plexiglas sleeve to provide additional mechanical strength. To reduce axial heat losses from the sample, the electrodes were made from copper clad fiberglass epoxy, rather than solid copper disks which have a much higher thermal mass. The electrodes were strengthened by gluing them to Delrin pistons and a divider network (see Figure 4.2) was connected to the electrodes to monitor electrical voltage and current delivered to the sample. For the shale samples used during these measurements the electrical resistance of the various samples ranged from approximately 150 Ω to 500 Ω.

To monitor the temperature rise of the sample, nine thermocouples were inserted radially, approximately 1.25 cm, into the sample and held in position by screw clamps. The response of the nine thermocouples was recorded by an HP 3052A Automatic Data Acquisition System.

The next section will outline the actual procedure used to determine the heat capacity of the shale samples.

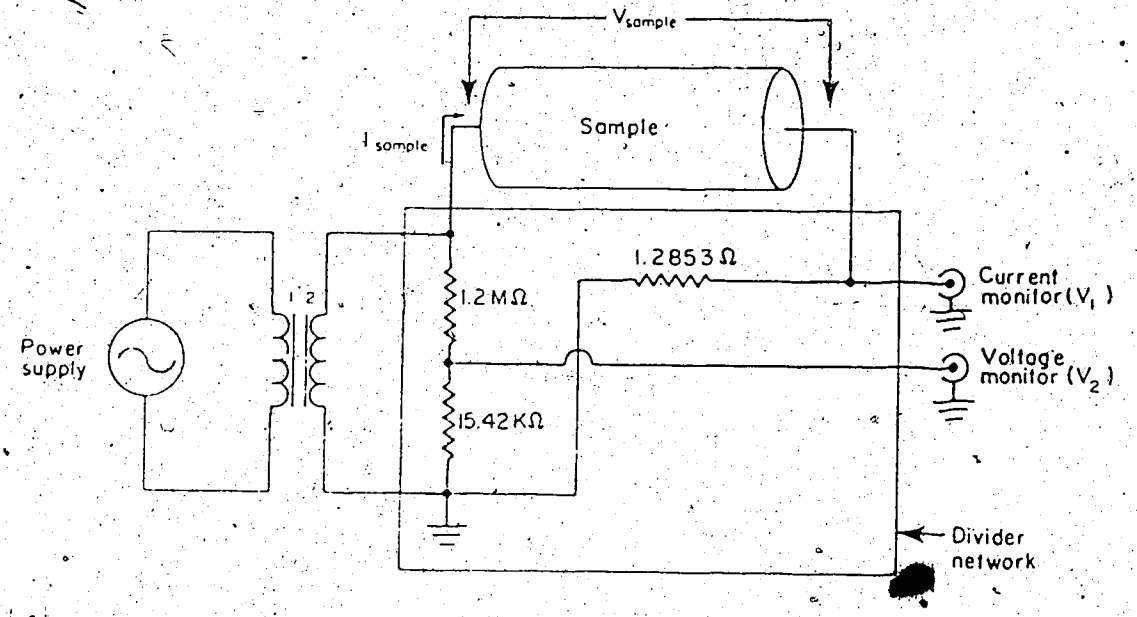

Figure 4.2 : Circuit Diagram for Transient Heat Capacity Method

4.2 Experimental Procedure Used to Determine the Thermal Heat Capacity of Shale

The following is a detailed outline of the procedure used to determine the thermal heat capacity of shale samples.

Procedure:

1) A shale sample is selected.

2) The composition of the sample is determined before experiment using the procedure outlined in step 2 of Section 3.3.

3) The shale sample is installed into the sample holder and the electrodes are placed at the ends of the sample.

   a) The mass of the heat capacity apparatus (including electrodes) is determined using a triple beam mass balance, with a resolution of 0.1 g and a maximum capacity of 2610 g ($M_{apparatus}$)

   b) Using a custom built extrusion device (Figure 4.3), the shale sample is extruded into the heat capacity apparatus. The shale samples are generally soft, with a consistency similar to cheese, and are easily shaped by a sharp object. By placing the shale sample in a PVC guide tube and applying pressure to one end of the sample, the sample is forced past a cylindrical brass cutting blade, which reduces the diameter of the sample to the same diameter as that of the heat capacity apparatus.

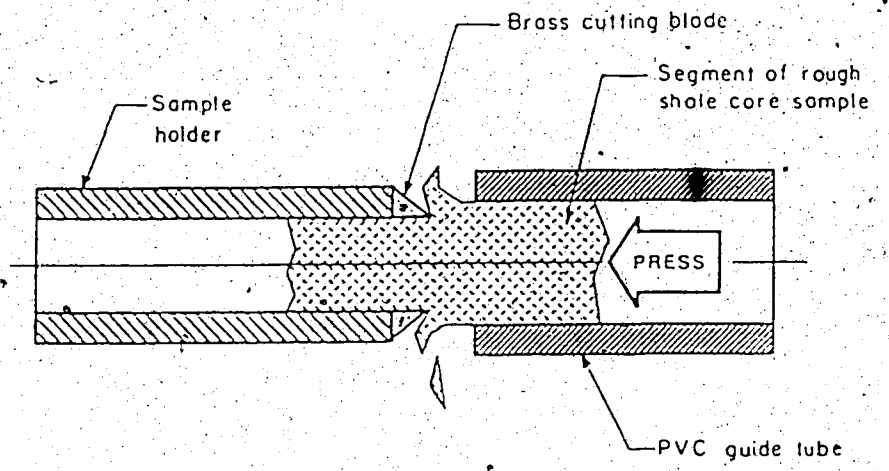

Figure 4.3 : Extrusion Device

c) After extruding the sample into the heat capacity apparatus, the ends of the sample are usually uneven and have to be planed before the electrodes can be placed on the ends. The ends of the sample are planed using a scalpel.

(Note, during this procedure the surface of the sample is exposed to the atmosphere for as short a period of time as possible to avoid drying of the sample.)

4) The mass of the shale sample inside the heat capacity apparatus is determined.

a) The mass of the apparatus (including electrodes) with the shale sample inside the apparatus is measured using the triple beam mass balance used

in step 3a), M_{total}.

b) Knowing the mass of the apparatus (including electrodes), $M_{apparatus}$, from step 3a), the mass of the sample can be found.

$$M_{sample} = M_{total} - M_{apparatus} \qquad (4.1)$$

5) Thermocouples are inserted into the sample and pressure is applied to electrodes.

a) Nine thermocouples are inserted radially to a depth of about 1.25 cm, into the sample, and held in position using screw clamps. The exact position of the thermocouples is not crucial in these experiments and if a thermocouple is difficult to insert, a sharp metal rod, with the same diameter as the thermocouple, is used to make a hole in the sample for the thermocouple.

b) Pressure (~1.3 MPa) is applied to the electrodes using a hydraulic press.

c) The thermocouples are connected to an HP 3495A scanner which is part of the HP-3052A Automatic Data Acquisition System. Inputs to the HP 3495A scanner are rated at 40 Volts peak to peak. To ensure that the HP 3495A scanner will not be damaged during the experiment the thermocouples

are checked for short circuits. The thermocouples are inside a metal sheath as shown in Figure 4.4 and are electrically insulated from the metal sheath.

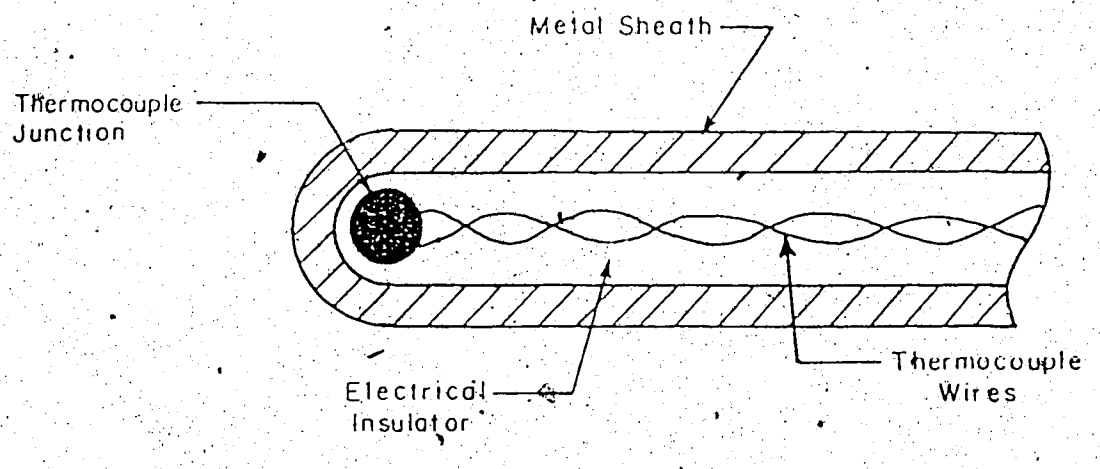

Figure 4.4 : Diagram of Thermocouple Used in Transient Heat Capacity Method

During a typical experiment the metal sheath may be floating at ~100 Volts RMS while the thermocouple inside is at ground potential. Consequently, if the electric insulator inside the metal sheath fails, the HP 3495A scanner would be damaged.

6) The volume and density of the sample are determined.

a) Knowing the dimensions of the apparatus, the

volume of the sample, V_{sample}, can be determined.

b) From step 4b) the mass of the sample, M_{sample}, is known and the density of the sample can be found using

$$\rho_{sample} = \frac{M_{sample}}{V_{sample}} \qquad (4.2)$$

7) The electrical resistance of the sample is determined. The electrical resistance of the sample is required so that an appropriate initial power (approximately 40 watts) can be delivered to the sample. In these experiments the sample is heated by applying a constant voltage across the sample. As the temperature of the sample increases its electrical resistance decreases and, as a result, the sample draws more power. Power increases from approximately 40 watts to 60 watts over approximately 3 minutes. To determine the constant voltage which is necessary, the electrical resistance of the sample is first determined by passing a small electric current through the sample, so as to avoid heating the sample. Once the sample resistance is known, the electrical power supply (a Variac Autotransformer with an output of 0-135 Volts and a maximum current of 10 Amps,

connected to a 2:1 step up transformer - see Figure 4.2) can be set to the appropriate voltage. Once the Variac power supply is set to the correct voltage, the Variac power supply and heat capacity apparatus are then connected to the divider network as shown in Figure 4.2.

8) Actual Measurement of Heat Capacity the begins.

An HP 3052A Automatic Data Acquisition System, under program control, is used to monitor the experiment and calculate the heat capacity of the sample.

a) A program controlling the HP system is started (see Appendix C for program).

b) The program records the initial temperature of the nine thermocouples (~25°C) and then waits for the Variac power supply, which heats the sample, to be turned on.

c) The Variac power supply is turned on and the program begins recording the response of the nine thermocouples and divider network.

d) When the temperature of the sample reaches ~40°C the Variac power supply is turned off by the operator.

e) The program then proceeds to calculate the specific heat of the sample as follows. First, the average temperature rise of the sample is calculated, as a function of time, by averaging the nine thermocouple responses. Next, the electrical power delivered to the sample is also calculated as a function of time. Once the average temperature rise of the sample and electrical energy delivered to the sample are known, the computer prompts the operator for the mass of the sample, and proceeds to calculate the specific heat of the sample, as a function of time, using

$$c = \frac{\Delta E}{\Delta T_{ave}(MASS)} \qquad (4.3)$$

where ΔE = the electrical energy delivered to the sample (J)

ΔT_{ave} = average temperature response of the nine thermocouples ($^{\circ}C$)

$MASS$ = mass of the sample (g)

The volumetric heat capacity can then be determined by simply multiplying the specific heat, c, of the sample by the density of the

sample, ρ_{sample}.

9) The composition and water saturation of the sample are determined, after the experiment has been completed.

a) The sample is removed from the apparatus and the composition of part of the sample is found using the procedure presented in step 2 of Section 3.3. The rest of the sample is saved, if possible, by sealing it in wax for future analysis.

b) The water saturation, S_w, of the sample is estimated using equation (3.6) of Section 3.3.

4.3 Testing of the Transient Heat Capacity Apparatus and Method

In Section 2.2 the theory used to develop this method was based upon homogeneous samples which are invariant during experiments. The samples used in actual experiments, however, are generally non-homogeneous, and their properties change during the experiments. As a consequence, the transient heat capacity method had to be tested to verify that it would produce useable results for non-homogeneous samples, which vary during experiments. To accomplish this, numerical simulations were conducted with the program MEGAERA. As well, actual experiments, using the transient

heat capacity method, were performed on samples with previously published thermal properties. The results of these tests are presented below.

4.3.1 MEGAERA Simulations of the Transient Heat Capacity Method

As previously mentioned in Section 3.1, MEGAERA was written by A. Hiebert[53,54] and simulates the electrical heating of composite or non-homogeneous materials with temperature dependent electrical conductivities. The electrical conductivity of the samples varied linearly with temperature in these simulations.

$$\sigma(T) = \sigma_{24}(1 - \alpha (T - 24^{\circ}C)) \qquad (4.4)$$

where $\sigma(T)$ = the electrical conductivity (S/m) at a temperature, T ($^{\circ}$C)

σ_{24} = the electrical conductivity (S/m) at 24°C

α = an experimentally determined temperature coefficient (1/$^{\circ}$C)

This program was used to simulate the transient heat capacity

---

[53]Hiebert, (1983)

[54]Hiebert, (1981)

method with homogeneous and non-homogeneous samples which have temperature dependent electrical conductivities. The program was used to predict the temperature changes in the sample. These temperatures were in turn used to estimate the volumetric heat capacity of the sample in a manner analogous to the experimental determination procedure described in step 8 of Section 4.2. The result was then compared to the actual volumetric heat capacity input to MEGAERA for the simulation in the first place. Ideally, the two values of volumetric heat capacity should agree exactly, however, quantization in the temperature response given by MEGAERA causes these two values to differ.

Unfortunately, MEGAERA does not allow the thermal properties of materials to be temperature dependent. However, Hepler[55] determined that the heat capacity of other reservoir minerals, such as Athabasca fine solids which were mostly clays (<325 mesh), only varies by approximately 5% over the temperature range involved in the experiments described in this research. A 5% variation in the heat capacity would be undetectable in actual experiments, which are estimated to be accurate to approximately 5% to 10%. The accuracy of the transient heat capacity method was estimated by comparing the results produced by this method on materials such as water, sand/water, and oilsands samples, with previously published thermal properties for these same materials.

---

[55]Hepler, (1985)

The homogeneous problem simulated by MEGAERA is the following. A cylindrical sample 10 cm in length and 2.5 cm in radius, with thermal conductivity 1.69 $\frac{W}{m\,^{o}C}$ and volumetric heat capacity 2.15 $\frac{J}{cm^{3}\,^{o}C}$, was electrical heated by electrodes placed at the ends of the sample (see Figure 4.5). To monitor the temperature rise of the sample, five simulated thermocouples were located 1.25 cm from the axis of the cylindrical sample and equally spaced 2 cm apart axially. The average temperature of the sample was determined by averaging the 5 simulated thermocouple responses.

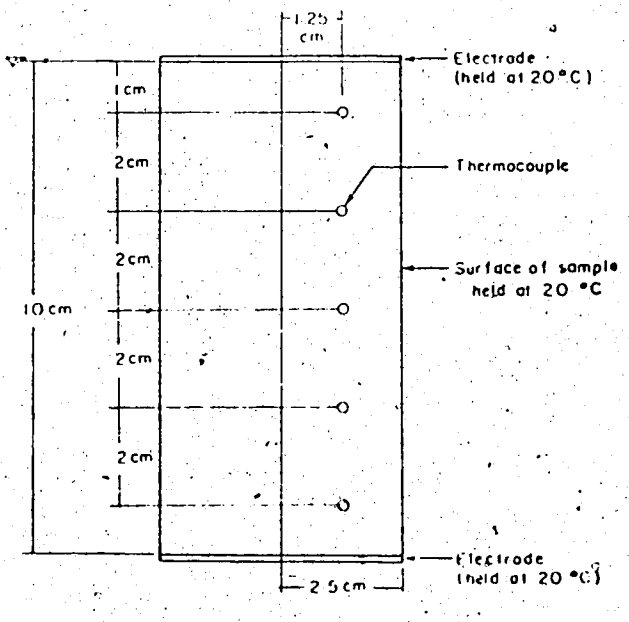

Figure 4.5 : Homogeneous Heat Capacity Problem Simulated by MEGAERA

In this simulation a constant temperature boundary condition was

imposed at the surface of the sample. Since the plexiglas sample holder used in the actual heat capacity apparatus acts as a partial thermal insulator, heat losses from actual experiments are lower than predicted by this simulation. Note that although there was no thermocouple lag in the simulated thermocouple responses, there was quantization error in these thermocouple responses. In other words the simulated temperatures were only given to a tenth of a degree. This quantization error in the thermocouple response initially caused the heat capacity results presented in Table 4.1 and other MEGAERA simulations of the transient heat capacity method to fluctuate greatly until the change in the sample temperature was great enough for quantization error to be negligible. This initial fluctuation in the MEGAERA simulation results is similar to Region 1 of Figure 2.8 in which noise and thermocouple lag caused the initial estimate of the heat capacity of the sample to be in error in actual experiments.

The results of this simulation are shown in the following table, where the heat capacities were calculated using equation (2.24) which, it should be recalled, is valid only so long as heat losses from the sample are negligible. In Table 4.1, the data between the dashed lines represent Region 2 of Figure 2.8, where valid estimates of the heat capacity can be made. The beginning of this region was determined by simply examining the heat capacity values in Table 4.1 and observing when the oscillation in the heat capacity values became a minimum. Similarly, the end of this region was chosen by examining when the heat capacity values continuously

time (s)	T_{ave} (°C)	Electrical Energy (J)	ρc $\left[\frac{J}{cm^3 °C}\right]$
0.5	20.10	25	1.2732
1	20.20	50	2.5465
2	20.40	100	2.5465
3	20.50	250	1.9099
4	20.60	200	2.0372
5	20.70	250	2.1221
6	20.80	300	2.1827
7	20.90	350	2.2282
8	21.10	400	2.2635
9	21.20	450	2.0835
10	21.30	500	2.1221
11	21.40	550	2.1546
12	21.50	600	2.1827
13	21.66	650	2.2070
14	21.76	700	2.1476
15	22.30	750	2.1703
20	22.32	1000	2.2143
30	23.34	1500	2.3010
40	24.34	2000	2.3470
50	25.16	2500	2.4675
60	25.98	3000	2.5550
70	26.66	3500	2.6765
80	27.30	4000	2.7907
90	27.92	4500	2.8937
100	28.48	5000	3.0029
110	28.96	5500	3.1263
120	29.44	6000	3.2371
130	29.86	6500	3.3574
140	30.28	7000	3.4680
150	30.60	7500	3.6035
160	30.92	8000	3.7311
170	31.20	8500	3.8652
180	31.52	9000	3.9789

Averaging ρc between 10s and 14s one obtains

$$\rho c_{est} = 2.163 \frac{J}{cm^3 °C}$$

Table 4.1 : Results of a MEGAERA Simulation of Transient Heat Capacity Method for a Homogeneous Sample with a Heat Capacity of $2.15 \frac{J}{cm^3 °C}$.

increased due to heat losses from the sample becoming significant.

From this simulation one can see that the transient heat capacity technique produces approximately the correct result even with the constant temperature boundary condition imposed at the surface of the cylinder. In other words, heat losses from the sample can be neglected without introducing serious error in the determination of the heat capacity of the sample. The difference between the estimated heat capacity, $\rho c_{est} = 2.163 \frac{J}{cm^3 {}^\circ C}$, and the actual heat capacity of $\rho c = 2.15 \frac{J}{cm^3 {}^\circ C}$ is only 0.6%.

As the diffusivity of the sample decreases the length of Region 2 of Figure 2.8 becomes longer because heat losses from the sample decrease. For instance, by doubling the heat capacity of the sample, $\rho c = 4.3 \frac{J}{cm^3 {}^\circ C}$, (or decreasing the diffusivity by a factor of two) one obtains the following results shown in Table 4.2.

Notice how the length of Region 2 has increases from 10-14 s to 7-50 s when the heat capacity of the sample has been doubled to $4.30 \frac{J}{cm^3 {}^\circ C}$. The difference between the simulated heat capacity and actual heat capacity is again less than 1%.

time (s)	T_{ave} (°C)	Electrical Energy (J)	ρc $\left[\frac{J}{cm^3 °C}\right]$
0.5	20.00	25	∞
1	20.10	50	2.5465
2	20.10	100	5.0930
3	20.20	250	3.8197
4	20.20	200	5.0930
5	20.30	250	4.2441
6	20.40	300	3.8187
7	20.40	350	4.4563
8	20.50	400	4.0744
9	20.50	450	4.5837
10	20.60	500	4.2441
11	20.66	550	4.2441
12	20.70	600	4.3654
13	20.80	650	4.1380
14	20.80	700	4.4563
15	20.90	750	4.2441
20	21.20	1000	4.2441
30	21.76	1500	4.3406
40	22.30	2000	4.4287
50	22.86	2500	4.4519
60	23.32	3000	4.6021
70	23.88	3500	4.5942
80	24.34	4000	4.6940
90	24.80	4500	4.7747
100	25.16	5000	4.9350
110	25.58	5500	5.0199
120	25.98	6000	5.1100
130	26.30	6500	5.2546
140	26.66	7000	5.3530
150	27.02	7500	5.4412
160	27.64	8000	5.5813
170	27.64	8500	5.6663
180	27.92	9000	5.7875

Averaging ρc between 10s and 14s one obtains

$$\rho c_{est} = 4.328 \frac{J}{cm^3 °C}$$

Table 4.2 : Results of a MEGAERA Simulation of Transient Heat Capacity Method for a Homogeneous Sample with a Heat Capacity of $4.3 \frac{J}{cm^3 °C}$.

To simulate the response in a non-homogeneous sample, the sample was divided into 5 regions of equal volume, as shown in Figure 4.6. The properties of each region were arbitrarily chosen. However, the variation of these properties are believed to be greater than the variation of these same properties in actual shale samples.

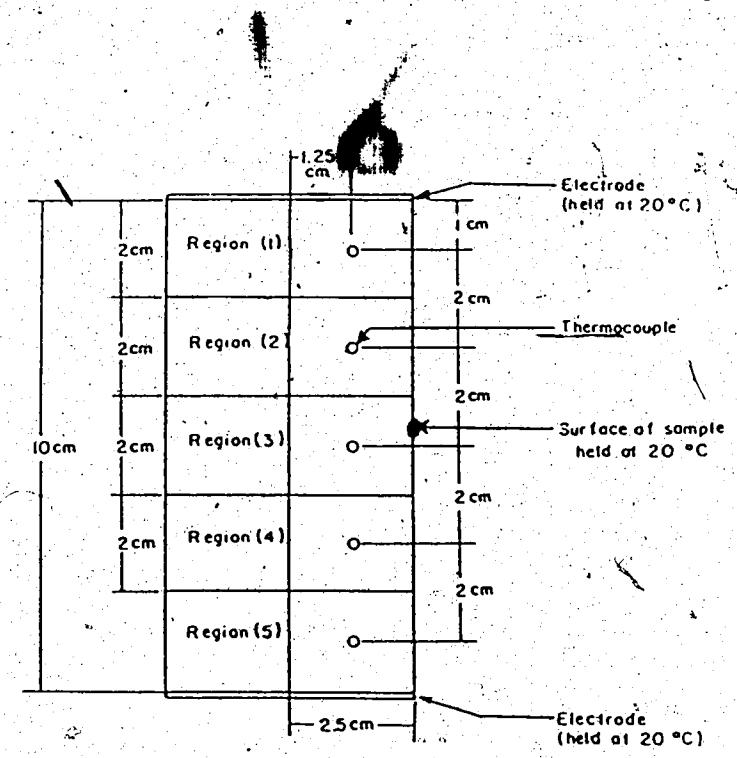

Figure 4.6 : Non-Homogeneous Heat Capacity Problem Simulated by MEGAERA

The properties selected for each of the regions were:

Region (1)	$\rho c = 2.3 \frac{J}{cm^3 {}^\circ C}$	$\sigma_{24} = 0.2 \frac{S}{m}$
	$K = 2 \frac{K}{m\,{}^\circ C}$	$\alpha = 0.03\ {}^\circ C^{-1}$
Region (2)	$\rho c = 2.225 \frac{J}{cm^3 {}^\circ C}$	$\sigma_{24} = 0.2125 \frac{S}{m}$
	$K = 1.875 \frac{K}{m\,{}^\circ C}$	$\alpha = 0.03\ {}^\circ C^{-1}$
Region (3)	$\rho c = 2.15 \frac{J}{cm^3 {}^\circ C}$	$\sigma_{24} = 0.275 \frac{S}{m}$
	$K = 1.75 \frac{K}{m\,{}^\circ C}$	$\alpha = 0.03\ {}^\circ C^{-1}$
Region (4)	$\rho c = 2.075 \frac{J}{cm^3 {}^\circ C}$	$\sigma_{24} = 0.3375 \frac{S}{m}$
	$K = 1.625 \frac{K}{m\,{}^\circ C}$	$\alpha = 0.03\ {}^\circ C^{-1}$
Region (5)	$\rho c = 2 \frac{J}{cm^3 {}^\circ C}$	$\sigma_{24} = 0.4 \frac{S}{m}$
	$K = 1.5 \frac{K}{m\,{}^\circ C}$	$\alpha = 0.03\ {}^\circ C^{-1}$

If one proceeds to calculate the heat capacity of the non-homogeneous sample, by using the average temperature rise of the thermocouples with time, as predicted by MEGAERA, one obtains average heat capacities as shown in Table 4.3.

time (s)	T_{ave} (°C)	Electrical Energy (J)	ρc $\left[\frac{J}{cm^3 °C}\right]$
0.5	20.06	25	2.1220
1	20.12	50	2.1221
2	20.26	100	1.9588
3	20.34	250	2.2469
4	20.46	200	2.2143
5	20.58	250	2.1952
6	20.70	300	2.1827
7	20.78	350	2.2853
8	20.92	400	2.2143
9	21.06	450	2.1621
10	21.18	500	2.1580
11	21.30	550	2.1547
12	21.40	600	2.1827
13	21.52	650	2.1779
14	21.60	700	2.2282
15	21.72	750	2.2208
20	22.28	1000	2.2338
30	23.32	1500	2.3010
40	24.22	2000	2.4134
50	25.08	2500	2.5064
60	25.84	3000	2.6162
70	26.54	3500	2.7256
80	27.18	4000	2.8373
90	27.76	4500	2.9534
100	28.28	5000	3.0755
110	28.78	5500	3.1903
120	29.18	6000	3.3287
130	29.64	6500	3.4305
140	30.00	7000	3.5651
150	30.34	7500	3.6941
160	30.64	8000	3.8293
170	30.94	8500	3.9571
180	31.22	9000	4.0853

Averaging ρc between 9s and 11s one obtains

$$\rho c_{est} = 2.158 \frac{J}{cm^3 °C}$$

Table 4.3 : Results of a MEGAERA Simulation of Transient Heat Capacity Method for a Non-Homogeneous Sample.

For non-homogeneous samples, an average or apparent heat capacity must be defined. To define such a heat capacity consider the following.

Assume that for a non-homogeneous sample, the temperature is changed from one *uniform* temperature distribution to another *uniform* temperature distribution. The change in the energy of the entire sample due to this temperature change is

$$\Delta E = \rho c_{ave} \Delta T \, (VOL) \qquad (4.5)$$

where ΔE = the change in the energy (J) of the entire sample

ρc_{ave} = average or apparent heat capacity of the entire sample $\left[\frac{J}{m^3 {}^\circ C}\right]$

ΔT = the change in the temperature ($^\circ C$) of the sample

(VOL) = volume of the sample (m^3)

For each region, i, in the sample with uniform volumetric heat capacity, ρc_i, the change in energy is

$$\Delta E_i = \rho c_i \Delta T \, (VOL_i) \qquad (4.6)$$

where ΔE_i = change in energy of region i (J)

ρc_i = volumetric heat capacity of region i $\left(\frac{J}{m^3 {}^\circ C} \right)$

ΔT = change in temperature of sample ($^\circ C$)

(VOL_i) = volume of region i (m^3)

Now equations (4.5) and (4.6) can be equated as follows

$$\Delta E = \sum \Delta E_i \rightarrow \rho c_{ave} \Delta T(VOL) = \sum \rho c_i \Delta T(VOL_i)$$

$$\text{or } \rho c_{ave} = \sum \rho c_i \frac{(VOL_i)}{(VOL)} \qquad (4.7)$$

For the MEGAERA simulation, the volume of each region is the same. Therefore the heat capacity of the sample is the average of all 5 regions or $\rho c_{ave} = 2.15 \frac{J}{cm^3 {}^\circ C}$.

The temperature distribution of non-homogeneous samples will generally be non-uniform. Hence, an average temperature change, ΔT_{ave}, must also be defined. This average temperature change in a non-homogeneous sample is defined such that

$$\Delta E = \rho c_{ave} \Delta T_{ave} (VOL) \qquad (4.8)$$

where ρc_{ave} = the average heat capacity $\left[\frac{J}{m^3 {}^\circ C}\right]$ of the sample as defined in equation (4.7)

ΔE_o = the total change in the heat energy (J) of the sample

(VOL) = the total volume of the sample (m^3)

For each region, i, in the sample with the same volumetric heat capacity, ρc_i, and temperature change, ΔT_i, the change in energy is

$$\Delta E_i = \rho c_i \Delta T_i (VOL_i) \tag{4.9}$$

where ΔE_i = change in energy of region i (J)

ρc_i = volumetric heat capacity of region i $\left[\frac{J}{m^3 {}^\circ C}\right]$

ΔT_i = change in temperature of region i ($^\circ C$)

(VOL_i) = volume of region i (m^3)

Equating equation (4.8) and (4.9), where each side of the latter is summed over the entire sample, and solving for ΔT_{ave} one obtains

$$\Delta E = \sum \Delta E_i \rightarrow \Delta T_{ave} = \frac{\sum \rho c_i \Delta T_i (VOL_i)}{\rho c_{ave} (VOL)} \tag{4.10}$$

Substituting equation (4.7) into (4.9), ΔT_{ave} can be expressed as

$$\Delta T_{ave} = \frac{\sum \rho c_i \Delta T_i (VOL_i)}{\sum \rho c_i (VOL_i)} \qquad (4.11)$$

In actual experiments the average temperature of the sample cannot be found using equation (4.11) since one has no prior knowledge regarding the distribution of non-homogeneities in the sample. Experimentally then, the average temperature of the sample can at best be estimated by simply averaging the thermocouple readings. Thus,

$$\Delta T'_{ave} = \frac{1}{N} \sum_{1}^{N} \Delta T_i \qquad (4.12)$$

and therefore

$$\rho c_{expt} = \frac{E}{\Delta T'_{ave} (VOL)} \qquad (4.13)$$

When $\Delta T'_{ave} \cong \Delta T_{ave}$

or $$\frac{1}{N} \sum_{1}^{N} \Delta T_i \cong \frac{\sum \rho c_i \Delta T_i (VOL_i)}{\sum \rho c_i (VOL_i)} \qquad (4.14)$$

equation (4.13) will produce an accurate estimate for the average heat capacity of the sample, $\rho c_{ave} \cong \rho c_{expt}$. The non-homogeneity of

the problem simulated by MEGAERA is believed to be greater than that in an actual experiment. Hence, if equation (4.14) is satisfied in this simulation, it is likely to hold true in an actual experiment. In this simulation at time t=11s, ΔT_{ave} and $\Delta T'_{ave}$, the two sides of equation (4.14) differed by only 1.3% even though there is a 14% variation in the heat capacity of the sample, as shown in the following table.

At time t=11 seconds

electrical energy = 550 Joules

$VOL_i = 2.5^2\pi 2 = 39.2699\ cm^3$

Region	ΔT	ρc_i	$\rho c_i VOL_i$	$\rho c_i \Delta T_i (VOL_i)$
1	1.9	2.3	90.3208	171.6095
2	1.5	2.225	87.3755	131.0633
3	1.2	2.15	84.4303	101.3164
4	1.0	2.075	81.4851	81.4851
5	0.9	2.0	78.5398	70.6858
	$\Sigma 6.5$		$\Sigma 422.1515$	$\Sigma 556.1601$

$$\Delta T_{ave} = \frac{556.1601}{422.1515} = 1.3174\ ^{\circ}C$$

$$\Delta T'_{ave} = \frac{6.5}{5} = 1.3\ ^{\circ}C$$

Table 4.4 : Verification of equation (4.14) by example.

From the results presented in Table 4.4, it would seem therefore that equation (4.12) provides an adequate definition for the average sample temperature. It should be noted that in actual

experiments, the location of non-homogeneities in the sample will be unknown. Consequently, when thermocouples are inserted into the sample they may not be located within all the non-homogeneities in the sample. This may cause concern that the average temperature, $\Delta T'_{ave}$, of the sample as calculated by equation (4.12) may significantly differ from the true average temperature, ΔT_{ave}, defined by equation (4.11). However, the variation of non-homogeneities in actual samples are believed to be less than those in the MEGAERA simulation problem above. Therefore, in view of the good agreement between ΔT_{ave} and $\Delta T'_{ave}$ in the foregoing example, equation (4.12) should be adequate for calculating the average temperature of typical samples used in actual experiments.

The ultimate test of the transient heat capacity method, for a non-homogeneous sample, is whether or not it produces the correct values for heat capacity. From Table 4.3 one can see that there is less than 1% difference between the value of heat capacity deduced from the temperature rise computed by MEGAERA, $\rho c_{est} = 2.158 \frac{J}{cm^3 °C}$, and the actual average value of heat capacity, $\rho c_{ave} = 2.15 \frac{J}{cm^3 °C}$, of the materials in the simulated sample.

4.3.2 Transient Heat Capacity Experiments on Materials with Published Thermal Properties

The transient heat capacity apparatus and method were tested on materials with known, or approximately known, thermal properties. Specifically, these materials were homogeneous sand/water samples,

tap water samples, and oilsand samples. The results of these experiments are shown below.

For the homogeneous sand/water sample, the apparatus and method presented in the previous two Sections 4.1 and 4.2 were used and the following results obtained.

Homogeneous sand/water experiment # 53

Composition of the sample by mass

	before expt	after expt
%water =	3.7%	(3.3%)
%sand =	96.3%	(96.7%)

Density of sample $\rho = 1.74 \frac{g}{cm^3}$

A published value for the heat capacity of the sand/water sample was determined using the compositional average specific heat (see equation (2.5)) based upon the component values by Hepler[56]. The specific heat of the sand used in this experiment was estimated from Table 5 of Hepler et al (1985) using the source *Athabasca coarse solids mostly* SiO_2 *>325 mesh*, at 27°C, and the following

---

[56]Hepler, (1985)

value calculated.

$$c_{sand} = 0.7556 \frac{J}{g\,^{\circ}C}$$

For water the specific heat value used was[57]

$$c_{water} = 4.18 \frac{J}{g\,^{\circ}C} \qquad \text{(from } 16^{\circ}C \text{ to } 61^{\circ}C\text{)}$$

and averaging the measured composition of the sample before and after the experiment one obtains

$$\%water = 3.5\%$$

$$\%sand = 96.5\%$$

Using equation (2.5) one obtains the following estimate for the heat capacity of the sand/water sample at 27°C.

$$c_{Hepler} = 0.8755 \frac{J}{g\,^{\circ}C}$$

$$\rho c_{Hepler} = 1.52 \frac{J}{m^3\,^{\circ}C}$$

[57] CRC Handbook of Chemistry and Physics, 55th Edition, (1974-1975)

Results from experiment

time (s)	T_{ave} (°C)	Electrical Energy (J)	$c\left[\frac{J}{g\,^{\circ}C}\right]$
2	25.70	84.50	0.9642
5	26.08	211.87	0.9331
7	26.40	297.49	0.8635
10	26.80	426.77	0.8689
12	27.11	513.27	0.8470
15	27.52	643.52	0.8523
17	27.80	730.76	0.8523
20	28.22	862.08	0.8517
23	28.64	994.38	0.8514
25	28.92	1083.24	0.8536
28	29.28	1217.26	0.8670
30	29.62	1307.06	0.8563
33	30.00	1442.79	0.8641
35	30.33	1533.44	0.8571
38	30.71	1670.10	0.8663
40	30.97	1761.58	0.8694
43	31.38	1899.75	0.8736
46	31.82	2039.28	0.8728
48	32.09	2132.56	0.8750
51	32.50	2272.70	0.8784
53	32.79	2366.73	0.8784
56	33.14	2509.51	0.8887
58	33.47	2605.23	0.8849
61	33.83	2749.21	0.8930
63	34.10	2845.68	0.8958
80	36.47	3679.71	0.9090
96	38.56	4492.96	0.9329
113	40.89	5385.32	0.9490
129	42.97	6254.17	0.9710
146	45.18	7205.10	0.9936

Averaging c between 7s and 38s one obtains

$$c_{expt} = 0.86\ \frac{J}{g\,^{\circ}C}$$

$$\rho c_{expt} = 1.49\ \frac{J}{g\,^{\circ}C}$$

Table 4.5 : Results of Heat Capacity Experiment # 53 on Homogeneous Sand/Water Sample.

The heat capacity, $\rho c_{expt} = 1.49 \frac{J}{cm^3 {}^\circ C}$, found by experiment # 53 is 2% less than the Hepler result of $\rho c_{Hepler} = 1.52 \frac{J}{cm^3 {}^\circ C}$.

A further experiment on a sand/water sample, described below, produced similar results.

Homogeneous sand/water experiment # 54

Composition of the sample by mass

	before expt	after expt
%water =	3.6%	(3.4%)
%sand =	96.4%	(96.6%)

Density of sample $\rho = 1.77 \frac{g}{cm^3}$

An estimate of the heat capacity of sample using results from Hepler et al (1985).

$$\rho c_{Hepler} = 1.54 \frac{J}{cm^3 {}^\circ C} \qquad (@\ 27^\circ C)$$

Result from experiment

time (s)	T_{ave} (°C)	Electrical Energy (J)	$c \left[\frac{J}{g\,^{\circ}C} \right]$
2	24.59	82.39	0.8660
5	24.97	206.41	0.8716
7	25.28	289.59	0.8221
10	25.66	415.11	0.8458
12	25.97	498.92	0.8254
15	26.35	625.02	0.8361
17	26.61	709.72	0.8426
20	27.03	837.58	0.8405
23	27.45	966.51	0.8383
25	27.73	1053.12	0.8392
28	28.08	1183.83	0.8561
30	28.38	1271.47	0.8500
33	28.76	1403.91	0.8584
35	29.07	1492.64	0.8530
38	29.46	1626.50	0.8593
40	29.76	1716.16	0.8558
43	30.12	1851.42	0.8656
46	30.39	1942.12	0.8681
48	30.79	2078.85	0.8723
51	31.21	2216.52	0.8723
53	31.49	2308.68	0.8736
56	31.84	2447.57	0.8825
58	32.14	2540.60	0.8808
61	32.51	2680.81	0.8877
63	32.77	2774.84	0.8904
80	35.05	3590.69	0.9073
96	37.09	4382.40	0.9306
113	39.35	5252.04	0.9476
129	41.38	6093.90	0.9685

Averaging c between 7s and 25s one obtains

$$c_{expt} = 0.84 \frac{J}{g\,^{\circ}C}$$

$$\rho c_{expt} = 1.48 \frac{J}{g\,^{\circ}C}$$

Table 4.6 : Results of Heat Capacity Experiment # 54 on Homogeneous Sand/Water Sample.

For this experiment the heat capacity, $\rho c_{expt} = 1.48 \frac{J}{cm^3 {}^\circ C}$, is 4% less than the theoretical value of $\rho c_{Hepler} = 1.54 \frac{J}{cm^3 {}^\circ C}$.

Experiments on tap water samples were done on a preliminary heat capacity apparatus, which failed because the apparatus was not strong enough to withstand the pressure applied to the electrodes. This apparatus consisted of a very thin 0.1588 cm plexiglas sleeve surrounded by Styrofoam insulation. The results of experiments with this apparatus were, nevertheless, useful in the design of the final apparatus. The heat capacity of tap water[58] used was

$$c_{water} = 4.18 \frac{J}{g {}^\circ C} \qquad \text{(from 16 °C to 61 °C)}$$

For the *Water experiment # 42*, shown in Table 4.7, the heat capacity of $c_{expt} = 4.24 \frac{J}{g {}^\circ C}$ found in this experiment is 1.4% higher than the theoretical value of $c_{water} = 4.18 \frac{J}{g {}^\circ C}$. A second experiment, *Water experiment # 43*, on a tap water sample, produced similar results. Table 4.8 contains the results from this experiment which produced a specific heat value, $c_{expt} = 4.09 \frac{J}{g {}^\circ C}$, that is 2.2% lower than $c_{water} = 4.18 \frac{J}{g {}^\circ C}$.

---

[58] CRC Handbook of Chemistry and Physics, 55th Edition, (1974-1975)

Water experiment # 42

time (s)	T_{ave} (°C)	Electrical Energy (J)	c $\left[\frac{J}{g\,^{\circ}C}\right]$
2.0	22.78	76.48	37.0005
5.0	22.86	191.47	10.2924
8.5	23.03	325.90	6.0642
12.0	23.19	460.39	5.3032
15.0	23.34	576.49	4.8930
18.5	23.49	712.23	4.7857
22.0	23.67	848.46	4.5609
25.0	23.83	965.74	4.4077
28.5	24.00	1103.10	4.3388
31.5	24.15	1221.11	4.2809
35.0	24.32	1359.42	4.2431
38.0	24.46	1478.38	4.2321
41.5	24.61	1617.51	4.2529
45.0	24.76	1756.92	4.2713
48.0	24.91	1876.60	4.2425
51.5	25.08	2016.57	4.2234
55.0	25.23	2156.87	4.2418
58.0	25.38	2277.79	4.2221
61.5	25.54	2419.32	4.2255
64.5	25.66	2540.89	4.2535
68.0	25.82	2682.80	4.2555
71.0	25.97	2804.92	4.2406
74.5	26.12	2947.85	4.2572
78.0	26.27	3091.39	4.2731
81.0	26.41	3214.97	4.2730
84.5	26.57	3359.78	4.2775
88.0	26.71	3504.93	4.3037
91.0	26.86	3629.69	4.2934

Averaging c between 38s and 74.5s one obtains

$$c_{expt} = 4.24\ \frac{J}{g\,^{\circ}C}$$

Table 4.7 : Results of Heat Capacity Experiment # 42 on Water Sample.

Water experiment # 43

time (s)	T_{ave} (°C)	Electrical Energy (J)	c $\left[\frac{J}{g\,^{\circ}C}\right]$
2.0	30.24	87.16	4.6853
5.0	30.42	218.11	3.9082
8.5	30.59	371.36	4.0832
12.0	30.76	524.83	4.1624
15.0	30.93	656.63	4.0727
18.5	31.11	811.18	4.0879
22.0	31.28	965.97	4.1357
25.0	31.46	1098.95	4.0585
28.5	31.64	1254.86	4.0744
31.5	31.78	1389.10	4.1229
35.0	31.96	1545.98	4.1322
38.0	32.13	1680.56	4.1063
41.5	32.29	1838.30	4.1559
45.0	32.44	1996.45	4.2178
48.0	32.61	2132.52	4.1939
51.5	32.78	2291.87	4.2159
55.0	32.95	2451.76	4.2362
58.0	33.13	2589.44	4.2039
61.5	33.31	2750.43	4.2109
64.5	33.46	2888.90	4.2224
68.0	33.65	3050.98	4.2173
71.0	33.82	3190.42	4.2057
74.5	34.00	3353.56	4.2141
78.0	34.17	3517.12	4.2327
81.0	34.33	3657.85	4.2336
84.5	34.50	3822.59	4.2514
88.0	34.67	3987.78	4.2683

Averaging c between 5s and 41.5s one obtains

$$c_{expt} = 4.09 \frac{J}{g\,^{\circ}C}$$

Table 4.8 : Results of Heat Capacity Experiment # 43 on Water Sample.

Finally, an experiment on an oil sand sample was done with the same apparatus that was used with water samples. However, in this oil sand experiment the thermocouples had an additional plastic sheath over the metal sheath as shown in Figure 4.7. Plastic sheath thermocouples were initially used in preliminary transient heat capacity experiments to protect the thermocouples from short circuiting with the sample. It was later discovered that the thermocouples could be used without the protective plastic sheath when appropriate precautions, as outline in Section 4.2, were taken.

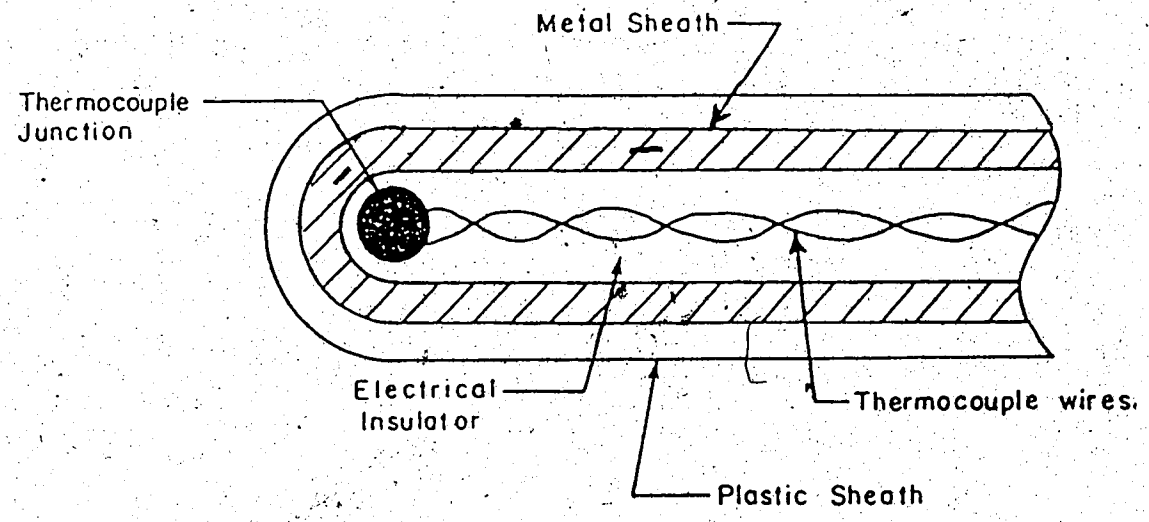

Figure 4.7 : Diagram of Plastic Sheath Thermocouple

This plastic sheath causes the response of the thermocouple to be very slow and might be expected to cause considerable error in the

heat capacity measurement.

This oilsand experiment, presented on the following pages, demonstrated that even with these plastic sheath thermocouples, which have a very slow response, the heat capacity apparatus still produced heat capacity results which were acceptable.

Oilsands experiment # 40

Composition of the sample by mass using the Dean Stark compositional analysis apparatus:

%water = 7.01%

%sand = 84.8%

%oil = 8.18%

Density of sample: $\rho = 2.04 \frac{g}{cm^3}$

An estimate of the heat capacity of the sample using the results of Hepler[59], with the specific heat of the bitumen estimated from Table 1 of Hepler et al (1985), using the source *Athabasca, from Alberta Research Council, Petro-Canada, and Syncrude,* at 36°C

[59]Hepler, (1985)

$$c_{bitumen} = 1.7361 \frac{J}{g\,^{o}C}$$

For the specific heat of the sand, Table 5 of Hepler et al (1985), using the source *Athabasca fine solids, mostly clays, <325 mesh*, at 36°C

$$c_{sand} = 0.8325 \frac{J}{g\,^{o}C}$$

The specific heat of water used was

$$c_{water} = 4.18 \frac{J}{g\,^{o}C} \qquad \text{(from 16°C to 61°C)}$$

Using equation (2.5) one obtains the following estimate for the heat capacity of the sand/water sample

$$c_{Hepler} = 1.141 \frac{J}{g\,^{o}C}$$

$$\rho c_{Hepler} = 2.33 \frac{J}{cm^{3}\,^{o}C}$$

Results from experiment

time (s)	T_{ave} (°C)	Electrical Energy (J)	$c \left[\frac{J}{g\,^\circ C} \right]$
6.5	26.29	421.29	1.5101
10.0	26.64	609.34	1.4504
13.5	27.01	799.26	1.3990
16.5	27.36	963.71	1.3441
19.5	27.72	1129.59	1.3060
22.5	28.05	1296.49	1.2963
26.0	28.40	1491.86	1.3042
29.5	28.79	1689.24	1.2952
32.5	29.18	1859.78	1.2727
35.5	29.56	2031.75	1.2572
38.5	29.90	2205.15	1.2545
42.0	30.27	2409.05	1.2613
45.5	30.68	2614.37	1.2581
48.5	31.06	2792.06	1.2504
51.5	31.46	2971.18	1.2409
54.5	31.84	3151.86	1.2354
58.0	32.22	3363.79	1.2416
61.5	32.62	3576.52	1.2451
64.5	33.03	3760.76	1.2377
67.5	33.43	3946.25	1.2322
70.5	33.79	4133.65	1.2340
74.0	34.19	4354.59	1.2384
77.5	34.62	4576.99	1.2398
80.5	35.03	4768.94	1.2354
83.5	35.46	4962.35	1.2304
86.5	35.84	5157.18	1.2308
90.0	36.26	5386.19	1.2349
93.5	36.70	5616.63	1.2361
100.5	37.61	6081.97	1.2374
110.5	38.98	6762.17	1.2345
120.5	40.28	7459.95	1.2414
130.5	41.67	8173.47	1.2421

Averaging c between 51.5s and 110.5s one obtains

$$c_{expt} = 1.24 \frac{J}{g\,^\circ C}$$

$$\rho c_{expt} = 2.52 \frac{J}{cm^3\,^\circ C}$$

Table 4.9 : Results of Heat Capacity Experiment # 40 on an Oil Sands Sample.

The experimental estimate of the heat capacity of this oilsand sample was 8.3% higher than predicted. This relatively large error was in part due to the delayed rise in the temperature of the plastic sheathed thermocouples. Such delays will increase the heat capacity value that is estimated from the transient heat capacity method.

In conclusion, MEGAERA simulation and experimental results on samples with known, or approximately known, thermal properties, demonstrate that the transient heat capacity method used in this research is capable of predicting the effective heat capacity of materials with acceptable accuracy.

4.4 Experimental Heat Capacity Results on Shale

The following tables summarize the experimental heat capacity results obtained on Clearwater shale samples. For a more thorough summary of the experiments presented in Tables 4.10a) and b) see Appendix E. The $c_{mineral}$ values in the following tables are estimates for the heat capacity of the mineral fraction of the Clearwater shale samples. These estimates for $c_{mineral}$ were determined using equation (2.5) where c_{eff} and the composition of the sample were experimentally found, and the specific heat of water was $4.18 \frac{J}{g\,^{o}C}$. Equation (2.5) could then be solved for $c_{mineral}$ using the composition of the sample before and after the experiment, and the results are listed in Tables 4.10.

For well 36-51-0-0

Experiment Number	Sample	$\rho c \left(\frac{J}{cm^3 {}^\circ C}\right)$	$c_{mineral} \left(\frac{J}{g\,{}^\circ C}\right)$	Composition of Sample	
				%mineral	%water
50	P4 ,A	3.17	0.74 - 0.81	80.3 - 82.1	19.7 - 17.9
55	P4 ,H	3.06	0.74 - 0.73	79.2 - 78.8	20.8 - 21.2
58	P27,E	2.70	0.80 - 0.89	87.2 - 84.9	12.8 - 15.1
61	P23,C	2.49	0.73 - 0.79	89.2 - 87.5	10.8 - 12.5
64	P19,L	3.02	0.86 - 0.91	85.2 - 86.5	14.8 - 13.5
65	P9 ,E	3.11	0.81 - 0.92	80.7 - 83.5	19.3 - 16.5
66	P16,B	2.96	0.80 - 0.86	84.4 - 85.6	15.6 - 14.4
69	P25,M	3.04	0.85 - 0.94	83.1 - 85.4	16.9 - 14.6
74	P24,D	3.20	0.77 - 0.88	79.9 - 82.5	20.1 - 17.5

$$c_{mineral,ave} = 0.82 \frac{J}{g\,{}^\circ C}$$

Table 4.10a) : Heat Capacity results for Well 36-51-0-0

For well 34-51-0-0

Experiment Number	Sample	$\rho c \left(\frac{J}{cm^3 {}^\circ C}\right)$	$c_{mineral} \left(\frac{J}{g\,{}^\circ C}\right)$	Composition of Sample	
				%mineral	%water
56	P17,A	2.87	0.74 - 0.79	84.2 - 85.2	15.8 - 14.8
57	P 2,C	2.78	0.73 - 0.75	84.3 - 84.0	15.4 - 16.0
59	P21,B	3.35	0.83 - 0.90	76.5 - 75.0	23.5 - 25.0
62	P29,A	2.90	0.69 - 0.85	82.5 - 86.6	17.5 - 13.4
67	P16,H	3.23	0.75 - 0.90	80.5 - 84.2	19.5 - 15.8
80	P 8,H	2.90	0.77 - 0.83	83.4 - 84.9	16.6 - 15.1

$$c_{mineral,ave} = 0.79 \frac{J}{g\,{}^\circ C}$$

Table 4.10b) : Heat Capacity results for Well 34-51-0-0

These results for the volumetric heat capacity of Clearwater shale are higher than a previously published result of Somerton[60] which was determined using a Bunsen-type calorimeter, and is

$$\rho c = 2.13 \frac{J}{cm^3 {}^\circ C}$$

However, as mentioned at the end of Section 3.5, the shale used by Somerton would appear to differ from Clearwater shale.

The average specific heat values for mineral fraction of the shale, $c_{mineral} = 0.81 \frac{J}{g\,{}^\circ C}$, however, did agree well with published results of Somerton[61] for the mineral fraction of shale and Hepler[62] for *Athabasca fine solids mostly clays, <325 mesh*, at 27 °C.

$$c_{mineral} = 0.80 \frac{J}{g\,{}^\circ C} \text{ (Somerton)}$$

$$c_{mineral} = 0.82 \frac{J}{g\,{}^\circ C} \text{ (Hepler)}$$

[60] Somerton, (1958)

[61] Somerton, (1958)

[62] Hepler., (1985)

5.0 Conclusions and Suggestions for Further Work

Two methods, one for measuring thermal conductivity and the other for measuring heat capacity, were studied by means of numerical simulations to gain a thorough understanding of their limitations. Concurrently, experimental apparatus capable of measuring the thermal conductivity and heat capacity of Clearwater shale samples were designed and built. Using these apparatus, the thermal conductivity and heat capacity of Clearwater shale were determined from temperature within carefully chosen intervals in the experimentally obtained temperature versus time data, to yield results that were unaffected by inherent shortcomings of the experimental apparatus. As well, thermocouple placement in the case of the heat capacity measurements was judiciously selected to minimize errors due to loss of heat from the transient heat capacity apparatus.

Values of thermal conductivity and heat capacity were obtained for Clearwater shale samples from two Syncrude Canada Limited wells, 34-51-0-0 and 36-51-0-0, located northeast of the Syncrude mine site at Section 8, Township 93, Range 11, west of the 4th Meridian. These values were

$$K = 1.74 \text{ to } 2.09 \ \frac{W}{m\,^{\circ}C} \quad \text{for well 36-51-0-0}$$

$$1.70 \text{ to } 2.26 \ \frac{W}{m\,^{\circ}C} \quad \text{for well 34-51-0-0}$$

$$\rho c = 2.49 \text{ to } 3.23 \ \frac{J}{cm^3\,^{\circ}C} \quad \text{for well 36-51-0-0}$$

$$2.78 \text{ to } 3.35 \frac{J}{cm^3 {}^oC} \text{ for well 34-51-0-0}$$

Using the weighted average method, equation (2.5), for determining the effective heat capacity of the mineral component of Clearwater shale, yields the following average specific heat value

$$c_{mineral,ave} = 0.81 \frac{J}{g\,{}^oC}$$

Using the MEGAERA numerical program, numerical simulations of the apparatus used in this research were conducted for a much greater range of conditions than those present in actual physical experiments. In numerical simulations of the transient heat probe method, axial heat flow was significantly increased by using solid probes which were shorter in length than the hollow probes used in actual experiments. Also, the simulated samples were smaller in diameter than actual samples. This greatly increased the effects that are caused by the heat front from the probe reaches the outer surface of the sample. For the transient heat capacity method, problems were simulated with samples which had larger variations in non-homogeneities than actual samples. Furthermore, heat losses from the sample were made larger than in actual experiments by imposing a constant temperature on the outer surface of the simulated sample. Both the transient heat probe and heat capacity simulations produced internally consistent results under these conditions, and increased confidence in the methods and apparatus

developed.

For future investigations of the thermal conductivity of shale with the transient thermal conductivity probe, further accuracy could be gained by using a more sensitive temperature measurement device.

Future investigations should consider, in addition to the methods presented here, the technique developed by Iida et al[63], which was briefly described in section 2.0 of this thesis. This transient method, by Iida et al, allows all of the thermal properties of a sample to be determined simultaneously. Very accuracy placement of thermocouples and frequent monitoring of the thermocouples is, however, necessary. Such a method used in conjunction with the methods described in this thesis, could provide valuable additional data in the determination of the thermal properties of shale.

---

[63]Iida, Ohtani, and Stephan, (1984)

Bibliography

Alberta Energy Resources Conservation Board (ERCB), December 31, 1986

ASTM, "Steady-State Heat Flux Measurements and Thermal Transmission Properties by Means of the Guarded-Hot-Plate Apparatus", C 177-85, (1985)

ASTM, "Using the Guarded-Hot-Plate Apparatus in the Onesided Mode to Measure Steady-State Heat Flux and Thermal Transmission Properties", C 1044-85, (1985)

Batty, W.J., O'Callaghan, P.W., and Probert, S.D., "Assessment of the Thermal Probe Technique for Rapid, Accurate Measurement of Effective Thermal Conductivities", Applied Energy, vol.16, pp83-113, (1984)

Blackwell, J.H., "Radial-Axial Heat Flow in Regions Bounded Internally by Circular Cylinders", Canadian Journal of Physics, vol.31, pp472-479, (1953)

Blackwell, J.H., "A Transient-Flow Method for Determination of Thermal Constants of Insulating Materials in Bulk", J. Appl. Phys., vol.25, no.2, pp137-144, (1954)

Blackwell, J.H., "The Axial-Flow Error in the Thermal Conductivity Probe", Canadian Journal of Physics, vol.34, pp412-417, (1956)

Bruijn, P.J., van Haneghem, I.A., Schenk, J., and Boshoven, H.P.A., "An Improved Nonsteady-State Probe Method for Measurements in Granular Materials", High Temperatures - High Pressures, vol.15, pp359-374, (1983)

Carslaw, H.S. and Jaeger, J.C., Conduction of Heat in Solids, Oxford University Press, London, (1959)

Cervenan, M.R., Vermeulen, F.E., and Chute, F.S., "Thermal Conductivity and Specific Heat of Oilsands Samples", Can. J. Earth Sciences, vol.18, no.5, pp926-931, (1981)

DeVries, D.A. and Peck, A.J., "On the Cylindrical Probe Method of Measuring Thermal Conductivity with Special Reference to Soils", Australian Journal of Physics, vol.11, pp255-271, (1958)

Erdman, C.A. and Schilmoeller, N.H., "Dymnamic Technique for Measuring Thermal Conductivity in Cylindrical Geometry", J. Appl. Phys., vol.44, no.7, pp3127-3129, (1973)

Glatzmaier, G.C. and Ramirez, W.F., "Simultaneous Measurement of the Thermal Conductivity and Thermal Diffusivity of Unconsolidated Materials by the Transient Hot Wire Method", Rev. Sci. Instrum., vol.56, no.7, pp1394-1398, (1985)

Hanafi, A. and Kiram, G.A., "The Thermal Conductivity of Oilsands Using a Transient Method", Journal of Energy Resources Technology, vol.108, no.4, pp315-320, (1986)

Hepler, L.G., et al, "Specific Heat Capacities of Bitumens and Heavy Oils, Reservoir Minerals, Clays, Dehydrated Clays, Asphaltenes, and Cokes", AOSTRA Journal of Research, vol.1, no.3, pp163-173, (1985)

Hiebert, A.D., "Computer Simulation of In-situ, Low Frequency, Electrical Heating of Oilsand Formations", M.Sc. Thesis, University of Alberta, (1981)

Hiebert, A.D., Capjack, C.E., Chute, F.S., and Vermeulen, F.E., "A Simulation Code for Investigating 2D Heating of Material Bodies by Loss Frequency Electric Fields", Appl. Math. Modelling, vol.7, pp366-371, (1983)

Holtz, R.D. and Kovacs, W.D., An Introduction to Geotechnical Engineering, Prentice-Hall, Inc., (1981)

Iida, Y., Ohtani, S., and Stephan, K., "Experimental Method to Determine the Heat Production Rate, Thermal Diffusivity, and Conductivity of Solid", Rev. Sci. Instrum., vol.55, no.10, pp1648-1653, (1984)

Jaeger, J.C., "Conduction of Heat in a Solid in Contact with a Thin Layer of Good Conductor", Quart. Journ. Mach. and Applied Math., vol.8, part 1, pp101-106, (1955)

Jaeger, J.C., "The Use of Complete Temperature-Time Curves for Determination of Thermal Conductivity with Particular Reference to Rocks", Australian Journal of Physics, vol.12, no.3, pp203-217, (1959)

Lillico, D.A.,"Development of an Oilsands Heat Transfer Cell", M.Sc. Thesis, University of Alberta, (1986)

Nancarrow, H.A., "A Method for the Determination of the Thermal Conductivities of Rocks", Proc. Phys. Soc., vol.45, pp447-461, (1933)

Özisik, M.N., Heat Conduction, John Wiley and Sons, Inc., (1980)

Sandberg, O., Andersson, P., and Bäckström, G., "Heat Capacity and Thermal Conductivity from Pulsed Wire Probe Measurements Under Pressure", Journal of Physics E. Scientific Instruments, vol.10, pp474-477, (1977)

Seto, A.C., "Thermal Testing of Oilsands", M.Sc. Thesis, University of Alberta, (1985)

Somerton, W.H., Keese, J.A., and Chu, S.L., "Thermal Behavior of Unconsolidated Oil Sands", Society of Petroleum Engineering Journal, vol.14, pp513-521, (1974)

Somerton, W.H., "Some Thermal Characteristics of Porous Rocks", Trans. AIME, vol.213, pp375-378, (1958)

Van Der Held, E.F.M. and Van Drunen, F.G., "A Method of Measuring the Thermal Conductivity of Liquids", Physica, vol.15, no.10, pp865-881, (1949)

Vos, B.H., "Measurement of Thermal Conductivity by Non-Steady Method", Appl. Sci. Res., section A, vol.5, pp425-428, (1955)

Wechsler, A.E., "Development of Thermal Conductivity Probes for Soils and Insulations", U.S. Army Cold Regions Research Engineering Laboratory, Technical Report 182, Hanover, NH., (1966)

Woodside, W. and Messmer, J.H., "a) Thermal Conductivity of Porous Media I. Unconsolidated Sands", J. Appl. Phys., vol.32., no.9, pp1688-1699, (1961)

Woodside, W. and Messmer, J.H., "b) Thermal Conductivity of Porous Media II. Consolidated Rocks", J. Appl. Phys., vol.32., no.9, pp1699-1706, (1961)

APPENDIX A : Least Squares Curve Fitting Routine Used to Calculate Thermal Conductivities

The following program listing is for the least squares curve fitting routine used to determine the thermal conductivity of shale samples in this research. This program was written in BASIC and reads an input file containing the temperature and time data of an experiment. The program then plots the temperature versus ln(time) data on the computer monitor and prompts the user to define various regions of the temperature versus ln(time) curve, for which the curve fitting routine should determine the thermal conductivity of the sample. The thermal conductivity of the sample is found using equations (3.7) and (3.8).

Based on the results obtained with this program when used on a personal computer, a log-linear region with a correlation coefficient greater than or equal to 0.95 is found and a range of thermal conductivities in this log-linear region is determined.

The following is a listing of the program:

```
'Initialize Variables

DEFDBL a-z
DIM t(240),tp(240)

'The following two functions are used to plot the
'temperature vs log(time) data on the computer's
'monitor

DEF FNx(t)=(500-10)*(LOG(t)-xmin)/(xmax-xmin)+10
DEF FNy(y)=(15-175)*(y-ymin)/(ymax-ymin)+175

pi=3.141592653589793#

'Open and read the appropriate data file containing
'the temperature, tp(i), and time, t(i), data
```

```
INPUT"file";file$
OPEN "i",#1,"dfl:expt"+file$

INPUT#1,q,dt
PRINT q,dt
i=1
WHILE NOT EOF(1)
  INPUT#1,t(i),tp(i)
  i=i+1
WEND
nn=i-1

'Close the data file

CLOSE#1

'To correct for the actual experiment not starting
'at time t=0, the time data is shifted by dt

FOR i=1 TO nn
  t(i)=t(i)-dt
NEXT

n1=24:n2=34

'Start least squared curve fitting of data between
'times t(n1) and t(n2) and calculate constants (a
'and b) for fit, thermal conductivity (k),
'correlation coefficients (r1 and r2), and the
'average error (min) between the fitted curve and
'the actual data

start:
xx=0
yy=0
x2=0
y2=0
xy=0
n=0
PRINT "Calculating new log-linear fit"
FOR i=n1 TO n2
  xx=xx+LOG(t(i))
  yy=yy+tp(i)
  x2=x2+LOG(t(i))*LOG(t(i))
  y2=y2+tp(i)*tp(i)
  xy=xy+tp(i)*LOG(t(i))
  n=n+1
NEXT

   d=x2*n-xx*xx
   IF(d = 0!) GOTO errr
```

```
    a=(xy*n-yy*xx)/d
    b=(x2*yy-xx*xy)/d
    IF(a = 0!) GOTO errr

    dd=y2*n-yy*yy
    IF(dd = 0!) GOTO errr
    aa=(xy*n-xx*yy)/dd
    bb=(y2*xx-yy*xy)/dd
    IF(aa = 0!) GOTO errr

    k=q/4/pi/a
    r1=a*aa
    r2=-a*bb/b

    min=(y2-2*a*xy-2*b*yy+a*a*x2+2*a*b*xx+b*b*n)/n
    min=SQR(min)

CLS
LOCATE 1,1
PRINT USING"t1=####.#          T1=####.#";t(n1),tp(n1)
PRINT USING"t2=####.#          T2=####.#";t(n2),tp(n2)
PRINT USING" a=##.######        b=####.#######";a,b
PRINT USING" k=##.######      min=  ##.#######";k,min
PRINT USING"r1=##.#######      r2=  ##.#######";r1,r2

'Find maximum and minimum extent of input data and
'plot it on the computer's monitor

FOR i=1 TO nn
  IF 0#<t(i) GOTO skip1
NEXT
skip1:
min=LOG(t(i))
xmax=LOG(t(nn))
ymin=100:ymax=0
FOR i=1 TO nn
  IF tp(i)<ymin THEN ymin=tp(i)
  IF ymax<tp(i) THEN ymax=tp(i)
NEXT

FOR i=1 TO nn
  IF t(i)<=0# GOTO skip2
  x=(500-10)*(LOG(t(i))-xmin)/(xmax-xmin)+10
  y=(15-175)*(tp(i)-ymin)/(ymax-ymin)+175
  PSET(x,y),3
  skip2:
NEXT
y1=a*LOG(t(n1))+b
y2=a*LOG(t(n2))+b
LINE(FNx(t(n1)),FNy(y1))-(FNx(t(n2)),FNy(y2)),1

'The following code reads the mouse position and
'buttons and finds the new region over which the
```

```
'user wants to fit equation (3.7)

again:
PRINT "Ready for new linear range"
CALL range(t1,xmin,xmax)
CALL range(t2,xmin,xmax)

FOR i=1 TO nn
  IF t1<t(i) GOTO skip3
NEXT
skip3:
n1=i
FOR i=n1 TO nn
  IF t2<t(i) GOTO skip4
NEXT
skip4:
n2=i
GOTO start

errr:
PRINT "Bad linear range. Try again"
GOTO again

SUB range(t,xmin,xmax)STATIC

WHILE (0=MOUSE(0))
WEND
x=MOUSE(5)
t=EXP((x-10)*(xmax-xmin)/(500-10)+xmin)
WHILE (0<>MOUSE(0))
WEND

END SUB
```

APPENDIX B : Program Used in HP 3052A Automatic Data Acquisition System for Transient Thermal Conductivity Experiments

The following HP BASIC language program was used during transient thermal conductivity experiments to monitor the temperature rise of the probe and temperature of the ice water reference, which was used to correct for drift in the thermocouple readings.

General Algorithm of program:

1) Reset clock to zero.
2) Read reference thermistor, which is used to calibrate the thermocouple responses.
3) Program stops and waits for the user to restart it, when they are ready to begin the actual thermal conductivity measurement. The program is restarted by the user just before the probe is turned on.
4) Begin monitoring the probe and ice water temperatures every second for the first 100 seconds and then every 10 seconds for the next 1400 seconds.
5) Print uncorrected probe and ice water temperatures.
6) Since the thermocouple readings drift during the experiments, the temperature of the probe must be corrected. This is accomplished by fitting a straight line to the measured ice water temperature, which should be constant but instead can drift by up to ~1 °C. The slope of this straight line is then used

to correct the transient heat probe temperature at a given time by subtracting (slope)×(time) from the measured transient heat probe temperature at this time.

7) Print the corrected probe temperature and the correction factor applied to the probe temperature.

The following is a listing of the actual program:

Set-up variables, initialize HP 3052A system and reset clock to zero.

```
1: dim T[4:5,251],X[3:5,251],W[5]
2: cll 'init'
3: wrt 708,"T"
```

Read reference themistor and wait for user to restart program when they are ready.

```
4: 0⇒r1
5: cll 'dvm'(4,7)
6: cll 'scnl'(0)
7: wait 100
8: 'ref jctn'('rdvm')⇒R
9: "hold":
10: stp
```

Start clock and prepare to read thermocouples by setting D.V.M. to D.C. volts.

```
11: wrt 708,"R"
12: cll 'dvm'(1,7)
```

Begin reading probe and ice water temperatures every second for 100 seconds.

```
13: for J=1 to 100
14: 'clkred'⇒Y
15: if frc(Y/100)*100+frc(int(Y/100)/100)*6000#J;gto 14
16: cll 'displ0'
17: next J
```

Begin reading probe and ice water temperatures

every 10 seconds for the next 1400 seconds.

```
18: for J=11 to 150
19: 'clkred'⇒Y
20: if frc(Y/100)*100+frc(int(Y/100)/100)*6000#J*10;gto 19
21: cll 'displ0'
22: next J
23: dsp "done"
24: beep
25: stp
```

Prepare to print out results

```
26: cll 'print'
27: stp
```

Routine to print out results and correct probe's

temperature

```
28: "print":
```

Print uncorrected probe and ice water temperatures.

```
29: for J=1 to 236 by 5
30: fmt 1,f5.0,f6.2,f6.2,z
31: fmt 2,f5.0,f6.2,f6.2
32: for M=J to J+4
33: X[3,M]⇒Y
34: M-J+1⇒L
35: frc(Y/100)*100+frc(int(Y/100)/100)*6000⇒W[L]
36: next M
37: for P=0 to 3
38: wrt 706.2,W[P+1],T[5,J+P],T[4,J+P]
39: next P
40: wrt 706.2,W[5],T[5,J+4],T[4,J+4]
41: next J
```

Begin to correct drift in measured probe temperature by fitting straight line to ice water results. The probe's temperature is then corrected as described in the algorithm and print out results.

```
42: wrt 706
43: fmt 1,f5.0,f6.2,f6.2,z
44: fmt 2,f5.0,f6.2,f6.2
45: 0⇒r1;0⇒r2;0⇒r3;0⇒r4;0⇒r5
46: for J=1 to 240
47: X[3,J]⇒Y
48: frc(Y/100)*100+frc(int(Y/100)/100)*6000⇒X[3,J]
49: r1+X[3,J]*X[3,J]⇒r1
50: r2+X[3,J]⇒r2
51: r3+1⇒r3
52: r4+T[5,J]*X[3,J]⇒r4
53: r5+T[5,J]⇒r5
54: next J
55: r1*r3-r2*r2⇒D
56: (r4*r3-r5*r2)/D⇒A
57: fmt 3,e.9
58: wrt 706.3,"A=",A
59: for J=1 to 236 by 5
60: for M=J to J+4
61: X[3,M]⇒W[M-J+1]
62: next M
63: for P=0 to 3
64: wrt 706.1,W[P+1],-A*X[3,J+P],T[4,J+P]-A*X[3,J+P]
65: next P
66: wrt 706.2,W[5],-A*X[3,J+4],T[4,J+4]-A*X[3,J+4]
67: next J
68: stp
```

The following are HP library routines required to initialize the HP 3052A system, read the thermocouple, etc.

```
69: "init":
70: if p0=0;rem 7;clr 7
71: fmt 9,f;dev "clk",708⇒p8,"ctr",725⇒p9,"dvm",
     722⇒p10,"ptr",715⇒p11
72: dev "scn",709⇒p12,"scn1",710⇒p13,"scn2",
     711⇒p14,"scn3",712⇒p15
```

```
 73: dev "svm",724⇒p16;8⇒p7
 74: wtb pp7;rds(7,p3,p4,p5)⇒p6;
     r0+2^(p7-8)bit(2,p5)⇒r0;1+p7⇒p7
 75: if p7<17;gto -1
 76: wtb "ptr.9",27,69
 77: ret
 78: "clkred":
 79: fxd 0
 80: 30⇒p6⇒p8⇒p13⇒p11⇒p16
 81: 31⇒p7⇒p9⇒p10⇒p12⇒p14
 82: 28⇒p15;0⇒p17
 83: 18-p1⇒p18;p2⇒p19
 84: if p18=17;p19-1⇒p19
 85: pp18+p19⇒p19
 86: p18+1⇒p18
 87: if p18<=17;jmp -2
 88: fmt 8,c2;wrt "clk","RP"
 89: 1⇒p18
 90: if p18>p19;jmp 3
 91: fmt 9,f4.0;wrt "clk.9","D"
 92: p18+1⇒p18;gto -2
 93: p3⇒p21;0⇒p18
 94: gto +1;if p18<p21;fmt 9,"H",z;wrt "clk.9";
     1+p18⇒p18;gto +0
 95: p4⇒p21;0⇒p18
 96: gto +1;if p18<p21;fmt 9,"M",z;wrt "clk.9";
     1+p18⇒p18;gto +0
 97: p5⇒p21;0⇒p18
 98: gto +1;if p18<p21;fmt 9,"S",z;wrt "clk.9";
     1+p18⇒p18;gto +0
 99: ret
100: "dvm":
101: 0⇒p5;fmt 9,f;clr "dvm";wrt "dvm.9","T3"
102: if p1<1 or p1>5;1⇒p5;1⇒p1
103: if p2<1 or p2>7;p5+2⇒p5;7⇒p2
104: if p3<0 or p3>1;p5+4⇒p5;0⇒p3
105: if p4<0 or p4>1;p5+8⇒p5;0⇒p4
106: fmt 9,"F",f1
107: wrt "dvm.9",int(p1),int(p2),int(p3),int(p4)
108: ret
109: "scn1":
110: if p0=0;wbb "scn,scn1,scn2,scn3";clr 731;ret
111: fmt 9,"0,1,2,3,4,5,6,7,",z;fmt 8,fz2.0,z
112: wrt "scn,scn1,scn2,scn3.9"
113: if p0=0;fmt 9,f;wrt "scn,scn1,scn2,scn3.9";ret
114: if pp0>319;p0-1⇒p0;gto -1
115: if pp0>239;wrt "scn3.8",pp0-240;p0-1⇒p0;gto -2
116: if pp0>159;wrt "scn2.8",pp0-160;p0-1⇒p0;gto -3
117: if pp0>79;wrt "scn1.8",pp0-80;p0-1⇒p0;gto -4
118: wrt "scn.8",pp0;p0-1⇒p0;gto -5
119: "ref jctn":
120: ret 5041.6/(ln(p1)+7.15)-314.052
121: "rdvm":
```

```
122: trg "dvm";fmt 9,f;red "dvm.9",p1
123: ret p1
124: "temp J":
125: if p2=0;p1⇒p20;gto +3
126: 0⇒p3;5.0373743e1⇒p4;3.0167011e-2⇒p5;-7.4293513e-5⇒p6
127: 'poly'(p2,p3,p4,p5,p6)/1e6+p1⇒p20
128: -.048868252⇒p3;19873.14503⇒p4;-218614.5353⇒p5
129: 11569199.78⇒p6;-264917531.4⇒p7;2018441314⇒p8
130: ret 'poly'(p20,p3,p4,p5,p6,p7,p8)
131: "clkred":
132: fmt 8,2x,f10.0;red "clk.8,p1;ret p1
133: "poly":
134: if p0<11;gto +2
135: ((((((p1p18+p17)p1+p16)p1+p15)p1+p14)p1+p13)p1+p12)
     p1+p11)p1⇒p20
136: (((((((p20+p10)p1+p9)p1+p8)p1+p7)p1+p6)p1+p5)p1+p4)
     p1+p3)p1⇒p20
137: ret p20+p2
138: "displ0":
139: r1+1⇒r1
140: 'clkred'⇒Y
141: for I=4 to 5
142: cll 'scn1'(I)
143: 'rdvm'⇒X[I,r1]
144: 'temp J'(X[I,r1],R)⇒T[I,r1]
145: next I
146: dsp T[4,r1],T[5,r1]
147: Y⇒X[3,r1]
148: ret
```

APPENDIX C : Program Used in HP 3052A Automatic Data Acquisition System for Transient Heat Capacity Experiments

The following HP BASIC language program was used during transient heat capacity experiments to monitor various responses of the apparatus and to calculate the heat capacity of the sample.

General Algorithm of program.

1) Reset clock to zero.
2) Read reference thermistor, which is used to calibrate the thermocouple responses.
3) Read initial temperature of the sample.
4) Wait for power supply which heats the sample to be turned on.
5) When power supply is turned on, program begins to record the response of the divider network (see figure 3.6) and the response of the 9 thermocouples in the sample every 3 to 3.5 seconds. This is done until either the power supply, which heats the sample, is shut off, or the memory of the computer is filled.
6) Once the heating of the sample has stopped, the program then proceeds to calculate and print out the temperature rise of the 9 thermocouples, the power and energy delivered to the sample, and the heat capacity of the sample. The heat capacity of the sample is found using equation (2.24).

The following is a listing of the actual program:

```
Set-up variables, initialize HP 3052A system and
reset clock to zero.

0: dim T[5:14,60],V[60],I[60],Z[13,60],C[60],
    A[60],Y[60],X[60],A$[10],E[60]
1: cll 'init'
2: wrt 708,"T"
3: 0⇒r1

Read reference themistor.

4: cll 'dvm'(4,7)
5: cll 'scnl'(0)
6: wait 100

Read initial sample temperature and display on
computer L.E.D. display and also on printer.

8: dsp "please wait"
9: 0⇒Q
10: wrt 722,"F1 R7 T3 M3 A1 H0"
11: for I=5 to 13
12: cll 'scnl'(I)
13: 'temp J'('rdvm',R)⇒T[I,1]
14: Q+T[I,1]⇒Q
15: next I
16: Q/9⇒Q
17: dsp "initial sample temp ",Q
18: wrt 706,"initial sample temp "
19: fmt 1,/,f5.0,z
20: fmt 2,z,f7.1,z
21: fmt 3,z,f5.0,f7.2,z
22: fmt 4,z,f7.2,/
23: wrt 706.1,0
24: for I=5 to 13
25: wrt 706.2,T[I,1]
26: next I
27: wrt 706.3,0,Q
28: wrt 706.4,0
```

Wait for power supply which heats sample to be turned on, by monitoring the current delivered to the sample.

```
29: cll 'dvm'(2,7)
30: cll 'scnl'(1)
31: 'rdvm'⇒I[1]
32: if abs(I[1])<.1;gto -1
```

Start clock.

```
33: wrt 708,"R"
```

Start recording the response of the 9 thermocouples in the sample and the divider network which monitors the voltage and current delivered to the sample. This is done until the power supply which heats the sample is turned off or the computer's memory is filled.

```
34: for J=1 to 60
35: if J>25;wait 15000
36: J⇒r1
37: 'clkred'⇒Z[1,r1]
38: wrt 722,"F1 R7 T3 M3 A1 H0"
39: for I=5 to 13
40: cll 'scnl'(I)
41: 'rdvm'⇒Z[I,r1]
42: next I
43: 'clkred'⇒Z[2,r1]
44: wrt 722,"F2 R7 T3 M3 A1 H0"
45: cll 'scnl'(1);'rdvm'⇒I[r1];'clkred'⇒Z[3,r1]
46: cll 'scnl'(2);'rdvm'⇒V[r1];'clkred'⇒Z[4,r1]
```

If V[r1] is less then 0.1 volts, the power supply was shut off. Therefore, the program stops recording responses of the apparatus and prepares to calculate the results of the experiment.

```
47: if abs(V[r1])<.1;gto +5
48: 'temp J'(Z[9,r1],R)⇒T[9,r1]
49: dsp T[9,r1]
50: next J
```

If the program ever reaches this point, the memory of the computer has been filled and, as a result, heating of the sample must be stopped and the results of the experiment calculated.

```
51: dsp "memory full";J-1⇒r1;r1⇒N;wait 1000;gto "print"
52: J⇒r1;J⇒N
53: I[r1-1]⇒I[r1]
54: V[r1-1]⇒V[r1]
55: (Z[4,r1-1]+Z[4,r1])/2⇒Z[3,r1]
56: Z[3,r1]⇒Z[4,r1]
57: "print":
```

Set-up format statements for printer.

```
58: dsp "press continue to get print out"
59: stp
60: fmt 2,3x,"t1",5x,"2",6x,"3",6x,"4",6x,"5",z
61: wrt 706.2
62: fmt 2,6x,"6",6x,"7",6x,"8",6x,"9",6x,"10",3x,
    "t2",3x,"Tave",3x,"time"
63: wrt 706.2
64: dsp "WAIT A MINUTE !"
65: fmt 1,/,f5.0,z
66: fmt 2,z,f7.1,z
67: fmt 3,z,f5.0,f7.2,z
68: fmt 4,z,f7.2
69: fmt 5,/,f5.0,f8.4,f7.2,f5.0,z
70: fmt 6,z,4x,f7.4,f7.4,2x,f10.2,4x,f10.2,1x,f5.1
71: fmt 7,/,f7.2,f7.2,f10.2,f10.4,z
72: fmt 8,z,4x,f7.4,z.
73: fmt 9,z,2x,f10.2,4x,f10.2,1x,f5.1
```

Calculate temperature of the sample.

```
74: for J=1 to N
75: for I=5 to 13
76: 'temp J'(Z[I,J],R)⇒T[I,J]
77: next I
78: next J
79: for J=1 to N
```

```
81: frc(Z[I,J]/100)*100+frc(int(Z[I,J]/100)/100)
     *6000⇒Z[I,J]
82: next I
83: next J
```

Print out temperature rise of the sample.

```
84: for J=1 to N
85: wrt 706.1,Z[1,J]
86: 0⇒T[14,J]
87: for I=5 to 13
88: wrt 706.2,T[I,J]
89: T[14,J]+T[I,J]⇒T[14,J]
90: next I
91: T[14,J]/9⇒T[14.J]
92: wrt 706.3,Z[2,J],T[14,J]
93: wrt 706.4,(Z[2,J]+Z[2,J])/2
94: next J
```

Calculate the current and voltage delivered to the sample.

```
95: for I=1 to N
96: I[I]*.7781-.0019⇒C[I]
97: V[I]*78.9965+.4229⇒A[I]
98: next I
```

Calculate the power delivered to the sample.

```
99: Z[4,1]⇒X[1]
100: (C[2]-C[1])/(Z[3,2]-Z[3,1])⇒S
101: (S*(X[1]-Z[3,2])+C[2])*A[1]⇒Y[1]
102: X[1]*Y[1]⇒E[1]
103: for I=2 to N-1
104: Z[4,I]⇒X[I]
105: (C[I+1]-C[I])/(Z[3,I+1]-Z[3,I])⇒S
106: (S*(X[I]-Z[3,I])+C[I])*A[I]⇒Y[I]
107: next I
```

Calculate the energy delivered to the sample by using an HP numerical integration routine.

```
108: Z[4,N]⇒X[N]
109: A[N]*C[N]⇒Y[N]
110: E[1]+(X[2]-X[1])*(Y[2]+Y[1])/2⇒E[2]
111: N⇒M;1e-6⇒E
```

```
113: for N=3 to M
114: gsb "INT"
115: A+Y[1]*X[1]⇒E[N]
116: next N
117: N-1⇒N
118: wrt 706;wrt 706
```

Print out energy and power delivered to the sample.

```
119: fmt 2,3x,"t1",5x,"I",6x,"V",5x,"t2",7x,"ch1",
     4x,"ch2",10x,"P",z
120: wrt 706,2
121: fmt 2,"              E       t"
122: wrt 706.2
123: for J=1 to N
124: wrt 706.5,Z[3,J],C[J],A[J],Z[4,J]
125: wrt 706.6,I[J],V[J],Y[J],E[J],Z[4,J]
126: next J
```

Program needs to know the mass of the sample, in order to calculate the heat capacity of the sample.

```
127: ent "mass ?",M
128: fmt 2,"  time    Tave        E          C"
129: wrt 706;wrt 706
130: wrt 706.2
```

Calculation of the heat capacity of the sample in performed using equation (2.23).

```
131: for I=1 to N-1
132: (Z[1,I]+Z[2,I])/2⇒A
133: (Z[1,I+1]+Z[2,I+1])/2⇒B
134: (T[14,I+1]-T[14,I])/(B-A)*(X[I]-A)+T[14,I]⇒T
135: E[I]/M/(T-Q)⇒C
136: wrt 706.7,Z[4,I],T,E[I],C
137: next I
138: stp
```

The following are HP library routines which are required to initialize the HP 3052A system, read the thermocouples, do the numerical integration, et cetera.

```
139: "init":
140: if p0=0;rem 7;clr 7
141: fmt 9,f;dev "clk",708⇒p8,"ctr",725⇒p9,
     "dvm",722⇒p10,"ptr",715⇒p11
142: dev "scn",709⇒p12,"scn1",710⇒p13,"scn2",711⇒p14,
     "scn3",712⇒p15
143: dev "svm",724⇒p16;8⇒p7
144: wtb pp7;rds(7,p3,p4,p5)⇒p6;
     r0+2^(p7-8)bit(2,p5)⇒r0;1+p7⇒p7
145: if p7<17;gto -1
146: wtb "ptr.9",27,69
147: ret
148: "clkred":
149: fxd 0
150: 30⇒p6⇒p8⇒p13⇒p11⇒p16
151: 31⇒p7⇒p9⇒p10⇒p12⇒p14 152: 28⇒p15;0⇒p17
153: 18-p1⇒p18;p2⇒p19
154: if p18=17;p19-1⇒p19
155: pp18+p19⇒p19
156: p18+1⇒p18
157: if p18<=17;jmp -2
158: fmt 8,c2;wrt "clk","RP"
159: 1⇒p18
160: if p18>p19;jmp 3
161: fmt 9,f4.0;wrt "clk.9","D"
162: p18+1⇒p18;gto -2
163: p3⇒p21;0⇒p18
164: gto +1;if p18<p21;fmt 9,"H",z;wrt "clk.9";
     1+p18⇒p18;gto +0
165: p4⇒p21;0⇒p18
166: gto +1;if p18<p21;fmt 9,"M",z;wrt "clk.9";
     1+p18⇒p18;gto +0
167: p5⇒p21;0⇒p18
168: gto +1;if p18<p21;fmt 9,"S",z;wrt "clk.9";
     1+p18⇒p18;gto +0
169: ret
170: "dvm":
171: 0⇒p5;fmt 9,f;clr "dvm";wrt "dvm.9","T3"
172: if p1<1 or p1>5;1⇒p5;1⇒p1
173: if p2<1 or p2>7;p5+2⇒p5;7⇒p2
174: if p3<0 or p3>1;p5+4⇒p5;0⇒p3
175: if p4<0 or p4>1;p5+8⇒p5;0⇒p4
176: fmt 9,"F",f1
177: wrt "dvm.9",int(p1),int(p2),int(p3),int(p4)
178: ret
179: "scn1":
180: if p0=0;wbb "scn,scn1,scn2,scn3";clr 731;ret
181: fmt 9,"0,1,2,3,4,5,6,7,",z;fmt 8,fz2.0,z
182: wrt "scn,scn1,scn2,scn3.9"
183: if p0=0;fmt 9,f;wrt "scn,scn1,scn2,scn3.9";ret
184: if pp0>319;p0-1⇒p0;gto -1
```

```
187: if pp0>79;wrt "scn1.8",pp0-80;p0-1⇒p0;gto -4
188: wrt "scn.8",pp0;p0-1⇒p0;gto -5
189: "ref jctn":
190: ret 5041.6/(ln(p1)+7.15)-314.052
191: "rdvm":
192: trg "dvm";fmt 9,f;red "dvm.9",p1
193: ret p1
194: "temp J":
195: if p2=0;p1⇒p20;gto +3
196: 0⇒p3;5.0373743e1⇒p4;3.0167011e-2⇒p5;
     -7.4293513e-5⇒p6
197: 'poly'(p2,p3,p4,p5,p6)/1e6+p1⇒p20
198: -.048868252⇒p3;19873.14503⇒p4;-218614.5353⇒p5
199: 11569199.78⇒p6;-264917531.4⇒p7;2018441314⇒p8
200: ret 'poly'(p20,p3,p4,p5,p6,p7,p8)
201: "clkred":
202: fmt 8,2x,f10.0;red "clk.8,p1;ret p1
203: "poly":
204: if p0<11;gto +2
205: (((((((p1p18+p17)p1+p16)p1+p15)p1+p14)p1+p13)
     p1+p12)p1+p11)p1⇒p20
206: (((((((p20+p10)p1+p9)p1+p8)p1+p7)p1+p6)p1+p5)
     p1+p4)p1+p3)p1⇒p20
207: ret p20+p2
208: "INT":1⇒I
209: if (I+1⇒I)>N-1;gto +3
210: .5(X[I]-X[I-1]⇒X)/X[I+1]-X[I-1]⇒H)⇒B[I]
211: 2(((Y[I+1]-Y[I])/(X[I+1]-X[I])-(Y[I]-Y[I-1])/X)
     /H⇒T)⇒S[I];3T⇒G[I];gto -2
212: 0⇒S[1]⇒S[N];8-4⇒W
213: 0⇒U;2⇒I
214: W(-S[I]-B[I]S[I-1]-(.5-B[I])S[I+1]+G[I])⇒T
215: if (abs(T)⇒H)>U;H⇒U
216: S[I]+T⇒S[I]
217: if I#N-1;I+1⇒I;gto -3
218: if U>=E;gto -5
220: if (I+1⇒I)>N-1;ret
221: A+(.5(X[I+1]-X[I]⇒H)(Y[I]+Y[I+1])-(1/24)
     H^3(S[I]-S[I+1]))⇒A;gto -1
```

APPENDIX D : Calibration of the Divider Network Used in the Heat Capacity Experiments

To ensure that the divider network shown in Figure 4.2 correctly monitors the voltage and current delivered to the sample, the divider network was calibrated by applying voltages and currents, at levels to be expected in the actual experiments, and by monitoring the response of the divider network. The response of the current monitor, V_1, and voltage monitor, V_2, were tabulated and a straight line fitted to the results.

For I_{sample}:

V_1	I_{sample}
0.272	0.210
0.385	0.297
0.518	0.402
0.663	0.515
0.667	0.516
0.517	0.400
0.425	0.328
0.272	0.210

Using a straight line fitting routine

$$I_{sample} = 0.7781\ V_1 - 0.0019 \qquad (D.1)$$

For V_{sample}:

V_2	V_{sample}
0.682	54.1
0.967	76.7
1.297	103.5
1.676	132.6
1.680	132.9
1.300	103.3
1.067	84.7
0.681	54.2

Using a straight line fitting rou

$$V_{sample} = 78.9965\ V_2 + 0.4229 \qquad (D.2)$$

APPENDIX E : Experimental Results

The experimental results presented here are divided into thermal conductivity and heat capacity results. These results are then presented in chronological order with appropriate comments regarding each experiment. The numbering system used to identify each experiment starts at 50 because many preliminary experiments were conducted in order to develop the final apparatus and methods. This numbering system is maintained here so that the results presented in this Appendix can easily be referred to the original, more complete experimental data results.

E.1 Thermal Conductivity Results

As previously mentioned in Section *3.3 Description of the Experimental Procedure for the Transient Heat Probe Method*, the power supplied to the probe had to be reduced to the point where noise and drift in the thermocouple reading became very significant. Therefore, the transient heat probe experiments were performed several times on the same sample and an average thermal conductivity for the sample calculated. To estimate the error in the average thermal conductivity result, the maximum deviation in the individual thermal conductivity runs from the average thermal conductivity was used.

The instrumentation used in this research, to monitor the temperature of the probe, was only accurate to ~0.1 °C. To reduce the error in the thermal conductivity results, a thermocouple with better temperature resolution (~0.01 to 0.001 °C) is required;

however, the shale sample may change physically during experiments. As a result, very accurate determination of the thermal conductivity of shale may not be possible. The work done by other researchers was on materials which allowed a larger temperature gradient within the sample than that within the Clearwater shale samples. For instance, Seto[64] used the transient heat probe method to measure the thermal conductivity of oilsands samples. In Seto's experiments, he ensured that the sample was 100% saturated by forcing water into the sample and pressurizing the sample. Since the samples were 100% saturated and pressurized, Seto was able to use higher temperature changes in his experiments without causing moisture migration in the samples.

The following pages summarize the thermal conductivity results obtained on Clearwater shale samples.

---

[64] Seto, (1985)

Experiment#71

Shale sample: May16/85
36-51-0-0
P25,"M"
147-152 ft

Density of sample: $\rho = 2.06$ g/cm^3

Composition of sample: mineral = 84.5%
water = 15.5%

Estimated Water Saturation: $S_w = 84\%$

Experimental results

Run	q $\left(\frac{W}{m}\right)$	K_{expt} $\left(\frac{W}{m\,^\circ C}\right)$	log-linear range (s)
1	4.33	----------	---------
2	1.73	1.33 - 1.35	5.5 - 480
3	2.21	1.78 - 1.88	7.5 - 325
4	2.20	1.68 - 1.71	13.5 - 360
5	2.46	1.68 - 1.73	5.5 - 315

Average thermal conductivity

$K_{ave} = 1.74 \pm 8\%$ (excluding 2nd run)

Comments:

a) Sample fractured radially.

b) First run drift in thermocouple not corrected.

c) It was believed that during the first run the probe power level was too high and caused

moisture to be evaporated from around the probe. Therefore, before the third run the probe was removed from the sample and water inserted into hole. The probe was then reinserted into sample.

Experiment#72

Shale sample: March17/87
36-51-0-0
P9,"D"
72-77 ft

Density of sample: $\rho = 2.09$ g/cm^3

Composition of sample: mineral - 81.2 - 79.1%
water - 18.8 - 20.9%

(Spread in results due to measurements made before and after experiment.)

Estimated Water Saturation: $S_w = 100\%$

Experimental results

Run	q $\left(\frac{W}{m}\right)$	K_{expt} $\left(\frac{W}{m\,^oC}\right)$	log-linear range (s)
1	2.41	----------	----------
2	2.41	1.75 - 1.87	14.5 - 440
3	2.41	1.67 - 1.72	21.5 - 525
4	3.26	1.66 - 1.90	12.5 - 370

Average thermal conductivity

$K_{ave} = 1.76 \pm 8\%$ (excluding 1st run)

Comments

a) During the first run the probe was not correctly grounded.

Experiment#73

Shale sample: March17/87
36-51-0-0
P16,"F"
112-117 ft

Density of sample: ρ = 2.17 g/cm^3

Composition of sample: mineral - 86.4 - 85.5%
water - 13.6 - 14.5%

Estimated Water Saturation: S_w - 90%

Experimental results

Run	q $\left(\frac{W}{m}\right)$	K_{expt} $\left(\frac{W}{m\,^oC}\right)$	log linear range (s)
1	2.73	2.06 - 2.16	10.5 - 1500
2	2.64	2.04 - 2.08	6.5 - 375
3	2.66	1.95 - 2.23	5.5 - 585
4	2.52	2.11 - 2.13	6.5 - 465
5	2.71	2.45 - 2.52	6.5 - 1200
6	2.71	2.01 - 2.14	7.5 - 485

Average thermal conductivity

K_{avg} = 2.09 ± 7% (excluding 5th run)

Comments

a) None

Experiment#75

Shale sample: April28/87
36-51-0-0
P24,"A"
142-147 ft

Density of sample: $\rho = 2.15$ g/cm^3

Composition of sample: mineral = 76.2 - 73.1%
water = 23.8 - 26.9%

Estimated Water Saturation: S_w = 124%

Experimental results

Run	q $\left(\frac{W}{m}\right)$	K_{expt} $\left(\frac{W}{m\,^oC}\right)$	log-linear range (s)
1	2.72	2.22	9.5 - 675
2	2.63	1.90 - 1.91	11.5 - 455
3	2.60	1.75 - 1.93	10.0 - 500
4	2.71	2.11 - 2.18	9.5 - 345
5	2.70	1.94 - 2.00	5.0 - 400

Average thermal conductivity

$K_{ave} = 1.99 \pm 12\%$ (using all runs)

Comments

a) None

Experiment#76

Shale sample: Nov16/86
34-51-0-0
P28, "I"
167-172 ft

Density of sample: $\rho = 2.47$ g/cm^3

Composition of sample: mineral = 90.3 - 88.1%
water = 9.7 - 11.9%

Estimated Water Saturation: $S_w = 118\%$

Experimental results

Run	q $\left(\frac{W}{m}\right)$	K_{expt} $\left(\frac{W}{m\,^oC}\right)$	log-linear range (s)
1	2.58	1.63 - 1.64	7.5 - 625
2	2.70	1.84 - 1.87	5.5 - 375
3	2.69	1.92 - 1.95	9.5 - 650
4	2.38	1.55 - 1.65	6.5 - 550

Average thermal conductivity

$K_{ave} = 1.76 \pm 12\%$ (using all runs)

Comments

a) Sample very sandy.

Experiment#77

Shale sample: Feb 6/87
34-51-0-0
P21,"C"
139-143 ft

Density of sample: ρ = 2.06 g/cm^3

Composition of sample: mineral = 77.2 - 75.8%
water = 22.8 - 24.2%

Estimated Water Saturation: S_w = 109%

Experimental results

Run	q $\left(\frac{W}{m}\right)$	K_{expt} $\left(\frac{W}{m\,^oC}\right)$	log-linear range (s)
1	2.39	1.64 - 1.69	10.5 - 475
2	2.28	1.78 - 1.87	7.5 - 430
3	2.30	1.63 - 1.65	6.5 - 550
4	2.31	1.46 - 1.51	15.5 - 400
5	2.24	1.65 - 1.67	9.5 - 580

Average thermal conductivity

K_{ave} = 1.70 ± 10% (excluding 4th run)

Comments

a) None

Experiment#78

Shale sample: March 3/87
34-51-0-0
P29,"G"
172-177 ft

Density of sample: ρ = 2.0 g/cm^3

Composition of sample: mineral = 88.6 - 87.5%
water = 11.4 - 12.5%

Estimated Water Saturation: S = unknown

Experimental results

Run	q $\left(\frac{W}{m}\right)$	K_{expt} $\left(\frac{W}{m\,^oC}\right)$	log-linear range (s)
1	2.05	2.22 - 2.27	10.5 - 450
2	2.11	2.30 - 2.33	6.5 - 525
3	2.27	2.21 - 2.30	7.5 - 250
4	2.08	2.19 - 2.25	10.5 - 500
5	1.82	1.85 - 1.96	9.0 - 300

Average thermal conductivity

K_{ave} = 2.26 ± 3% (excluding 5th run)

Comments

a) Sample very sandy with bitumen traces.

b) In the fifth run, the probe current drifted by -3.5%

Experiment#79

Shale sample: May20/87
34-51-0-0
P8,"D"
77-82 ft

Density of sample: $\rho = 2.22$ g/cm^3

Composition of sample: mineral = 86.4 - 83%
water = 13.4 - 17%

Estimated Water Saturation: $S_w = 95\%$

Experimental results

Run	q $\left(\frac{W}{m}\right)$	K_{expt} $\left(\frac{W}{m\,^oC}\right)$	log-linear range (s)
1	2.10	2.30 - 2.35	6.5 - 500
2	2.31	2.12 - 2.18	6.5 - 550
3	2.35	2.15 - 2.16	5.5 - 500
4	2.35	2.20 - 2.21	7.5 - 500
5	2.35	2.27 - 2.32	5.5 - 550

Average thermal conductivity

$K_{ave} = 2.23 \pm 5.4\%$ (using all the runs)

Comments

a) None

E.2 Thermal Heat Capacity Results

Thermal heat capacity values were obtained experimentally for three substances, these being tap water, sand/water, and oilsands. These experimentally obtained values were compared with previously published values, in order to acquire some approximate estimate of the accuracy of the transient heat capacity method used in this research. A meaningful comparison can, however, only be made for the case of tap water. Based on heat capacity values for tap water, as obtained by the transient heat capacity method and as quoted in the literature, it is thought that the experimental error in the heat capacity values determined by the transient heat capacity method is in the neighbourhood of 5%.

The heat capacity of the mineral fraction of the sample, $c_{mineral}$, was determined using equation (2.5) where the effective heat capacity, c_{eff}, of the sample was experimentally determined and the value used for the heat capacity of the water was $4.18 \frac{J}{g\,^{o}C}$. Two values for $c_{mineral}$ were calculated using the composition of the sample measured before and after the experiment.

The following pages summarize the heat capacity results obtained for Clearwater shale samples.

Experiment#50

Shale sample: Aug20/86
36-51-0-0
P4, "A"
47-52 ft

Density of sample: $\rho = 2.24\ g/cm^3$

Composition of sample: mineral = 80.3 - 82.1%
water = 19.7 - 17.9%

Estimated Water Saturation: $S_w = 113\%$

Experimental results

$$c_{expt} = 1.42\ \frac{J}{g\ ^oC}$$

$$\rho c_{expt} = 3.17\ \frac{J}{cm^3\ ^oC}$$

$$c_{mineral} = 0.81 \text{ to } 0.74\ \frac{J}{g\ ^oC}$$

Comments

a) The metal sheath of two thermocouples in the sample were accidentally touching each other. This caused very high localized heating rates at the thermocouple locations and as a result the response of these two thermocouples had to be ignored in the calculation of the heat capacity of the sample.

Experiment#55

Shale sample: Aug20/86
36-51-0-0
P4,"H"
47-52 ft

Density of sample: $\rho = 2.09\ g/cm^3$

Composition of sample: mineral = 79.2 - 78.8%
water = 20.8 - 21.2%

Estimated Water Saturation: $S_w = 106\%$

ental results.

$c_{expt} = 1.46\ \frac{J}{g\,^\circ C}$

$\rho c_{expt} = 3.06\ \frac{J}{cm^3\,^\circ C}$

$c_{mineral} = 0.74$ to $0.73\ \frac{J}{g\,^\circ C}$

Comments

a) None

Experiment#56

Shale sample: Aug 1/86
34-51-20-0
P17, "A"
119-124 ft

Density of sample: $\rho = 2.22\ g/cm^3$

Composition of sample: mineral = 84.2 - 85.2%
water = 15.8 - 14.8%

Estimated Water Saturation: $S_w = 101\%$

Experimental results

$$c_{expt} = 1.29\ \frac{J}{g\,^{\circ}C}$$

$$\rho c_{expt} = 2.87\ \frac{J}{cm^3\,^{\circ}C}$$

$$c_{mineral} = 0.74 \text{ to } 0.79\ \frac{J}{g\,^{\circ}C}$$

Comments

a) None

Experiment#57

Shale sample: Sept30/86
34-51-0-0
P2,"C"
53-57 ft

Density of sample: $\rho = 2.17$ g/cm^3

Composition of sample: mineral = 84.3 - 84%
water = 15.4 - 16%

Estimated Water Saturation: $S_w = 97\%$

Experimental results

$$c_{expt} = 1.28 \frac{J}{g\,^oC}$$

$$\rho c_{expt} = 2.78 \frac{J}{cm^3\,^oC}$$

$$c_{mineral} = 0.75 \text{ to } 0.73 \frac{J}{g\,^oC}$$

Comments

a) Sandy sample.

Experiment#58

Shale sample: Nov 3/86
36-51-20-0
P27,"E"
162-167 ft

Density of sample: $\rho = 2.06\ g/cm^3$

Composition of sample: mineral = 87.2 - 84.9%
water = 12.8 - 15.1%

Estimated Water Saturation: $S_w = 74\%$

Experimental results

$$c_{expt} = 1.31\ \frac{J}{g\,^oC}$$

$$\rho c_{expt} = 2.70\ \frac{J}{cm^3\,^oC}$$

$$c_{mineral} = 0.89 \text{ to } 0.80\ \frac{J}{g\,^oC}$$

Comments

a) Sample very sandy with bitumen traces.

Experiment#59

Shale sample: Feb.6/87
34-51-0-0
P21,"B"
139-143 ft

Density of sample: $\rho = 2.00\ g/cm^3$

Composition of sample: mineral - 76.5 - 75.0%
water - 23.5 - 25.0%

Estimated Water Saturation: $S_w = 104\%$

Experimental results

$$c_{expt} = 1.67\ \frac{J}{g\,^oC}$$

$$\rho c_{expt} = 3.35\ \frac{J}{cm^3\,^oC}$$

$$c_{mineral} = 0.90 \text{ to } 0.83\ \frac{J}{g\,^oC}$$

Comments

a) Note that the moisture content in this sample was very high, and that this sample also produced the highest heat capacity of all transient heat capacity experiments performed on Clearwater shale samples.

Experiment#61

Shale sample: Feb 6/87
36-51-0-0
P23, "C"
137-142 ft

Density of sample: $\rho = 2.15\ g/cm^3$

Composition of sample: mineral = 89.2 - 87.5%
water = 10.8 - 12.5%

Estimated Water Saturation: $S_w = 79\%$

Experimental results

$$c_{expt} = 1.16\ \frac{J}{g\,^oC}$$

$$\rho c_{expt} = 2.49\ \frac{J}{cm^3\,^oC}$$

$$c_{mineral} = 0.79 \text{ to } 0.73\ \frac{J}{g\,^oC}$$

Comments

a) The sample was very sandy with streaks of shale mixed with the sand.

Experiment#62

Shale sample: Mar 3/87
34-51-0-0
P29,"A"
172-177 ft

Density of sample: $\rho = 2.24\ g/cm^3$

Composition of sample: mineral = 82.5 - 86.6%
water = 17.5 - 13.4%

Estimated Water Saturation: $S_w = 98\%$

Experimental results

$$c_{expt} = 1.30\ \frac{J}{g\,^oC}$$

$$\rho c_{expt} = 2.90\ \frac{J}{cm^3\,^oC}$$

$$c_{mineral} = 0.69 \text{ to } 0.85\ \frac{J}{g\,^oC}$$

Comments

a) The sample was very sandy with clumps of shale mixed in and bitumen traces present.

Experiment#64

Shale sample: Oct24/85
36-51-Q-0
P19,"L"

Density of sample: $\rho = 2.23\ g/cm^3$

Composition of sample: mineral = 85.2 - 86.5%
water = 14.8 - 13.5%

Estimated Water Saturation: $^{\circ}S_w = 97\%$

Experimental results

$$c_{expt} = 1.35\ \frac{J}{g\,^{\circ}C}$$

$$\rho c_{expt} = 3.02\ \frac{J}{cm^3\,^{\circ}C}$$

$$c_{mineral} = 0.86 \text{ to } 0.91\ \frac{J}{g\,^{\circ}C}$$

Comments

a) None

Experiment#65

Shale sample: Mar17/87
36-51-0-0
P9, "E"
72-77 ft

Density of sample: $\rho = 2.13\ g/cm^3$

Composition of sample: mineral = 80.7 - 83.5%
water = 19.3 - 16.5%

Estimated Water Saturation: $S_w = 96\%$

Experimental results

$$c_{expt} = 1.46\ \frac{J}{g\,^\circ C}$$

$$\rho c_{expt} = 3.11\ \frac{J}{cm^3\,^\circ C}$$

$$c_{mineral} = 0.81 \text{ to } 0.92\ \frac{J}{g\,^\circ C}$$

Comments

a) None

Experiment#66

Shale sample: Mar17/87
36-51-0-0
P16,"B"
112-117 ft

Density of sample: $\rho = 2.22\ g/cm^3$

Composition of sample: mineral = 84.4 - 85.6%
water = 15.6 - 14.4%

Estimated Water Saturation: $S_w = 99\%$

Experimental results

$$c_{expt} = 1.33\ \frac{J}{g^{\circ}C}$$

$$\rho c_{expt} = 2.96\ \frac{J}{cm^3\,^{\circ}C}$$

$$c_{mineral} = 0.80 \text{ to } 0.86\ \frac{J}{g^{\circ}C}$$

Comments

a) The metal sheath of two thermocouples were touching during the experiment and produced the same effects as described in Experiment#50.

Experiment#67

Shale sample: Mar17/86
36-51-0-0
P16,"H"
112-117 ft

Density of sample: $\rho = 2.28$ g/cm

Composition of sample: mineral - 80.5 - 84.2%
water - 19.5 - 15.8%

Estimated Water Saturation: $S_w = 114$

Experimental results

$$c_{expt} = 1.42 \frac{J}{g\,^{o}C}$$

$$\rho c_{expt} = 3.23 \frac{J}{cm^{3}\,^{o}C}$$

$$c_{mineral} = 0.75 \text{ to } 0.90 \frac{J}{g\,^{o}C}$$

Comments

a) None

Experiment#69

Shale sample: May16/87
36-51-0-0
P25,"M"
147-152 ft

Density of sample: $\rho = 2.16\ g/cm^3$

Composition of sample: mineral = 83.1 - 85.4%
water = 16.9 - 14.6%

Estimated Water Saturation: $S_w = 93\%$

Experimental results

$$c_{expt} = 1.41\ \frac{J}{g\,^oC}$$

$$\rho c_{expt} = 3.04\ \frac{J}{cm^3\,^oC}$$

$$c_{mineral} \quad 0.85 \text{ to } 0.94\ \frac{J}{g\,^oC}$$

Comments

a) None

Experiment#74

Shale sample: April28/87
36-51-0-0
P24, "D"
142-147 ft

Density of sample: $\rho = 2.19$ g/cm^3

Composition of sample: mineral = 79.9 - 82.5%
water = 20.1 - 17.5%

Estimated Water Saturation: $S_w = 108\%$

Experimental results

$$c_{expt} = 1.46 \frac{J}{g\,^oC}$$

$$\rho c_{expt} = 3.20 \frac{J}{cm^3\,^oC}$$

$$c_{mineral} = 0.77 \text{ to } 0.88 \frac{J}{g\,^oC}$$

Comments

a) The sample was very badly fractured axially and radially.

Experiment#80

Shale sample: May 20/87
34-51-0-0
P8, "H"
77-82 ft

Density of sample: $\rho = 2.17\ g/cm^3$

Composition of sample: mineral = 83.4 - 84.9%
water = 16.6 - 15.1%

Estimated Water Saturation: $S_w = 96\%$

Experimental results

$$c_{expt} = 1.34\ \frac{J}{g\,^\circ C}$$

$$\rho c_{expt} = 2.90\ \frac{J}{cm^3\,^\circ C}$$

$$c_{mineral} = 0.77 \text{ to } 0.83\ \frac{J}{g\,^\circ C}$$

Comments

a) None

APPENDIX F : Derivation of Equation (2.25)

The following derivation uses the integral transform method outlined by Özisik[65]. For the problem as described in Section 2.2.2 the following partial differential equation applies.

$$K\nabla^2 T(r,z,t) + q = \rho c \frac{\partial T}{\partial t} \qquad (F.1)$$

where the parameters on this equation are the same as in Section 2.2.2.

The boundary conditions for this problem are as follows

1) $T(r,z,0) = f(r,z) = 0$ (F.2a)

2) $T(r,0,t) = 0$ (F.2b)

3) $T(r,\ell,t) = 0$ (F.2c)

4) $T(b,z,t) = 0$ (F.2d)

5) $T(0,z,t)$ finite (F.2e)

For the integral transform method, the required homogeneous problem is

$$K\nabla^2 T(r,z,t) = \rho c \frac{\partial T}{\partial t} \qquad (F.3a)$$

---

[65] Özisik, pp552-593, (1980)

or in cylindrical coordinates

$$\frac{1}{r}\frac{\partial}{\partial r}\left[r\frac{\partial T}{\partial r}\right] + \frac{\partial^2 T}{\partial z^2} = \frac{1}{D}\frac{\partial T}{\partial t} \qquad \text{(F.3b)}$$

Applying separation of variables

$$T(r,z,t) = R(r)Z(z)Q(t) \qquad \text{(F.4)}$$

Equation (F.3b) becomes

$$\underbrace{\frac{1}{rR}\frac{\partial}{\partial r}\left[r\frac{\partial R}{\partial r}\right]}_{-\beta^2} + \underbrace{\frac{1}{Z}\frac{\partial^2 Z}{\partial z^2}}_{-\lambda^2} = \underbrace{\frac{1}{DQ}\frac{\partial Q}{\partial t}}_{-(\beta^2+\lambda^2)} \qquad \text{(F.5)}$$

For the time solution Q(t):

$$\frac{dQ}{dt} = -(\beta^2+\lambda^2)QD \Rightarrow Q(t) = e^{-D(\beta^2+\lambda^2)t} \qquad \text{(F.6)}$$

For the axial component Z(z):

$$\frac{d^2Z}{dz^2} = -\lambda^2 Z \Rightarrow Z(z) = A\cos(z\lambda) + B\sin(z\lambda) \qquad \text{(F.7a)}$$

where A and B are constants to be determined later.

From Table 2.2 of Özisik

$$Z_m(z) = A_m \sin(\lambda_m z) \qquad \text{(F.7b)}$$

where $\lambda_m = \frac{m\pi}{\ell}$

and $\frac{1}{N(\lambda_m)} = \frac{2}{\ell}$

(normalization constant)

and the A_m's are constants to be determined later.

For the radial component R(z):

$$\frac{d}{dr}\left[r\frac{dR}{dr}\right] + \beta^2 rR = 0 \Rightarrow R(r) = CJ_0(\beta r) + DN_0(\beta r) \qquad \text{(F.8a)}$$

where C and D are constants to be determined later.

and $J_0()$ and $N_0()$ are Bessel and Neuman functions.

From Table 3.1 of Özisik

$$R_n(r) = C_n J_0(\beta_n r) \qquad \text{(F.8b)}$$

where β_n's are the roots of

$$J_0(\beta_n r) = 0$$

and $\frac{1}{N(\beta_n)} = \frac{2}{b^2 J_1^2(\beta_n b)}$

(normalization constant)

and the C_n's are constants to be determined later.

The homogeneous solution is therefore

$$T(r,z,t) = \sum_m \sum_n C_{mn} \sin(\lambda_m z) J_0(\beta_n r) e^{-D(\lambda_m^2+\beta_n^2)t} \qquad (F.9a)$$

$$\text{where } C_{mn} = \frac{4}{\ell b^2 J_1^2(\beta_n b)} \int_0^b \int_0^\ell r \sin\left[\frac{m\pi}{\ell} z\right] J_0(\beta_n r)\, \partial z\, \partial r \qquad (F.9b)$$

Using equation (13.15) from Özisik the solution to the original problem is obtained.

$$T(r,z,t) = \sum_m \sum_n C_{mn} \sin(\lambda_m z) J_0(\beta_n r) e^{-D(\lambda_m^2+\beta_n^2)t} * \frac{D}{K} \int_0^t q e^{D(\lambda_m^2+\beta_n^2)t}\, \partial t \qquad (F.10)$$

Solving the integral in equation (F.9b), one obtains equation (2.25) presented in Section 2.2.2.